UNIVERSIDAD DE INVESTIGACIÓN DE TECNOLOGÍA EXPERIMENTAL YACHAY

Escuela de Ciencias biológicas e Ingeniería

TÍTULO: Use of Natural Diatoms doped with gold nanoparticles for Gentamicin Drug Delivery

Trabajo de integración curricular presentado como requisito para la obtención
del título de Ingeniero/a Biomédico

Autor:

Chavez Chico Eva Anai

Tutor:

PhD. González Vásquez Gema

Urcuquí, diciembre 2020

SECRETARÍA GENERAL
(Vicerrectorado Académico/Cancillería)
ESCUELA DE CIENCIAS BIOLÓGICAS E INGENIERÍA
CARRERA DE BIOMEDICINA
ACTA DE DEFENSA No. UITEY-BIO-2020-00054-AD

A los 21 días del mes de diciembre de 2020, a las 16:00 horas, de manera virtual mediante videoconferencia, y ante el Tribunal Calificador, integrado por los docentes:

Presidente Tribunal de Defensa	Dra. SPENCER VALERO, LILIAN MARITZA , Ph.D.
Miembro No Tutor	Dr. CAETANO SOUSA MANUEL , Ph.D.
Tutor	Dra. GONZALEZ VASQUEZ, GEMA , Ph.D.

El(la) señor(ita) estudiante **CHAVEZ CHICO, EVA ANAI**, con cédula de identidad No. **1723100226**, de la **ESCUELA DE CIENCIAS BIOLÓGICAS E INGENIERÍA**, de la Carrera de **BIOMEDICINA**, aprobada por el Consejo de Educación Superior (CES), mediante Resolución **RPC-SO-43-No.496-2014**, realiza a través de videoconferencia, la sustentación de su trabajo de titulación denominado: **Use of Natural Diatoms doped with gold nanoparticles for Gentamicin Drug Delivery.**, previa a la obtención del título de **INGENIERO/A BIOMÉDICO/A**.

El citado trabajo de titulación, fue debidamente aprobado por el(los) docente(s):

Tutor	Dra. GONZALEZ VASQUEZ, GEMA , Ph.D.

Y recibió las observaciones de los otros miembros del Tribunal Calificador, las mismas que han sido incorporadas por el(la) estudiante.

Previamente cumplidos los requisitos legales y reglamentarios, el trabajo de titulación fue sustentado por el(la) estudiante y examinado por los miembros del Tribunal Calificador. Escuchada la sustentación del trabajo de titulación a través de videoconferencia, que integró la exposición de el(la) estudiante sobre el contenido de la misma y las preguntas formuladas por los miembros del Tribunal, se califica la sustentación del trabajo de titulación con las siguientes calificaciones:

Tipo	Docente	Calificación
Tutor	Dra. GONZALEZ VASQUEZ, GEMA , Ph.D.	9,0
Presidente Tribunal De Defensa	Dra. SPENCER VALERO, LILIAN MARITZA , Ph.D.	9,0
Miembro Tribunal De Defensa	Dr. CAETANO SOUSA MANUEL , Ph.D.	9,5

Lo que da un promedio de: **9.2 (Nueve punto Dos)**, sobre 10 (diez), equivalente a: **APROBADO**

Para constancia de lo actuado, firman los miembros del Tribunal Calificador, el/la estudiante y el/la secretario ad-hoc.

Certifico que *en cumplimiento del Decreto Ejecutivo 1017 de 16 de marzo de 2020, la defensa de trabajo de titulación (o examen de grado modalidad teórico práctica) se realizó vía virtual, por lo que las firmas de los miembros del Tribunal de Defensa de Grado, constan en forma digital.*

CHAVEZ CHICO, EVA ANAI
Estudiante

LILIAN MARITZA SPENCER VALERO
Firmado digitalmente por LILIAN MARITZA SPENCER VALERO
Fecha: 2020.12.23 10:03:30 -05'00'

Dra. SPENCER VALERO, LILIAN MARITZA , Ph.D.
Presidente Tribunal de Defensa

Dra. GONZALEZ VASQUEZ, GEMA , Ph.D.
Tutor

CERTIFICACIÓN ELECTRÓNICA
BANCO CENTRAL DEL ECUADOR
Firmado Digitalmente por: GEMA GONZALEZ VAZQUEZ
Hora oficial Ecuador: 28/12/2020 11:09

MANUEL
CAETANO SOUSA

Dr. CAETANO SOUSA MANUEL , Ph.D.
Miembro No Tutor

KARLA ESTEFANIA
ALARCON FELIX

ALARCON FELIX, KARLA ESTEFANIA
Secretario Ad-hoc

AUTORÍA

Yo, **EVA ANAI CHAVEZ CHICO**, con cédula de identidad 1723100226, declaro que las ideas, juicios, valoraciones, interpretaciones, consultas bibliográficas, definiciones y conceptualizaciones expuestas en el presente trabajo; así cómo, los procedimientos y herramientas utilizadas en la investigación, son de absoluta responsabilidad de el/la autora (a) del trabajo de integración curricular. Así mismo, me acojo a los reglamentos internos de la Universidad de Investigación de Tecnología Experimental Yachay.

Urcuquí, diciembre 2020.

_____
Eva Anai Chávez Chico
CI: 1723100226

AUTORIZACIÓN DE PUBLICACIÓN

Yo, **EVA ANAI CHAVEZ CHICO,** con cédula de identidad 1723100226, cedo a la Universidad de Tecnología Experimental Yachay, los derechos de publicación de la presente obra, sin que deba haber un reconocimiento económico por este concepto. Declaro además que el texto del presente trabajo de titulación no podrá ser cedido a ninguna empresa editorial para su publicación u otros fines, sin contar previamente con la autorización escrita de la Universidad.

Asimismo, autorizo a la Universidad que realice la digitalización y publicación de este trabajo de integración curricular en el repositorio virtual, de conformidad a lo dispuesto en el Art. 144 de la Ley Orgánica de Educación Superior

Urcuquí, diciembre 2020.

_____
Eva Anai Chavez Chico
CI: 1723100226

Resumen

Las diatomeas son algas fotosintéticas unicelulares cubiertas de pared celular silícea, con un notable interesante estructura porosa ordenada con diferentes niveles de porosidad jerárquica desde nano hasta macroporos. Tienen paredes de células nano y macroestructura muy espectaculares y diversas que imparten una arquitectura diferente a su estructura. La compatibilidad de la matriz silícea se ha demostrado en otros sistemas. Por lo tanto, debido a la estructura ordenada de los poros, la alta superficie, la biocompatibilidad, la disponibilidad y el bajo procesamiento costo, pueden tener un gran potencial para la administración de fármacos en comparación con otros sistemas de sílice utilizados para esta aplicación que requirió procesos de síntesis mucho más difíciles y uso de reactivos costosos. Natural y las diatomeas cultivadas contienen varios compuestos terapéuticos como proteínas y polisacáridos complejos que se puede utilizar en diversas aplicaciones terapéuticas. Se ha encontrado que las diatomeas marinas contienen ácidos grasos poliinsaturados y compuestos bioactivos con potenciales propiedades antioxidantes y anticancerígenas. Por tanto, en el presente trabajo se propone explorar el uso de una diatomea natural (Aulacoseria) de la región de Guayllabamba de Ecuador dopada con nanopartículas de oro como posibles sistemas de administración de fármacos. Las diatomeas se caracterizan por espectroscopía ultravioleta-visible, difracción de rayos X en polvo (XRD), escaneo Microscopía electrónica (SEM), Microscopía de fluorescencia, Raman y Área de superficie (BET). Las muestras fueron desaluminados y funcionalizados con nanopartículas de oro y se estudió la entrega controlada utilizando gentamicina como fármaco modelo.

Palabras Clave:

Diatomeas; Biosilica; Funcionalización de superficies; Nanopartículas de oro; Gentamicina; Administración de medicamentos.

Abstract

Diatoms are unicellular photosynthetic algae covered with siliceous cell wall, with a remarkably interesting ordered porous structure with different levels of hierarchical porosity from nano to macropores. They have a very spectacular and diverse nano and macrostruture cellwalls that impart different architecture to their structure. The compatibility of siliceous matrix has been proved in other systems. Therefore, due to the ordered pore structure, the high surface area, biocompatibility, availability, and low processing cost, they can have a great potential for drug delivery compared with other silica systems used for this application that required much more difficult synthesis processes and used of expensive reactants. Natural and cultured Diatoms contain various therapeutic compounds such as proteins and complex polysaccharides which can be used in various therapeutic applications. It has been found that the marine diatoms contain polyunsaturated fatty acids and bioactive compounds with potential antioxidant and anticancer properties. Therefore, in the present work it is proposed to explore the use of a natural diatom (*Aulacoseria*) from the Guayllabamba region of Ecuador doped with gold nanoparticles as potential drug delivery systems. The diatoms are characterized by Ultraviolet-Visible Spectroscopy, X-ray Powder Diffraction (XRD), Scanning Electron Microscopy (SEM), Fluorescence Microscopy, Raman, and Surface area (BET). The samples were dealuminated and functionalized with gold nanoparticles and the controlled delivery was studied using Gentamicin as model drug.

Key Words:

Contents

List of Figures

List of Tables

Chapter 1

Introduction

Nowadays, diatoms are fascinating nanotechnologists who are hoping these impressive pore structures can show them how to obtain new properties for new applications. The first time that the idea of utilizing diatoms as news materials with potential properties came in 1999 (by Morse) due to their nano-scale design and the hierarchical porosity in different scales and the genetic control, crucial features for the human engineering applications[1]. Thanks to the usefulness of biotechnology, we have been capable of generating more specific and complex medicines, making their administration very intricate. The most advanced systems include the use of microspheres and polymer microcapsules, nanoparticles, and natural polymers[2]. In order to consider a explicit type of drug delivery, it is necessary to contemplate the clinical needs and the factors that characterize them, such as the physicochemical properties of the drug, the disease to be treated, in which part of the body has its interaction if the treatment will be for chronic or acute diseases, among others[2]. One of the principal objectives in drug delivery is to create new and efficient carries for drugs with less toxicity for the patient and lower the risk of handle high amounts of drugs incorporations[3,4]. Through the years, several experiments have been made facing of the struggles for drug delivery, and as a result, bio-templating was developed, and diatoms came up as attractive carriers and delivery system[5]. The diatom nanostructure has suitable characteristics such as adsorption capacity and packing for drug delivery[6]. Using diatoms for drug delivery permits us to understand the effect of surface functionalization on controlling diffusion rates, due to the drug packing and release in bare and modified diatoms[1]. The use of silica-based particles has been growing over the years, creating a wide variety of porosities and scales for drug delivery; these synthetic particles have excellent characteristics such as a high surface area, thermal stability, biocompatibility, among others. However, their high cost, the production time and the use of toxic materials have motivated researches

to look for alternative natural sources of these silica structures for the drug delivery, with diatoms being the best positioned due to their exceptional characteristics[6]. *In vitro* tests and experiments have been made using diatoms as carriers of certain drugs, such as indomethacin. A loading capacity of 22 wt% and prolonged drug release over two weeks was obtained promising giving results in the use of diatoms for drug delivery[6]. Other drugs that have been tested in diatoms were mesalamine and prednisone both are standard drugs for the treatment of gastrointestinal disorders, the drug delivery property of diatoms with these two drugs where tested in monolayers of colon cancer cells and prove a low toxicity at concentration of 1000 μg/mL and a stable release, moreover, this study proved that the diatoms enhanced the permeability of the drug by the permeation of the monolayer cell culture[7]. Dolatabadi and de la Guardia reported some studies about functionalization of diatom biosilica frustules with antibodies and enzymes[8]. Additionally, diatom-silica microcapsules were functionalized with dopamine- modified iron-oxide NPs, and new properties of magnetic diatoms were obtained with an enormous potential to be used as magnetically-guided drug-delivery micro-carriers. In 2019, Delasoie and Zobi in their study "Natural Diatom Biosilica as Microshuttles in Drug Delivery Systems" commented that diatoms have the ability to be functionalized with various types of components, this added to the high drug-loading capacity, of these micro-algae a promising material in the pharmaceutics field and also in biomedical applications. Additionally, these systems are an eco-friendly and inexpensive nanoporous biosilica material[9]. According to Uthappa, *et al*, modified diatoms with silica xerogel and obtained a notable increase in drug loading capacity in comparison with the control diatomaceous earth sample[10].The functionalization of diatoms with gold nanoparticles has been reported by different authors[11,12] , Terracciano, *et al*, performed *in vitro* cytotoxicity tests, resulting in high viability, therefore these materials are considered safe for application in biomedicine. In the present work, it is proposed to explore the use of natural diatoms (*Aulacoseira genus*) from the Guayllabamba region of Ecuador undoped and doped with gold nanoparticles as potential Gentamicin drug delivery systems. The diatoms were characterized by UV-vis, XRD, SEM, Raman, and surface area. The samples studied are natural and dealuminated diatoms, functionalized and not functionalized with Au nanoparticles, and loaded with Gentamicin as a model drug.

Chapter 2

Motivation

2.1 Problem Statement

The use of natural diatoms is currently a topic of interest to both medical and scientific community due to their use and facilities in the field of drug delivery and other related fields. As the world is advancing its needs grow, one of them is the demand of new contolled delivery systems of medications. Diatoms appear as a natural alternative eco-friendly biomaterial for this purpose.

Nanomaterials of silica have been used to work in drug delivery, but the process of obtaining them is harmful to the environment. So, diatoms are a "greener" option for the same purpose. This marvelous nanostructures have some essential characteristics that are needed for drug delivery such as biocompatibility and biodegradability. Using the natural micro algae instead of synthetic materials implies reducing the cost of production too. To reach this goal, functionalized diatoms are needed to improve the drug release, reduce the waste of materials, the contamination and the environmental toxicity.

In this perspective, this project proposes the use of natural diatoms doped with gold nanoparticles *In-situ*, and *Ex-situ* for the drug delivery of Gentamicin and compare with the not functionalized samples.

2.2 General and Specific Objectives

2.2.1 General objective

To use natural diatoms undoped and doped with gold nanoparticles for Gentamicin drug delivery.

2.2.2 Specific objectives

- Obtain, dealuminize, functionalize, and characterize a natural diatom genus *Aulacoseira* from Guayllabamba intermontane basin.

- Synthetized gold nanoparticles on the diatom by *In-situ* and *Ex-situ* methods.

- Characterize the diatoms undoped and doped with gold nanoparticles using UV-vis, XRD, SEM, Raman, and surface area.

- Load the different samples with Gentamicine and carried out drug release experiments in Simulated Body Fluid (SBF).

- Evaluate the drug release behavior of the different functionalized diatoms.

Chapter 3

Theoretical Background

3.1 Diatoms

Diatoms are unicellular microalgae that are the most outstanding natural supplier of porous silica, these species can be found in every aqueous habitat, there exits probably around 100000 species of them. During their accelerated growth cycle, diatoms absorb important quantities of trace elements and nutrients from the surface water layer, especially silicon to form their shells, and zinc, which performs a vital physiological role in their development[13]. Diatom shells have a combination of chemical, mechanical and structural characteristics that surpass the obstacles associated with the delivery of therapeutic agents and offer several advantages over existing synthetic microparticle delivery systems, they have a pillbox structure with a hollow and large inner space with micro- and nano-scale porosity, high surface area, excellent biocompatibility, amorphous silica, high permeability, low density, non-toxicity and the ability to mimic the nature of constituents for natural bone and medical implant, these properties make diatoms silica a promising biomaterial for drug-delivery applications[6]. Diatoms with distinct 3-D of silica cell walls and highly-ordered pore structures, offer a great potential to replace synthetic mesoporous materials also they are a suitable carrier system for delivering small interfering ribonucleic acid (siRNA) inside the human epidermoid cancer cells[4,14].

3.1.1 Diatoms structure

The diatoms have an outer wall composed of silica called frustule which consists of two leaflets, a small one called hypotheca and a larger one called an epitheca, each of which is formed from a leaflet that forms the outer surface and a girdle that is a circular band of silica on the edges of the valve[15]. These

leaflets are situated from different sheets, which gives them a variation in porosity that can range from microns to nanometers and their distribution depend on the species. The use of frustules diatoms has diversed over time and can be found in these physical properties that allow its application in fields such as nanotechnology and biotechnology, where we can highlight its use for the production of bio-inspired solar cells due to its capacity of collecting light with great efficiency, such as nano-structured substrates in plasmonic, optical sensors and biosensors, nanoparticles as vectors in drug delivery. It is possible to generate variations in the frustule diatoms in terms of their porosity, morphology and geometry to be able to generate new more efficient techniques, this is possible through the modification of certain genes that are involved in the formation of the frustule diatom[16].

3.1.2   Diatoms used in this work

The diatoms used in this work correspond to the genus *Aulacoseira*. They have a centric morphology and it contains various number of species. It has apparently a better adaptation to develop life in lakes, large rivers and ponds[17]. The species to which correspond these amazing microalgae is plantonik, which means that they are centric; this fact can be confirmed just with the observation in the morphology. In concept, the structure of these diatoms that have the characteristic to be centric, are consistent and stable, which facilitates the identification of the specie[17].

3.2   Nanotechnology

Physicist Richard Feynman firstly revealed the conceptual bases regarding nanotechnology in 1959,although some properties of small materials were known from 1857 when Michael Faraday observed the interaction of light with metal nanoparticles[18]and this is considered the birth of nanotechnology, although at that time the word nano was not used. Feynman proposed that molecules and atoms of materials could be modified completely. The term, nanotechnology, was not used until 1974[19]. When referring to nanotechnology, it means "nano" one billionth part of a meter, and "technology." So, with this, it can be stated that it is the technology that worked in the nanoscale. Nanotechnology entails manipulating all kinds of nanomaterials to work as a system and make it function in all sorts of areas. Some to mention can be medicine, energy, environmental, security, agriculture, and others[19].

The principle idea of nanomaterials, is, due to their size, they possess some qualities that only appear at the nanoscale. With this, the expected was to develop the next generation of different fields. Together with the electrical and mechanical characteristics, the biology field joins them to form the nanobiotechnology

world. It is well known these days that biological structures have some sort of organization in the dimension of nanoscale, as well as some synthetic nanomaterials that can be associated with DNA, and proteins[20].

3.3 Nanoparticles

Nanoparticles (NPs) are particles that are in the range of size between 1 and 100 nm in diameter. NPs are widely being employed in many industries because of their distinctive properties[21]. This NPs as quantum dot has an adjustable bandgap, which can be managed by making variations in the size of these QDs[22]. Different attributes of the nanoparticles will depend entirely on their nature, their size, the chemical composition, the surface area, and others[21]. Nanoparticles (NPs) have several substantial implications, principally in biomedical engineering, agriculture, and environmental remediation practices.

3.3.1 Gold nanoparticles

Gold Nanoparticles (AuNPs), due to the variety of their size and shape, have a broad spectrum of areas where can be applied, including medicine, food industry, water purification, and biological applications. Its applications in bionanotechnology are countless, some to mention: sensing, therapeutic, imaging[23], drug delivery, photothermal therapy, catalysis, and antimicrobial[24]. The conjugation or bioconjugation is one of its incredible properties, it allows the nanoparticles to bond to other materials and these will acquire new properties or improve the ones that they already had[23].
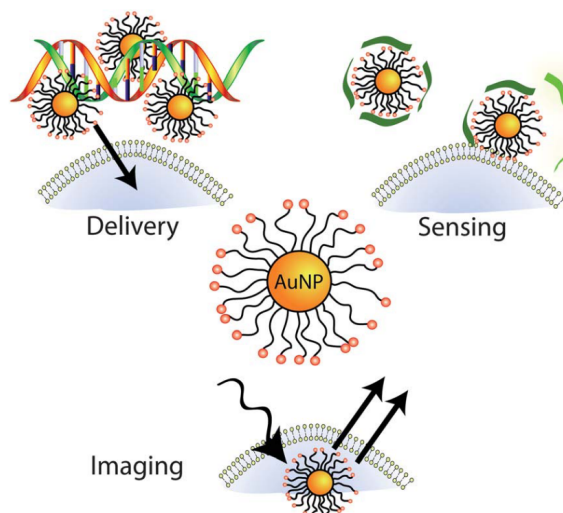
Figure 3.1: Applications of AuNPs in bionanotechnology, taken from Yeh. et al. "Nanoscale, 2012, 4, 1871"[23]

In the figure 3.1 it can be observed an example of AuNPs been utilized in bionanotechnology, in some areas mentioned before as imaging,delivery and sensing.

Synthesis of gold nanoparticles

To control the size, shape, and surface functionality was developed, a wide range of solution approaches were developed[23]. Turkevich et al. in 1951 established a synthetic method for producing AuNPs by processing hydrogen tetrachloroaurate ($HAuCl_4$) in boiling water with citric acid (figure 3.2), where the citrate performs as both reducing and stabilizing agent[25]. Another author, Frens, accomplished the procedure by changing the ratio of gold/citrate to obtain a better control of particle size[26]. This protocol has mainly been used to formulate dilute solutions of relatively stable spherical AuNPs with a tendency of 10 to 20 nm of diameter, also larger AuNPs can be prepared, for example, of 100nm[23].
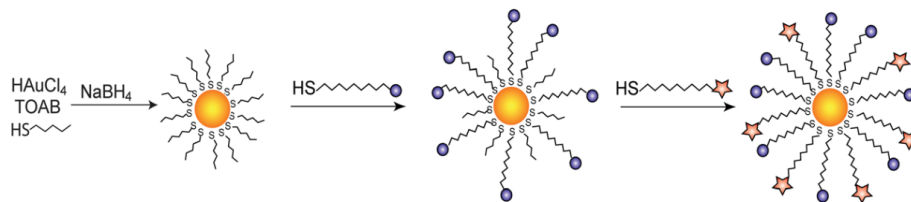
Figure 3.2: Two-phase synthesis of AuNPs by reduction of *HAuCl*$_4$ in presence of alkanethiols as the stabilizing ligands and *NaBH*$_4$ as reducing agent. Place-exchange reaction for alkanethiol-protected AuNPs can then be performed with functionalized thiols. Adapted from Yeh. et al.[23]

In 1994, Brust and Schriffin synthesized AuNPs by producing organic soluble alkanethiol-stabilized AuNPs through a biphasic reduction protocol as seen in figure 3.2 utilizing tetraoctylammonium bromide (TOAB) as the phase transfer reagent and sodium borohydride (*NaBH*$_4$) as reducing agent[27].

Properties of gold nanoparticles

Sphere-shaped AuNPs have essential qualities such as shape- and size- associated with optoelectronic properties, significant surface-to-volume ratio, exceptional biocompatibility, and low toxicity[28]. These characteristics make AuNPs a valuable implement in bionanotechnology[23].

Some of the properties are redox activity, surface-enhanced Raman scattering (SERS), surface plasmon resonance (SPR), and Fluorescence quenching, and their application areas are electronic devices and electrochemical sensing, imaging and sensing, colorimetric sensing and photothermal therapy, sensor fabrication, and materials science[23]. Spherical AuNPs can exhibit a selection of colors like brown, orange, red and purple, in aqueous solution as the core size intensifies from 1 to 100 nm, and frequently show a size relative absorption peak from 500 to 550 nm[29].

3.4   Oxidation-reduction method

An oxidation-reduction reaction is basically a transfer of electrons. It consists of two sub-reactions, reduction, and oxidation. In the phase of oxidation there are three principle concepts, it gains oxygen, losses electrons and the element increase its oxidation number. In reduction's phase there are also three principles: it gains oxygen, losses electrons and the element increase its oxidation number. In reduction's phase there are also three principles that it might be known as the opposite of oxidation, these are loss

of oxygen, gain of electrons and the element decrease its oxidation number[30]. For the preparation of AuNPs, there are various procedures to follow, but the most known is still the reduction method, which is the reduction of tetrachloroauric acid in aqueous solution with sodium citrate. In general the reduction of Au(III) to Au(I) takes place due to the addition of the citrate[31].

3.5 Drug delivery

Drug delivery is one of the technological innovations whose major objective is the administration or release of medications in the individual. The use of medications is a common practice in the human history, but the way in which medications are administered has varied and improved over time, being much more efficient[32]. Drug delivery is an extensive area in researching the development of new materials or transporters to improve the efficient of delivery of medicines or treatments[33,34]. According to the National Institute of Biomedical Imaging and Bioengineering of the USA, the most recent drug delivery systems investigation can be described in 4 different categories such as: administration routes, administration vehicles, cargo and mark strategies[32]. Some referents that a system of drug delivery could have is to be controlled, to be steady or to be targeted[34]. When referring to administration routes, skin, buccal and nasal mucosal membranes are good examples of it. But a new area is rising inside this field, and it is referred as controlled release technology[34]. These controlled systems suggest the most of trans-mucosal and trans-dermal for drug delivery. Even there are some other variations of notions and techniques that can benefit the methods of the controlled stage of drug delivery[34,35].

3.5.1 Controlled drug delivery

Regarding drug delivery, there exists controlled systems that are used to maintain adequate levels of drugs in the body, which is necessary for the administration of certain medications making their use more effective. The main objective for which this systems were conceived is to maintain constant levels of medications in the patients' blood for a period of time, thus evading a decrease in the concentration of medication between administrations, ensuring that the dose does not reach toxic levels for the patient[36]. Chemical-controlled systems of the bioerosion or biodegradation structure consists in the degradation of the polymers where the medicine is distributed in water soluble molecules, can also use the system Pendant chain of a biodegradable polymer which, upon contact with water destroys these bonds by releasing the medication in the body[37]. The appearing of controlled drug delivery systems represents one of the prominent areas in science. Bringing a multidisciplinary enrollment of fields that are all supporting the healthcare area[34].

3.6 Drug release

The procedure of drug release is managed by dissolution and diffusion, separately or together. When it comes to the diffusion part, the model of square root of time of Higuchi shows the best fitting where applied it is to porous materials[38].

$$Q = \sqrt{\frac{D\varepsilon}{\tau}(2A - \varepsilon C)C_t)} \tag{3.1}$$

In the equation of Higuchi's model, Q represents the drug released after a time t, D is the diffusivity in a fluid of the drug, τ the tortuosity factor of the capillary system, A is the amount of drug present in the matrix, C is the solubility of the drug in the fluid and ϵ is the porosity of the matrix[38,39]. Usually the release is a process of two stages, the first that is fast and the second one has a slower velocity[39].

3.7 Gentamicin

The Gentamicin is part of the antibiotics called aminoglycosides. It's chemical structure include amino sugars merged by a glycoside linkage[40,41]. This medication, through its liaison to the 30S ribosomal subunit, is known to permanently inhibit bacterial protein synthesis[41,42]. The diseases produced by aerobic gram-negative bacteria are primarily treated by this type of medicine. However, the medicine group, to which Gentamicin belongs, are an important part in the treatment of severe gram-negative sepsis, even though their extremely cationic, polar nature, which it implies that the circulation across membranes is restricted[40]. For the gram-positive bacteria, the aminoglycosides performance synergistically against them[41]. Generally, Gentamicin has a powerful antimicrobial activity[42]. In figure 3.3 it can be observed the molecule of Gentamicin, its formula is $C_{21}H_{43}N_5O_7$.
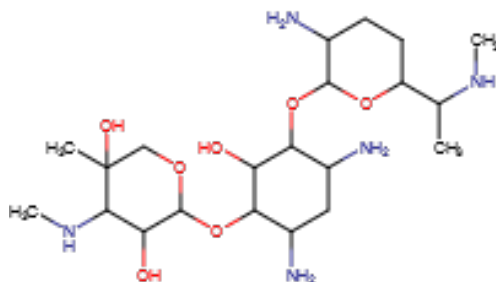
Figure 3.3: Gentamicin chemical structure.

3.7.1   Characteristics of Gentamicin

Gentamicin has a low molecular weight, it is only bond weakly to plasma proteins, and as the primary route of excretion, is easily discharged into the glomerular filtrate[43]. Gentamicin has shown good response of being rapidly and well absorbed via intramuscular and subcutaneous injection of routes of administration, but cannot being absorbed via orally[40]. The recommended is to apply a single dosage per day. This is known to maximizes the efficacy and decreases toxicity. To set an example, lets speak about the concentrations applied. A concentration between the limits of 0.5 to 5.0 μg/mL of Gentamicin is considered bactericidal for gram-positive and for a few types of gram-negative bacteria. If the concentration changes to the range of 10 to 15 μg/mL, the treatment of Gentamicin is more effective, even for the most resilient bacteria, like *Pseudomonas aeruginosa, Klebsiella pneumoniae, and Proteus mirabilis*[40].

3.8   Simulated Body Fluid (SBF)

Simulated body fluid, is a solution which is synthesized from certain quantities of explicit compounds to acquire ion concentrations that can emulate the same composition as in human blood plasma. The reagants presents in the SBF formula are the following: sodium chloride (NaCl), sodium hydrogen carbonate ($NaHCO_3$), potassium chloride (KCl), Hydrochloric Acid (HCl), di-potassium hydrogen phosphate trihydrate ($K_2HPO_4.3H_2O$), magnesium chloride hexahydrate ($MgCl_2.6H_2O$), calcium chloride ($CaCl_2$),

sodium sulfate (Na_2SO_4), Tris-hydroxymethyl aminomethane: (($HOCH_2$)$3CNH_2$)(Tris), Hydrochloric Acid (used to balance the pH). The last two components are used to get a stable pH of 7.4. It is important to know that the reactive previously mentioned, should be added in certain order to obtain a good solution[44].

Chapter 4

Characterization techniques

4.1 UV-visible Spectroscopy (UV-vis)

Ultraviolet spectroscopy covers the absorption spectroscopy and reflectance spectroscopy, which works in the ultraviolet-visible (UV-vis) spectral region[45,46]. Is a method that is considered to be fast and low-cost that determines the concentration of an analyte in a solution[47]. The absorption has as result the excitation of the electrons from lower to higher energy levels[45]. The molecules that include p-electrons or non-bonding electrons (n-electrons) are capable of absorb ultraviolet or visible light energy[46]. In general, UV-vis spectroscopy, as it is mentioned before, serve to establish elemental concentrations quantitatively in some solution, all these is directed by the Bee-Lambert law,

$$A = log_{10}(\frac{I_0}{I}) = \varepsilon CL \tag{4.1}$$

In this equation A stands for the measured absorbance, I_0 for the intensity of the incident light at a certain wavelength, I is for the transmitted intensity, C holds for the concentration of the absorbing species, ε represents a constant that is the molar absorptivity or extinction coefficient for each species and wavelength, and L refers the path length through the sample[46].

This method corresponds to the absorbances of ultraviolet (180-390 nm) and the visible (390-780 nm). These regions of the spectrum offer an exact amount of energy that ends up in electronic transitions, starting with the highest occupied molecular orbital (HOMO) to the lowest unoccupied molecular orbital (LUMO). The difference in energy between these two is what is known as band gap. Consequently, each wavelength of light is associated to a unique energy[48,49]. To estimate the energy gap, the wavelength value could be analyzed with these two equations[50]:

$$E_g = \frac{hc}{\lambda} \tag{4.2}$$

$$E_g = h\frac{1240}{\lambda} \tag{4.3}$$

Where E_g is the band gap energy, h represents the Planck's constant, λ is the wavelength, and c stands for speed of light. By far, it is known that molecules with different chemical structures have different energy band gaps and the absorption spectra is also different. The usual transitions that fall in the range of UV-vis are $\pi - \pi*$ and $n - \pi*$[51]. In figure 4.1 it can be observed a sample of UV-vis spectra, retrieved from Ojea, et al[31].
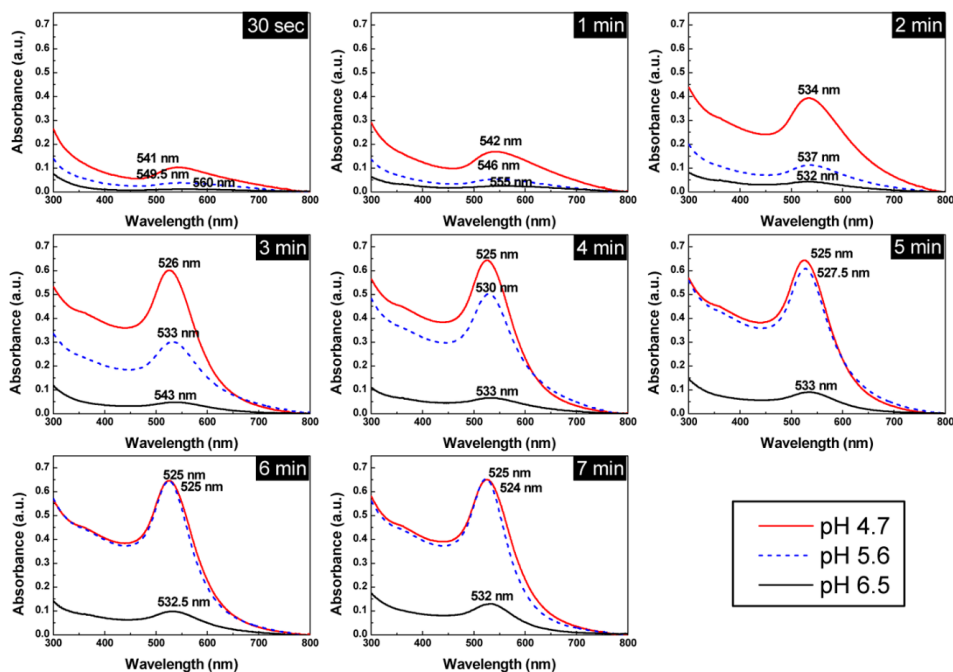
Figure 4.1: Time evolution of the UVvis absorbance spectra of AuNPs synthesized using 0.165 mM of $HAuCl_4$ and a sodium citrate: $HAuCl_4$ ratio of 13.6 at 90 °C, under acidic, mild acidic and neutral conditions. The appearance of a peak at approximately 525 nm is characteristic of the SPR of Au colloids. Adapted from Ojea. et al[31].

4.2   Scanning Electron Microscopy (SEM)
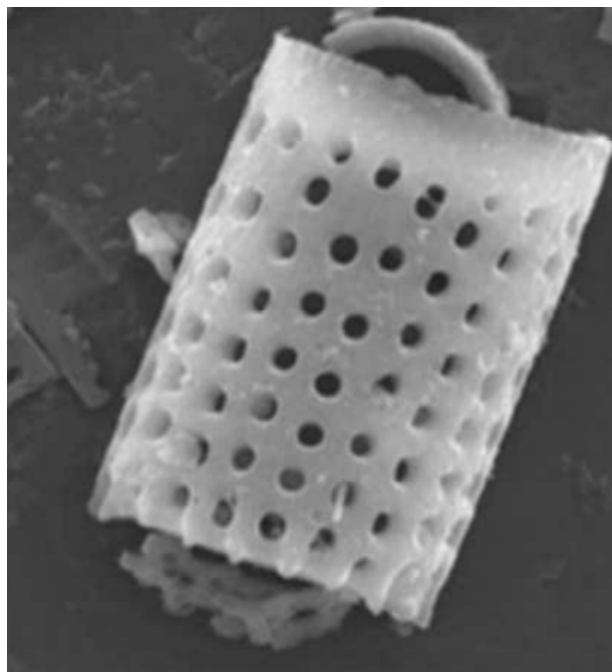
Figure 4.2: Image of Diatom (DE) frustule (scale bar –1μm). Adapted from Uthappa. et al. Xerogel modified diatomaceous earth microparticles for controlled drug release studies [10]

One of the usual techniques for imaging and examining the microstructure and morphology of the materials in a micro- and nanoscale is the Scanning Electron Microscopy [52,53]. In SEM, an energetic electron beam, is spread to the material and scans the surface of the object. Numerous of various interactions take place while the beam achieves the material, which takes them to the release of photons and electrons that are in the object [52]. Subsequently, the beam rasters the sample surface with assistance of scan coils. Images are produced from the beam interaction with the specimen. The backscattered and secondary electrons released from the sample above the vacuum level are captured by a correctly placed detector [53,54]. The surface topography of a sample with the high spatial resolution is observed [53].

A standard SEM, according to Omidi et al, consists of a variety of elements, such as: The electron gun which is located on top of the column and emits electrons. The electrons are then accelerated to energy levels of typically 0.1-30 keV; electromagnetic lenses and apertures which focus and shape the electron beam to form a small concentrated electron spot on the sample; and a high-vacuum environment that allows

electrons moving without being scattered or absorbed by the air, although there are also systems that work in low vacuum and even under environmental conditions[52].

4.3   Energy Disperse X-Ray (EDX)

EDX analysis, or also known as EDS, is also named energy dispersive X-ray analysis/spectroscopy or additionally found as energy dispersive X-ray microanalysis. It is an analytical method employed for the fundamental analysis or chemical characterization of a sample[55]. This technique is the most commonly used for bringing out compositional analysis in SEM. The method depends on the ionization of atoms in the specimen by the expulsion of an electron from an internal shell by an incident electron. The particle can then relax in several ways, one of which is the loss of energy by an external shell electron, which saturates the hole left behind by the emitted electron[56]. When it is used in combination with SEM it permits the analysis of near-surface components and their amount at distinct spots offering a map of the sample[57]. The energy loss ends in the emission of an X-ray photon, and the energy of this X-ray is the variation in the energy levels between the ejected and external shell electrons implicated. Consequently, the energy of the radiated X-ray is element-specific and can be applied to perform chemical analysis with a dispersive energy indicator. Elements that are in concentrations > 1% by mass are regularly detected, although mitigating factors such as spectral cover can make difficult such recognition for a thorough treatment of these procedures. Quantification of the EDX spectral indication can be accomplished by adequately correcting the raw signal through background subtraction, rectification for absorption, and fluorescence effects, and comparison to spectra obtained under comparable conditions from reference materials of identified composition[56]. Sections for analysis are carefully chosen by focusing the incoming beam, and the released X-rays are perceived and their energies recognized by a solid-state X-ray energy-dispersive spectrometer (XEDS). The output of this method is an XEDS spectrum, which is a plot of X-ray counts vs. energy[58]. Almost all the elements in the periodic table can be analyzed by EDS; just hydrogen and helium produce no X-rays; beryllium (Be Kα at 108.8 eV) and still lithium (Li Ka at 54.4 eV) can only be identified with very modern EDS methods[59]. The X-rays are generated from an area about 2 microns deep. The electron beam is moved throughout the material, and then the elements in the specimen form an image[57]. figure 4.3, and table 4.1 show an EDX sample:
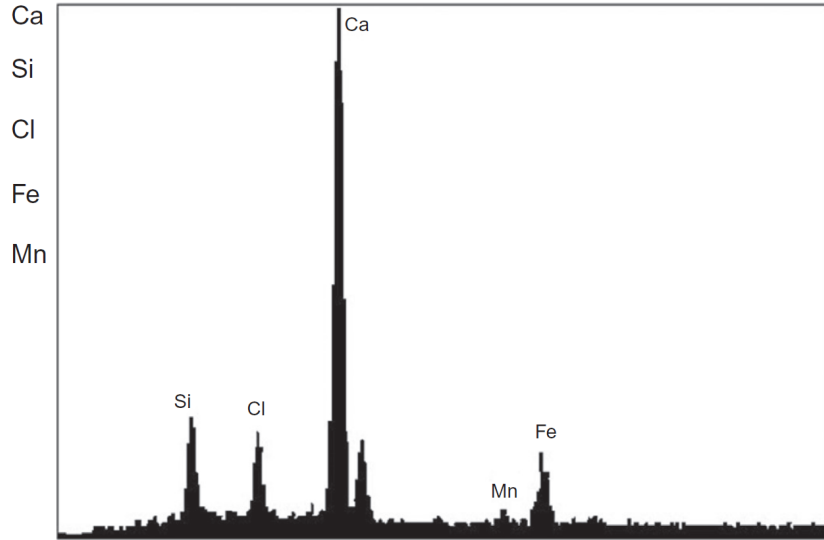
Figure 4.3: EDX sample. A test result of cracked surface of a BOF slag particle using EDS, adapted from Wang. et al.[55]

EDS analysis result for BOF slag			
Element	Shell	Weight %	Atomic%)
Ca	K	60.8899	60.1600
Si	K	12.2610	17.2873
Cl	K	8.5383	9.5369
Fe	k	15.5730	11.0423
Mn	k	5730	11.0423

Table 4.1: EDS analysis result for BOF slag, adapted from Wang. et al.[55]

In figure 4.3 it can be observed a sample from Wang. et al[55], precisely the spectrum, and in table4.1 can be observed the analysis of the spectrum in figure 4.3.

4.4   Raman Spectroscopy (RS)

Raman spectroscopy (RS), is a potent method for investigating the distinctive "chemical fingerprints" of liquid and solid samples, to make possible to identify different molecules[60,61], used to examine vibrational, rotational, and other low-frequency modes in a scheme[61]. For the past 25 years, RS has been extensively utilized in molecules to inquiry bonds, to give distinctive chemical evidence about the effects on the cell biochemistry of drugs, to comprehend the mechanisms of differentiation and cell death, and to distinguish between different types of cells[60]. In RS, the samples are frequently used immaculate, making this spectroscopy easier than infrared spectroscopy when talking about preparing the sample[62]. RS is known as a second procedure of infrared examination that lights samples with short wavelength, that is not infra-red, light and later evaluates the light that is scattered at right angles to the illuminating beam. The laser typically produces illumination and the molecules in the laser beam absorb light as they vibrate and change the wavelength of some of the emitted illuminated light to wavelengths similar to IR absorption bands. These are more known as Raman spectra[63]. RS is a somewhat old system for the presence of inelastic light scattering based on theoretical projections[64]. The spectrum of this technique offers information that complements to the IR spectrum in that both are vibrational spectra. Usually the signals that are considered the weakest in the IR spectrum, in the Raman spectra are the strongest signals[65]. RS offers unique data about the molecular distinctiveness of the sample: as mentioned before, these are the "chemical fingerprints," the 3D structural changes in alignment, placement and configuration of bio-molecules like collagen, the intermolecular interactions, and the dynamics of biological phenomenon; different types of Raman systems have been developed for different needs. The most popular for biological purposes are Confocal Raman Spectroscopy (CRS), Modulated Raman Spectroscopy (MRS), Surface-Enhanced Raman Spectroscopy (SERS), and Tip-Enhanced Raman Spectroscopy (TERS)[60].

There exist several options of lasers for Raman offered in the area. Generally, they are categorized into three separate classifications that depends on their wavelength: UV lasers (wavelength <360 nm), visible lasers (wavelength of approximately 450 nm up to 660 nm), and NIR lasers (wavelength in the range 785–1064 nm)[62].
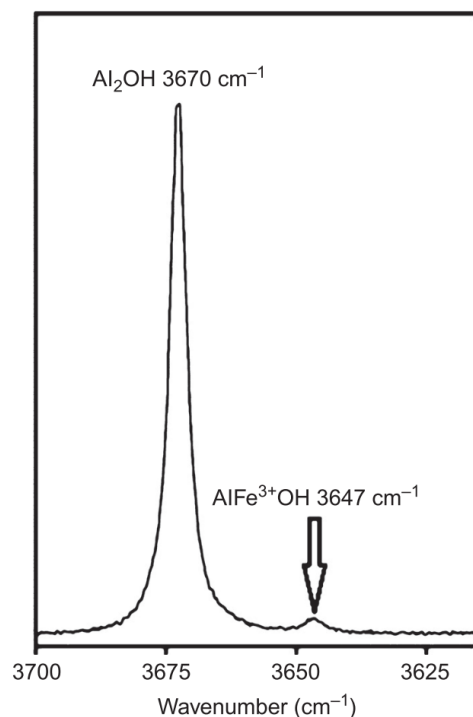
Figure 4.4: Raman Spectrometer example. Raman spectrum of natural pyrophyllite in the hydroxyl stretching region showing the strong mode associated with n(Al_2OH) at 3670 cm^{-1} and the n($AlFe_3+OH$) at 3647 cm^{-1} due to substitution of Al^{3+} by Fe^{3+} in the octahedral sheet. Adapted from Kropogge. Raman Spectroscopy of Clay Minerals[64]

4.5 Fluorescence Microscopy

Between microscopy methods, there is Fluorescence Microscopy that is used to characterize fluorescent or fluorescent-labeled NPs[66]. Fluorescence microscopy is a procedure where samples that are marked with dyes that have fluorescent properties are monitored with a fluorescent microscope[67]. This microscope has been accepted as one of the most flexible optical imaging techniques[68]. In this imaging technique, fluorophores are intended to normally label certain types of cells and organelles, or at the same time, to indicate the existence of particular molecules[69], these are situated in close proximity to the position of concern, and are excited by an external source of light and then redirected at another wavelength that can be identified[68]. Therefore, the optical sign in fluorescence microscopy greatly depends on the fluorophore

properties. Some examples of fluorophores that are typical can be organic dyes, quantum dots (QDs), and lanthanide compounds, these can be utilized in living cells for the optical imaging[68].
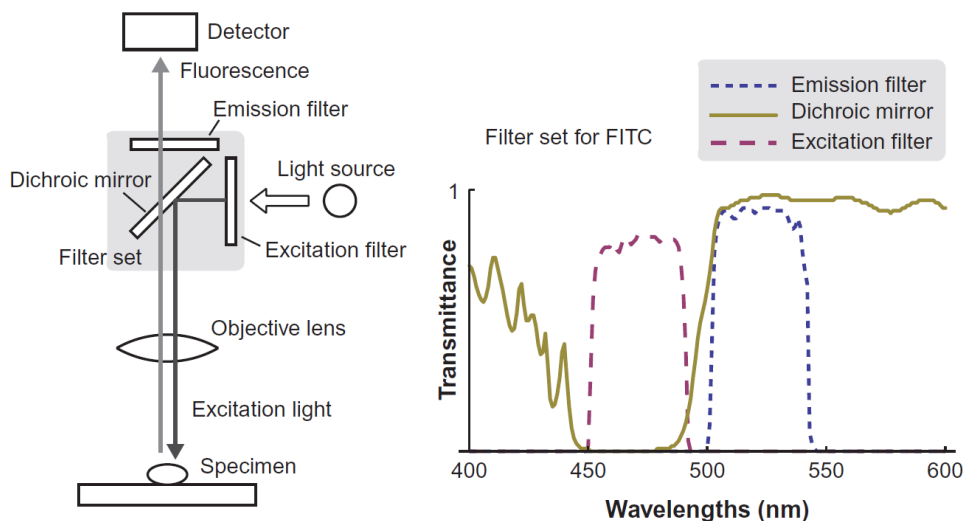
Figure 4.5: Schematic of a fluorescence microscope and the spectra of a fluorescence filter cube. Image retrieved from Optical transducers: Optical molecular sensing and spectroscopy. Chapter 5 from Zhang, et al.[67]

In the figure 4.5 we can see a fluorescent microscope's basic composition. The light source, the excitation filter, the dichroic mirror, and the emission filter are the crucial elements for fluorescence microscope. The light source is typically a xenon lamp, a tungsten halogen lamp, or a mercury lamp, which has a large band of emission. The excitation light that goes through the excitation filter is mirrored by the dichroic mirror and light up the sample. When for excitation, a laser or a monochromatic light source is used, the excitation filter is not required. Fluorescence from the sample goes through the emission filter and the dichroic mirror. A package of an excitation filter, a dichroic mirror, and an emission filter is normally packed in an approximately 1 in. size box called a filter cube or filter package. Packages of filters have to be selected for distinct types of fluorescent dyes[67]. Also in the figure 4.5 there can be appreciated an example of a filter cube's transmission spectra, which involves a long-pass dichroic mirror, a bandpass excitation filter, and a band-pass emission filter intended for fluorescein isothiocyanate (FITC). FITC is one of the most popular fluorescent dyes utilized[67]. In the biological field, fluorescence microscopy is a procedure often applied to uncover cellular composition or sub cellular activities[69]. FITC has been applied

for the tagging of antibodies. Immunofluorescence is the most valuable technique for molecular sensing and imaging[67].

4.6   X-Ray Difractometry (XRD)

Simulated body fluid, is a solution which is synthesized from certain quantities of explicit compounds to acquire ion concentrations that can almost emulate the same composition as in human blood plasma.[53,70,71], it also provides information of crystal defects, phases, preferred crystal orientations (texture)[71]. XRD is also considered to be a formidable non-destructive procedure for characterizing crystalline materials[70,71]. (XRD), or also referred to as x-ray powder diffraction, uses x-ray radiation on crystalline inorganic and organic experiments[72].

In X-ray technique the rays are diffracted in a configuration defined by the position, size, and arrangement of the components of the crystal. Scattered photons, which may experience subsequent interference, a guide to a characteristic diffraction model, which is particular to the crystalline powder, and it could be work as its 'fingerprint'[72]. XRD peaks are generated by constructive interference of a monochromatic beam of X-rays scattered at precise positions from each set of lattice planes in an experiment. The peak intensities are defined by the atomic situations within the lattice planes. Therefore, the XRD configuration, as mentioned before, is the fingerprint of periodic atomic arrangements in a given material[71]. Minor changes in the lattice spacing because of compression or tension could be quantified with specific incident optics or high resolution. In incident optics and generators, some current studies say that it could make it possible to calculate strain in patterned features even if they are small as $70\,\mu$m. By now, X-ray procedures are presently regularly employed to supervise strain in epitaxial films in the state-of-the-art semiconductor assembly features. The utilization of XRD in the pharmacological investigation is significantly increasing due to its full application[53]. XRD functions on the principle of Bragg's equation,

$$n\lambda = 2d\sin\theta \qquad (4.4)$$

which can be explained concerning the reflection of collimated X-ray beam incidence on a crystal plane of the sample that is going to be characterized[53,73]. The wide-angle elastic scattering is what the XRD bases on and is commonly employed for ordered material, and for disordered material is not preferred. All measurements are taken out in Angstroms (1Å 50.1 nm or 10210m). To verify the results acquired employing XRD, they could be contrasted with microscopy methods or other alike. Nevertheless, XRD can be time-consuming and may necessitate a considerable quantity of sample. Even though some restrictions, XRD is extensively used to establish the material structure at an atomic level[53].

Retaking Bragg's law, a one-color beam of X-rays is permitted to incident on a sample, and a detector identifies the reflected X-rays. The X-ray diffraction configuration is distinctive of the material under investi¬gation. X-ray diffraction procedure helps establish the percent crystallinity in the natural structures before and after chemical or physical treatment. Usually, according to Patel. et al, says that "X-ray diffractogram of the sample is recorded on an X-ray diffractometer working at known voltages and current applying a Cu Kα X-rays (λ = 0.15406 nm) over the 2θ range from 10 to 100 degrees in the steps of 0.01 degree at room temperature in open quartz sample holders." Amorphous regions of the samples produce a broad peak, whereas crystalline regions produce sharp peaks[73]. The degree of crystallinity (Xc) can be determined by determining the intensities of the crystalline (Ic) and amorphous (Ia) show in the sample of the following equation[73] :

$$X_c = \frac{I_c}{(Ia + Ic)} \times 100 \tag{4.5}$$

4.7 Brunauer-Emmett-Teller Surface Area (BET)

Brunauer-Emmett-Teller (BET) premise intends to explain the physical adsorption of gas molecules on a solid surface. It works as the basis for a critical analysis method for the measurement of the specific surface area of materials. BET hypothesis applies to systems of multilayer adsorption and typically utilizes probing gases that, chemically talking, do not react with material surfaces as adsorbates to quantify particular surface area. Nitrogen is considered the most commonly employed gaseous adsorbate used for surface investigating by BET methods. For this reason, standard BET analysis is frequently directed at the boiling temperature of N_2. Additional probing adsorbates are also employed, albeit with lower frequencies, allowing the measurement of surface area at distinct temperatures and measurement ranges. These involve water, carbon dioxide, and argon. Specific surface area is a scale-dependent property, without a particular correct value of particular surface area definable. Thus quantities of a specific surface area determined through BET theory may vary on the adsorbate molecule used and its adsorption cross-section[74].
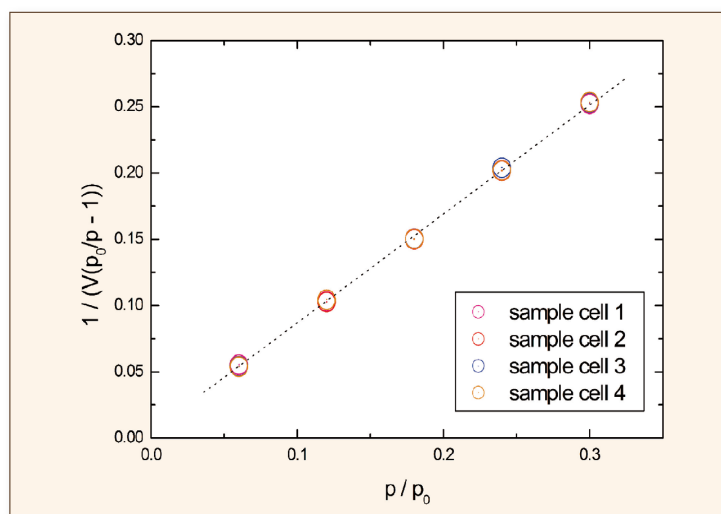
Figure 4.6: BET sample. BET plots of 5-point BET measurements of one material in all four measurement stations, took from magazine "Particle World. Technical papers of 3P instruments. Edition 20. September 2019" .[75]

In figure 4.6 it can be observed the good reproducibility on the based upon the BET line of 5-point BET measurements of one material in all four measuring positions (standard deviation ± 0.019 m^2/g). The complete analysis time varies on the number of samples, number of measuring spots and the total surface in the measuring cell (sample weight)[75].

Chapter 5

Experimental

5.1 Methology

5.1.1 Recollection

The diatoms studied in this work come from the valley of Guayllabamba, specifically in the Tanda and Puellaro locations, in the province of Pichincha, Ecuador. These diatoms, belong to the species Plantonic, which means that they have a centric morphology, these microalgae belong to the genus *Aulacoseira*. Centric diatoms have considerable variability in frustule structure and types of species. *Aulacoseira* genus includes a significant number of species and quite a few diverse forms as a product of either silica limitations or growth processes[17]. As in this specie exist a wide variation of sub-classification of *Aulacoseira*, this leads to having morphological differences, and these characteristics are attributed to factors like environment, geographic location, and others. These diatoms that have centric frustules, finding bilaterally symmetrical construction are rare. The structures that can be seen as frustules are concentric, radial, or irregular. They have no raphe or pseudoraphe. The surfaces valve can present circular, polygonal or elliptical, and not often boat-shaped irregular shapes[76]. *Aulacoseira* seems to be very adaptable when to different environments develop life. Large rivers, ponds, and lakes are some of their habitats. It is well distributed in time and space compared to all freshwater of the plantoniks[17]. It can be found in numerous lakes around the world[17,77].

For the preparation or the different samples, the diatoms were functionalized and "clean" with different treatments described as dealuminization with sulfuric acid, piranha treatment and ethanol washed, all of these are explained in the next section.

The different samples studied were: diatom dealuminized (D), diatom dialuminized doped with gold

nanoparticles by *In-situ* (DG); diatom dealuminized broken structure (DB), doped with gold nanoparticles by *In-situ* (DBG) and *Ex-situ* (DBE) methods, diatom washed in ethanol (E), and doped with gold nanoparticles by *In-situ* (EG), diatom treated with piranha (P), and doped with gold nanoparticles by *In-situ* (PG) methods.

5.1.2   Dealuminization

This procedure is able to add acid groups to the surface of the diatom. In this treatment, the diatoms were washed with sulfuric acid (H_2SO_4) for 16 hours to take off most of the aluminum (Al) present in the sample. For this process we have two types of samples broken structures and complete structures, described below:

Broken structure

For the first type, the protocol followed was the next one:

The first step was to prepare 100 mL of sulfuric acid (1M). Weight 1 g of the original sample of diatom. After, place the weighted gram of diatom with the solution previously prepared of sulfuric acid in a flask of 500 mL with a magnetic stir. Then, the samples were placed in a support system of sand, in order to keep a constant temperature, (figure 5.1). Initiate the stirring system and stabilize to a temperature of 60°C. Then the sample was left for 16 h with the stirring system by reflux. At the end of the time the temperature was checked. Thus, a vacuum wash with distilled water was carried out. A total of 400 mL of water were utilized to proceed with the washing. After that, check with NaOH (0.5 M) to see if in the sample there was still presence of Al. After checking there is no longer presence of aluminum, the sample was placed in the oven, the temperature ideally needed should be at approximately 60°C for 3 days. The material was ground, and then stored until use.

Figure 5.1: Support system.

Complete structure

For this type, the same procedure of "Broken structure" was followed, with the difference that the concentration of the solution of sulfuric acid was 2M. and the sample of original diatom used was 5 g, and consequently, 500 mL of solution was needed. To vacuum wash was needed 1.5 L of distilled water. And the last difference, this sample wasn't ground, so we will consider this diatom as the structure is intact or "complete".

5.1.3 Piranha treatment

The piranha treatment consists in placing the diatoms in a solution 3/1 of H_2SO_4/H_2O_2, in a total solution of 20 mL; this treatment functionalizes the surface of the diatom, adding OH groups. The protocol applied started with a solution of 15 mL of H_2SO_4 and 5 mL of H_2O_2. The original natural diatom was weighted 1 g. The diatom was placed in the concentrated solution of H_2SO_4 and H_2O_2 in a flask with a stirring bar. The system was placed in a support platform with sand. The stirring was on and place in controlled temperature at 80°C approximately for 30 min. Then, it was washed with approximately 300 mL of distilled water. After that it was placed in the oven for three days at 60°C.

5.1.4 Ethanol treatment

From the natural diatom, 1 g was weighted and mixed with 20 mL of ethanol. Next the sample was sonicated for 20 min. Then, the extraction of the clean diatom was carried out, leaving the dirtiness in the bottom. After that, the diatom was dried in the oven for 2 hours at 60°C.

5.1.5 Diatom coated with gold nanoparticles

Ex-situ and *In-situ* methods

For the diatoms decoration with gold nanoparticles, two protocols were applied, one the *In-situ* protocol, which consists in synthesize *in situ* the nanoparticles over the diatomite frustule. This protocol was applied to the four different types of diatoms that we have treated (complete, broken, dealuminized and clean). The second protocol is the *Ex-situ* method, consists in attaching to the diatom surface the nanoparticles already synthesized in a solution of Au/CTAB. This protocol was applied only to the dealuminated ground sample. Giving us a total of five samples (diatom dealuminazed doped with gold nanoparticles, diatom dealuminazed with broken structure doped with gold nanoparticles, diatom dealuminazed with broken structure doped with Au/CTAB, diatom washed with ethanol doped with gold nanoparticles and diatoms treated with piranha doped with gold nanoparticles). The two protocols are described in detail below:

In-situ **protocol:**

Synthesis of gold nanoparticles on the diatoms

This is the procedure applied to the four type of treated diatoms (diatom dealuminazed, diatom dealuminazed with broken structure, diatom washed with ethanol and diatoms treated with piranha). To decorate the diatoms with gold nanoparticles a solution of 0.5 g of sodium citrate in 50 mL of distilled water was prepared and a solution of 0.085 g of $NaBH_4$ in 50 mL of distilled water. 0.5 g of Diatoms were mixed in 25 mL of distilled water with 1.2 mL of the sodium citrate. Then 0.2 mL of $HAuCl_4$ (0.1 g/100 mL) was added at 60°C under continuous stirring. After that 0.58 mL of the solution of $NaBH_4$ should be added drop by drop. The size of the nanoparticles depends on this step. A change of color can be observed (figure 5.2 (b)). The solution continues stirring at 60°C for about 2 hours and 30 minutes.

In table 5.1 we can observe the quantities used for every type of diatoms sample decorated with gold nanoparticles by the *In-situ* method.

CHAPTER 5. EXPERIMENTAL

Quantities employed in the In-situ method		
Type of diatom sample	Quantity of diatom (g)	$HAuCl_4$ (mL)
Dealuminized complete	0.3	0.16
Dealuminized broken	0.36	0.20
Ethanol	0.2	0.11
Piranha	0.25	0.13

Table 5.1: Diatoms quantities used in the *In-situ* procedure
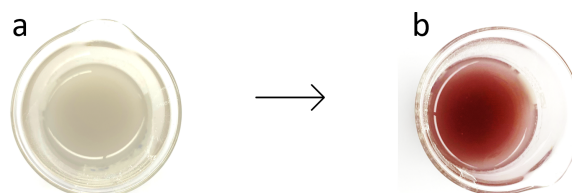
Figure 5.2: In-situ protocol. a)Solution of diatoms with sodium citrate and $HAuCl_4$, b)Solution after $NaBH_4$ is added drop by drop.

Ex-situ **protocol:**

Synthesis of Au/CTAB nanoparticles

In a typical synthesis, 0.83 g (2.2 mmol) of chloroauric acid ($HAuCl_4$) 3.1 g (1.2 mmol) of 1,2-hexadecanediol, 0.5 mL (1.5 mmol) of oleic acid, 3 mL (6 mmol) of oleylamine were added into 30 mL of phenyl ether. Under argon atmosphere and vigorous stirring, the reaction solution was heated to 180°C and was kept at this temperature for 1.5 hours. After cooling to room temperature, ethanol was added into the solution. A dark-purple material was precipitated and separated by centrifugation. The precipitated product was washed with ethanol, and redispersed in a solution of CTAB with a concentration of 0.1 g/100 mL. For the incorporation of the Au/CTAB NPs on the diatom, 0.36 g of diatom dealuminized and ground was weighted. Placed the amount of diatom in 20 mL of distilled water at 60°C. 0.20 mL of Au/CTAB were added (figure 5.3). Then they were left for approximately two hours and thirty minutes at 60°C under stirring.
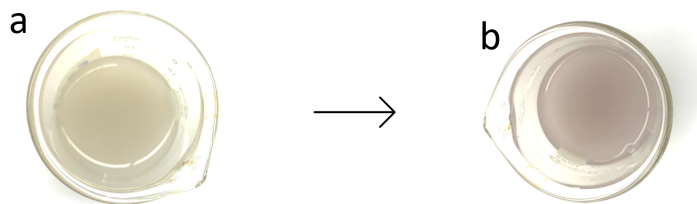
Figure 5.3: *Ex-situ* protocol. a) Solution of diatoms in distilled water, b)Solution of diatoms after adding Au/CTAB. A faint change of color can be seen in figure (b) due to the gold nanoparticles.

Codes

In table 5.2 the codification for each of the nine different samples is given. With these codes will be refered to in the following sections.

Diatoms codification			
Treatment	Simple	*In situ* gold decorated	*Ex-situ* gold decorated
Dealuminized complete	D	DG	-
Dealuminized broken	DB	DBG	DBE
Ethanol	E	EG	-
Piranha	P	PG	-

Table 5.2: Diatoms sample codes

5.1.6   Simulated Body Fluid (SBF)

For the preparation of the Simulated Body Fluid (SBF) the protocol proposed by Kokubo *et al.* was followed; whose steps are detailed below: All the containers and utensils that were used in the preparation of the SBF are washed, very well with a neutral detergent and then with a dilute HCl solution (they are immersed in this solution for a couple of hours) and then they are thoroughly rinsed with distilled water (several times) and dried in a stove at 50°C. Then they were wrapped in aluminum foil until they are going to be used. The materials that must be included to prepare 1000 mL of solution are the following: A 2000 mL beaker, a magnetic stirrer, six beakers, a funnel, a disposable pipette to adjust the pH (to be used with 1N HCl), a bottle 1000 mL plastic (polyethylene or polypropylene), a 1000 mL volumetric ball, six plastic spoons, gloves and a mouth cap. For the preparation of the solution it should be used only distilled and

deionized water (of high purity). The water was boiled before use, cooled to room temperature and store in a closed container. The solution was prepared at 37°C. Using a heating plate (or thermal bath) with a Teflon-coated magnetic stirrer. The solution was prepared in a dust-free environment, as clean as possible. Approximately 700 or 750 mL of water is added to the 2000 mL beaker (made of new polyethylene or polypropylene) and stirred by means of a magnetic stirrer at 37°C. Then the reagents are added following the order shown in table 5.3 and waiting for each reagent to be completely dissolved before adding the next one, shake vigorously for approximately 3 min each after adding each reagent one by one, (3 min stirring after each one). Reagents with their respective amounts for the preparation of 1 L of SBF solution mentioned in the table 5.3.

SBF reagents		
Reagant	C-SBF(g)	Purity
NaCl	7.996	99.5
$NaHCO_3$	0.352	99.5
KCl	0.225	99.5
$K_2HPO_4.3H_2O$	0.23	99.5
1.M-HCl	40 mL	98.0
$MgCl_2.6H_2O$	0.311	99.9
$CaCl_2.2H_2O$	0.293	95.0
Na_2SO_4	0.072	99.0
$C_4H_{11}O_3N$(tris)	6.063	99.9
1.M-HCl	0.2 mL	-

Table 5.3: SBF reagents, showing their corresponding quantities needed for the solution and the purity.

The TRIS was added in little quantities at a time (less than 1 g at a time), to avoid sudden increase in pH. When TRIS is added the solution becomes cloudy, keep stirring until clear, if not discard. After adding the TRIS the pH was checked, and the temperature was at $36 - 37°C$. The pH of the solution was adjusted to 7.4 by adding 30 mL 1M HCl previously prepared. Using a pH meter, it was added very slowly using a 5 mL to 5 mL pipette (5 + 5 + 5 + 5 + 5 + 5 mL = 30mL). The pH was 7.4. The solution is kept under continuous stirring, and carefully with the last addition of HCl (drop exhausts) the pH is controlled to 7.4, the solution must be clear. The solution was cooled down to room temperature and transferred to a 1000 mL volumetric balloon and the total volume was adjusted by adding distilled water. The solution was kept at 4°C in a plastic container.

5.2   Equipment

5.2.1   UV-vis

Figure 5.4: UV-vis spectrometer JENWAY Genova Nano.

The UV-vis spectra was taken with an Ultraviolet-Visible spectrometer JENWAY Genova Nano, this apparatus belong to Yachay Tech University, to the School of Physical Sciences and Nanotechnology, the principle of this equipment worked only measuring a drop of the sample, been calibrated before with a drop of the "zero" solution. in figure 5.4 it can be observed a picture of the equipment used.

5.2.2   Scanning Electron Microscopy

The Scanning Electron Microscopes used for these work were two, one belonging to ESPE University, the TESCAN MIRA 3 Schottky field scanning electron microscope, working with an acceleration voltage of 10 KV attached with an energy dispersive X-ray microanalysis (EDS Bruker Quantax), and the second one was the PHENOM PRO X, with software prosuite detector fast SDD from AMPTEK located at the School of Earth Sciences, Energy and Environment, of Yachay Tech University. For the sample measure it was

need a minimum quantity placed in a carbon support in powder form.

5.2.3 EDX

For the measurement of EDX, the equipment used were EDS Bruker Quantax from ESPE University, and from Yachay Tech University FAST SDD from AMPTEK with the Phenom Prosuite software.

5.2.4 RAMAN
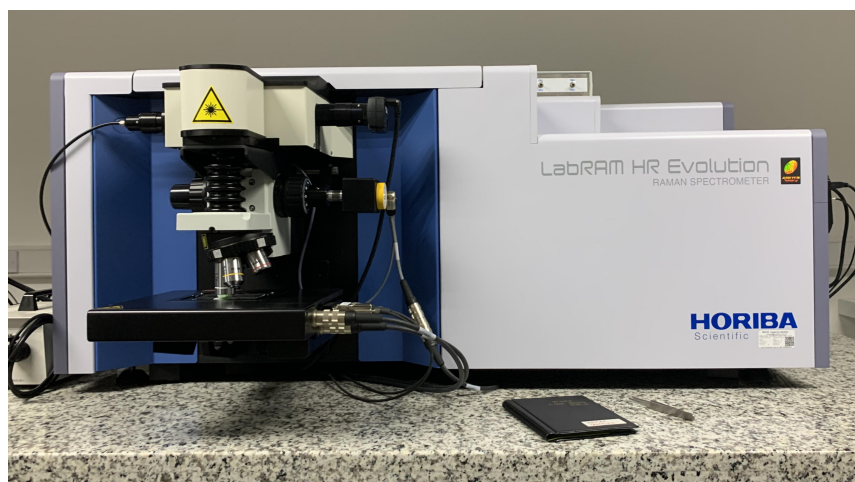
Figure 5.5: Raman spectrometer, HORIBA LabRAM HR Evolution.

The Raman spectra was taken with a Raman spectrometer HORIBA LabRAM HR Evolution, this equipment belongs to Yachay Tech University, to the School of Physical Sciences and Nanotechnology, in figure 5.21 can be appreciated a photo of the actual apparatus.

5.2.5 FLUORESCENCE

The Fluorescence microscope utilized in the present work was the Olympus BX63optical microscope with a fluorescence device, belonged to the School of Earth Sciences, Energy and Environment of Yachay Tech University.

5.2.6   XRD

Figure 5.6: X-Ray Diffractometer, Rigaku MiniFlex.

The powder diffractometer used in this characterization was a Mini-flex-600, from Rigaku, with a D/tex Ultra 2 detector. The measurement conditions were 40 kV and 15 mA for the X-ray generator in a sealed tube CuK (α) radiation source. This equipment belongs to the Yachay Tech University, for this characterization the sample was ground and then placed in a little plate, the amount of sample needed for this procedure is considerable, because it needs to cover the hole plate surface, which is approximately $(1.5\text{cm})^2$ and 1 mm of depth. figure 5.6 shows a picture of the actual XRD used.

5.2.7 BET

The equipment applied to analyze the Brunauer–Emmett–Teller technique was an ASAP from Micromeritis that belongs to Instituto Venezolano de Investigaciones Cientificas, Center of Materials Engineering and Nanotechnology. To proceed with this analysis, a minimum quantity of sample was needed in the original form of powder.

5.3 Results & Discussion

5.3.1 BET Surface Area

The Brunauer-Emmett-Teller method was performed in two samples, natural and dealuminated diatoms. BET surface area analysis was performed to be aware of the physical characteristics of the samples natural diatom, and dealuminated diatom, the results are shown in table 5.4. For natural diatom, the surface area and pore volume was 59.52 m^2/g and 0.24 cm^3/g respectively. After the surface modification, for the dealuminated diatom, the surface area increased, almost double the value and pore volume slightly decreased, the values were 102.30 m^2/g and 0.22 cm^3/g, respectively. The increase in the surface area on the diatom frustule is due to removal of impurities with piranha treatment[10]. A larger surface area is an advantage for drug adsorption and drug delivery, more surface area means more space where the drug could attach in the frustrule[10,78]. The obtained results are in accordance with those reported in the literature[78].

Natural Diatom
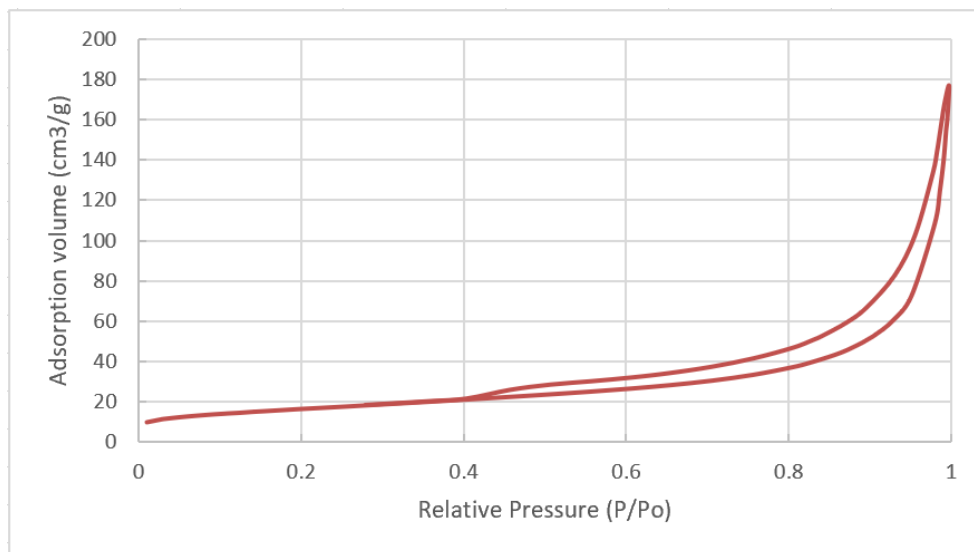
Figure 5.7: BET. Adsorption volume of natural diatom.
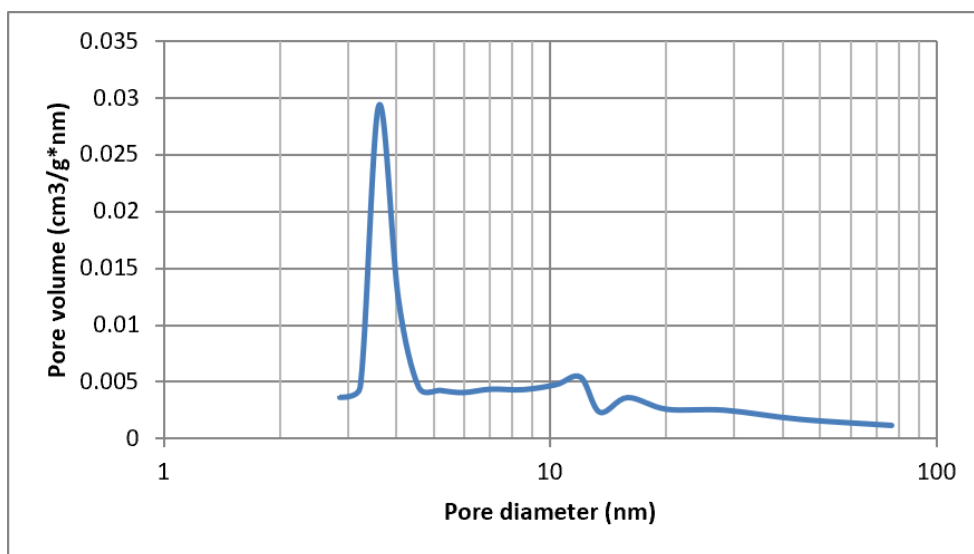
Figure 5.8: BET. Pore volume of natural diatom.

Dealuminated Diatom
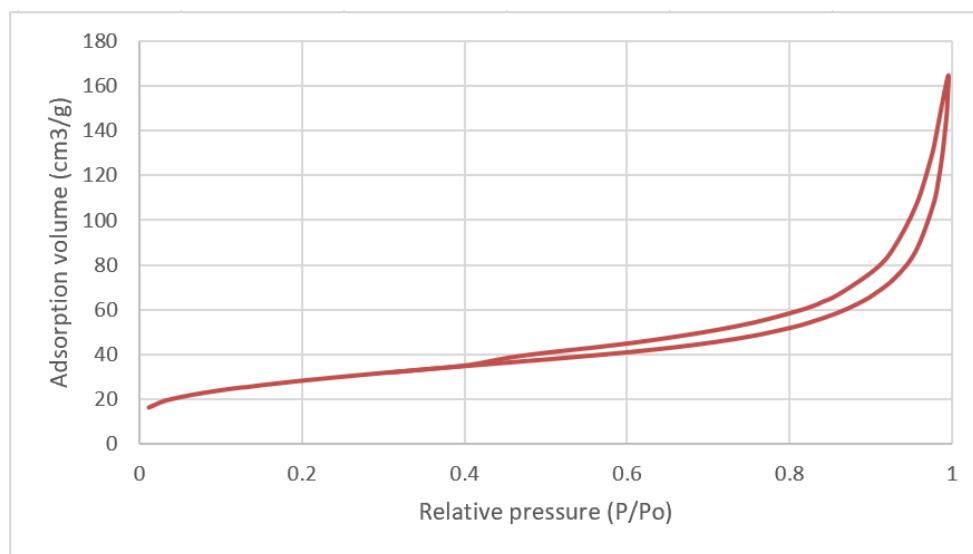
Figure 5.9: BET. Adsorption volume of dealuminated diatom.
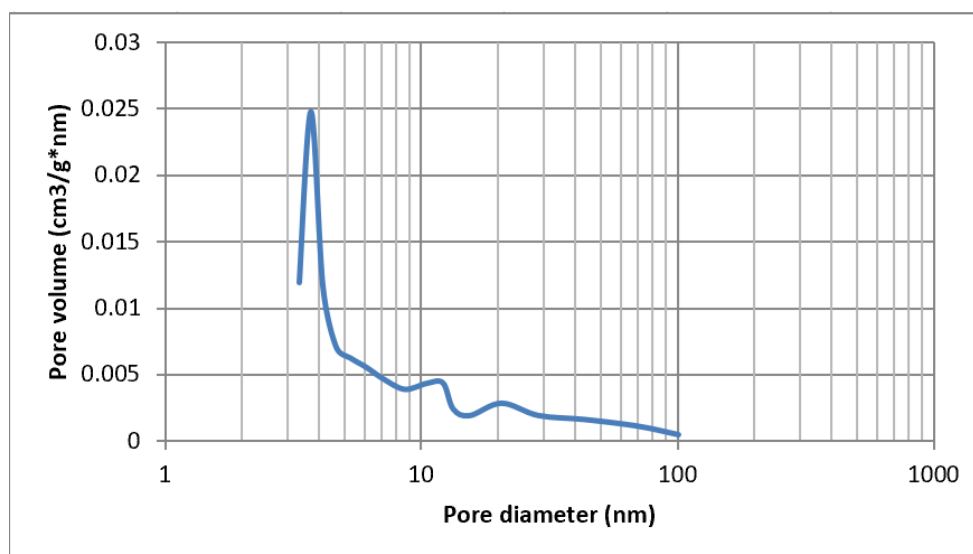
Figure 5.10: BET. Pore volume of dealuminated diatom.

Sample	Surface area ($m^{2/g}$)	Pore volume (cm^3/g)
Natural diatom	59.52	0.24
Dealuminated diatom	102.30	0.22

Table 5.4: BET data obtained from natural and dealuminated diatom.

5.4   Ultraviolet-Visible spectroscopy (UV-vis)

UV-vis spectra of diatoms doped with gold nanoparticles
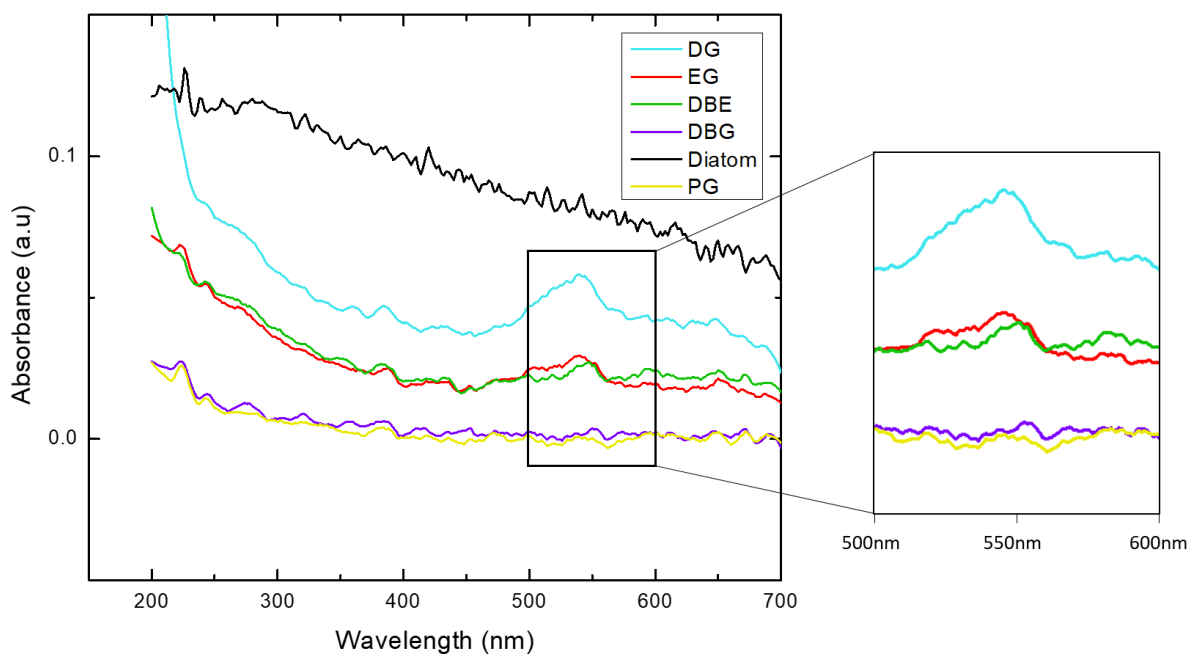
Figure 5.11: UV-vis Spectrums of diatoms doped with gold nanoparticles: EG (ethanol-gold) in red, DG (dealuminated-*In situ* gold decorated) in cyan, DBE (dealuminated broken-*Ex-situ* gold decorated) in green, DBG (dealuminated broken-gold) in purple, PG (piranha-gold) in yellow and the UV-vis spectra of the natural diatom in black..

As can be appreciated in figure 5.11 there are 6 UV-vis spectrums, these correspond to the samples that are doped with gold nanoparticles, DG (dealuminated-gold), DBG (dealuminated broken-gold), DBE

(dealuminated broke-Au/CTAB-*Ex situ* method), EG (ethanol-gold) AND PG (piranha-gold); and also there is the Uv-Vis spectrum of the natural diatom in color black to compare. In the spectrum of the doped diatoms with gold, a peak can be observed between 500 nm and 550 nm, that according to the literature is where the absorbance of gold should be with a particle size between 20 and 60 nm[31]. In the spectrum of the diatom, there is no existence of peak in the mentioned wavelength. So, this verifies that AuNPs are present in the samples decorated with the gold nanoparticles by *In situ* and *Ex-situ* methods.
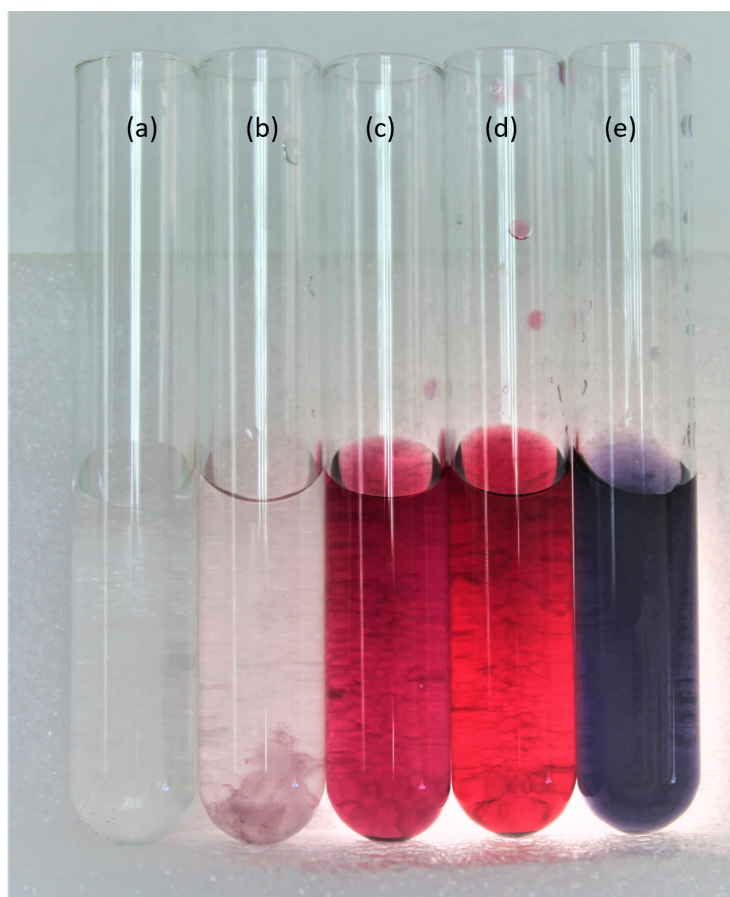
Figure 5.12: Diatoms doped with gold nanoparticles solutions. (a) sample DBE "dealuminated broken-Au/CTAB-*Ex situ*", (b) sample DBG "dealuminated broken-gold *In situ*", (c) sample DG "dealuminated-gold", (d) sample PG "piranha-gold", and (e) sample EG "ethanol-gold".

Figure 5.12 shows the solutions of each sample doped with gold nanoparticles. The variation in

color demonstrates that there is a different particle size in each of them. In Fig. 5.12 (a) the solution is practically colorless, this sample is the one prepared by the *Ex-situ* method, where the already synthesized gold nanoparticles, the Au/CTAB, were added. This solution despite it shows a light color, in its UV-vis spectra, characteristic gold signal at 550 nm. It has been reported that smaller nanospheres have peaks near 520 nm, while larger nanoparticles increased scattering and have peaks that broaden significantly and shift towards longer wavelengths. If the particles aggregate, the solution will appear blue/purple (sample e) EG "ethanol-gold), however unaggregated gold nanoparticles will have a red color in solution, as seen for samples (b) sample DBG "dealuminated broken-gold", (c) sample DG "dealuminated-gold", (d) sample PG "piranha-gold", this implies that the dealuminated and piranha treatment induce a good dispersion of the gold nanoparticles. On the other hand the a) sample DBE "dealuminated broken- Au/CTAB -Ex situ" , presents a greyish color , this is attributed to the presence of CTAB that changes the refractive index around the gold nanoparticles , additionally it can also change the shape of the Au NPs[79]. All of this contributes to the color of the these gold nanoparticles in solution, however , their presence is clearly seen in the UV.

5.5   X-ray diffraction (XRD)
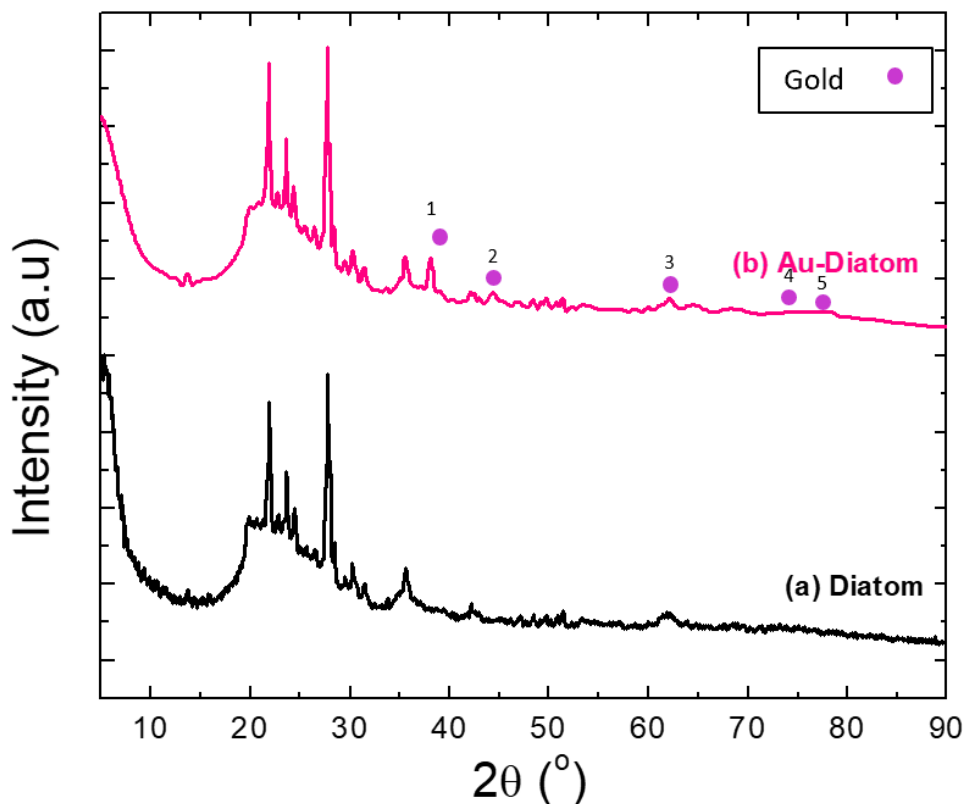
Figure 5.13: XRD patterns of a) Natural Diatom (D) without any treatment and b)Diatom doped with gold nanoparticles (DG).

The XRD patterns of the natural diatom in figure 5.13 shows some peaks corresponding mainly to quartz and cristobalite[80]. The amorphous part in the region20-30 degrees corresponds to diatoms. The structure of diatom, consequently, may be studied as a random network of tetrahedrally bound silicon atoms. This relates to a poorly ordered silica. Moreover in figure 5.13 there is also the patterns of diatoms doped with gold nanoparticles, in there 5 peaks can be observed that reveal the presence of gold on the diatom structure. In table 5.5 shows the crystallographic data for gold.

XRD pattern of gold				
No.	$2\theta,°$	d,Å	h k l	Norm. l.
1	38.09204	2.36050	1 1 1	100.00
2	44.27252	2.04425	2 0 0	48.42
3	64.40193	1.44551	2 2 0	29.92
4	77.34523	1.23273	3 1 1	34.11
5	81.48415	1.18025	2 2 2	9.85

Table 5.5: XRD data for gold

5.6   Scanning Electron Microscopy (SEM)

Scanning Electron Microscopy analysis was used to observed the morphological characteristics of the diatoms such as the diameter of the pores, the presence of gold nanoparticles, and their distribution on the diatoms surface. The determination of the AuNPs particle size was made using the ImageJ software.
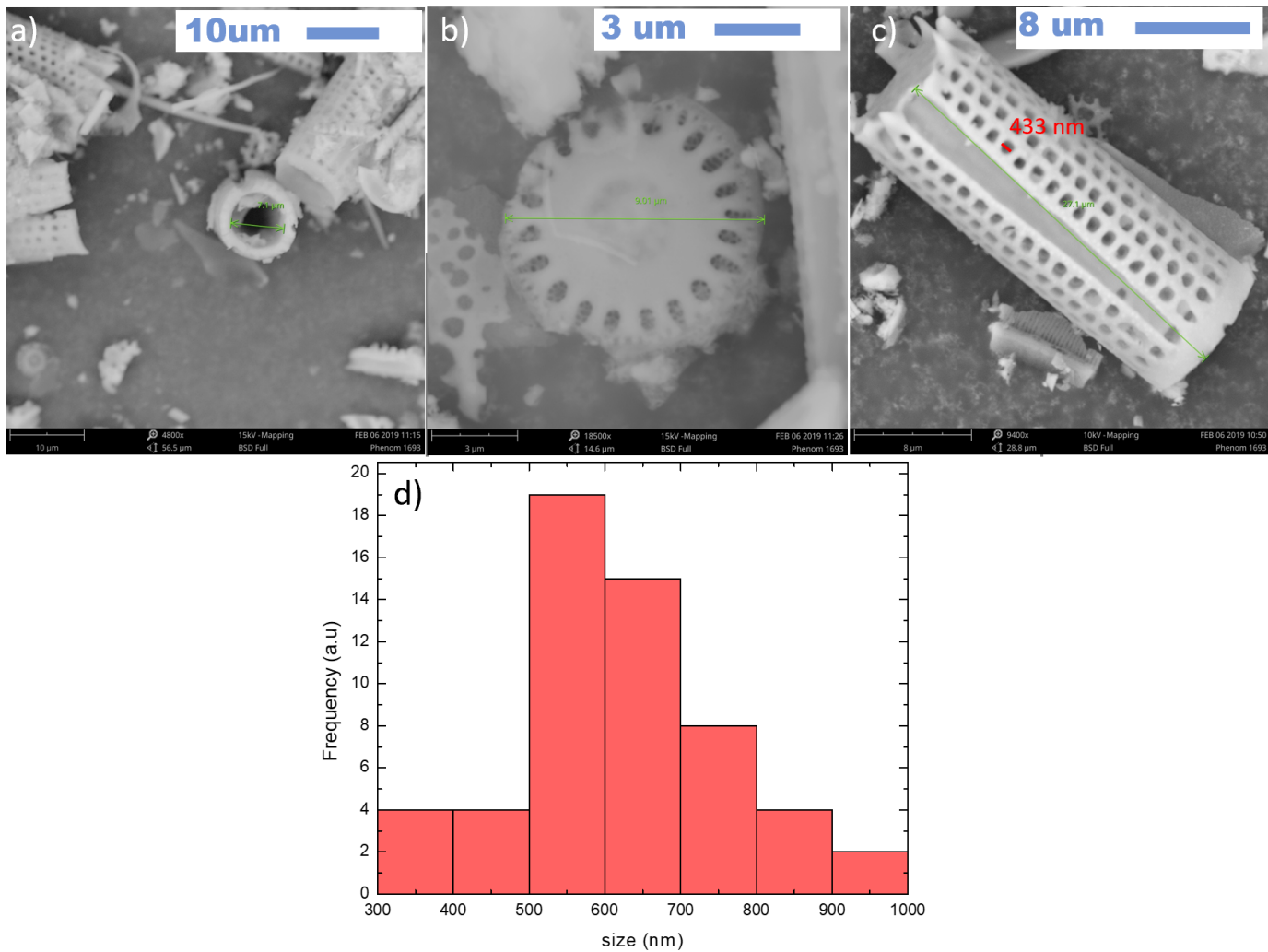
Figure 5.14: SEM micrographs of the complete Diatom (D) and pore size distribution.

Figure 5.14 show the micrographs of diatoms appreciated from different perspectives; a) a diatom from a side view where it can be seen its diameter of 7.1 μm; b) a diatom from a top view, with a diameter of 9.01 μm; and c) a cylindrical diatom of 27.1 μm of length. Here, it can be observed the pores and its structure. The size of pores were measured with ImageJ, with an average size of 500 nm. In the plot in

5.14 d) there is a histogram of pore size of (c). It can be seen that the majority of the 56 pores measured are in an average of 500 nm.
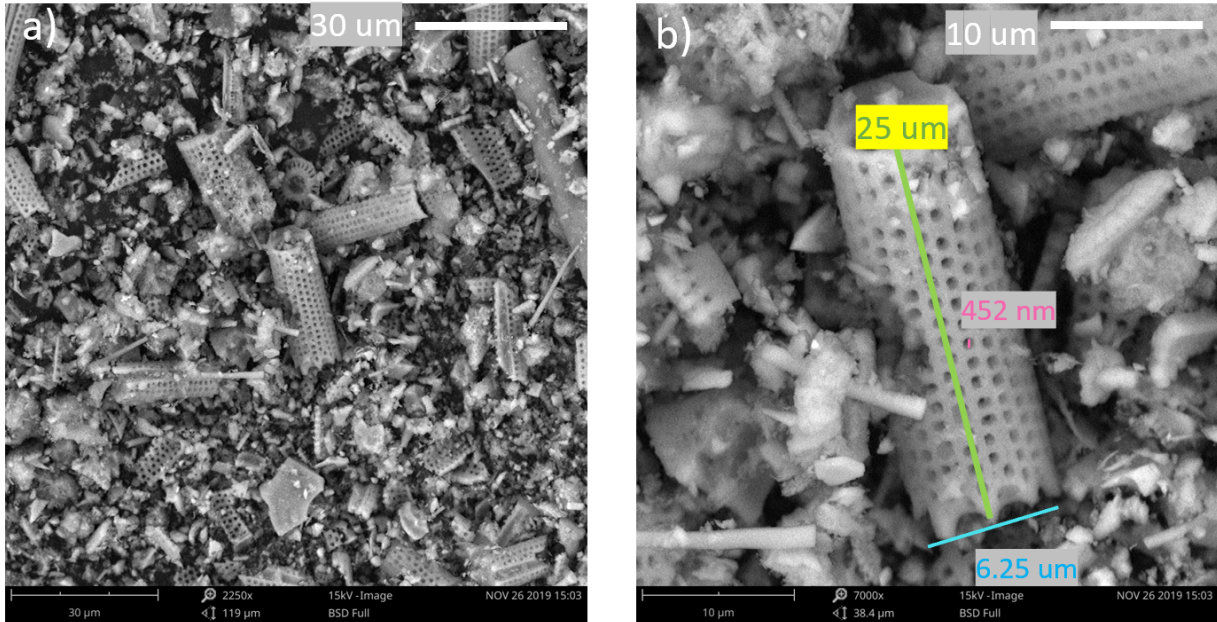
Figure 5.15: SEM micrographs of natural diatom a) general low magnification view and b) detail at high magnification of a diatom *Aulacoseira*

Figure 5.15 shows the micrographs of the natural diatoms (D). This diatom is referring to be natural because it does not have any treatment and has not been clean up. That is why it can be observed a variety of impurities, like clay or sponges. In Fig. 5.15 (b), it can be appreciated the length, diameter and pore size, which are 25 μm, 6.25μm, and 452 nm. According to the literature, these values correspond to *Aulacoseira* genus[17].
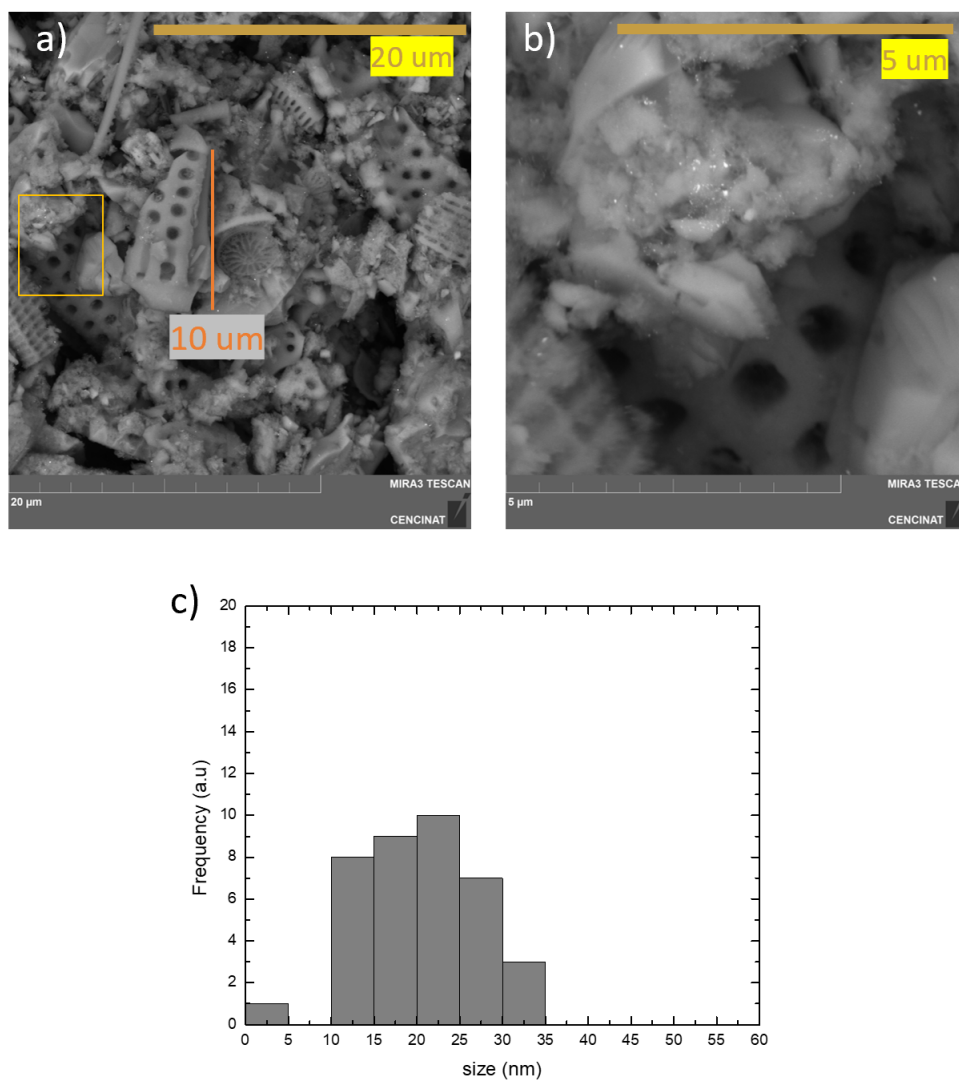
Figure 5.16: SEM micrographs of dealuminated diatom with broken structure, doped with gold nanoparticles (*Ex-situ* protocol) , a) large perspective and b) closer look of a), and pore distribution histogram.

Figure 5.16 a) shows a SEM micrograph of the broken diatom (sample DBE) doped with the AuNPs using the *Ex-situ* protocol. As can be appreciated, it presents a broken structure, which appears to be 10 μm long. AuNPs appear as white dots contrasting with the diatom. Yellow square inset is magnified is micrograph b), a closer look at 5μm of a). Both images revealed the AuNPs. In figure c) is presented

an histogram of the nanoparticles sizes presented in a). A total of 38 NPs were counted, showing a wide distribution of particle size between 10 and 35 nm. This indicates an average particle size of 25 nm, however some agglomerates can also be observed.
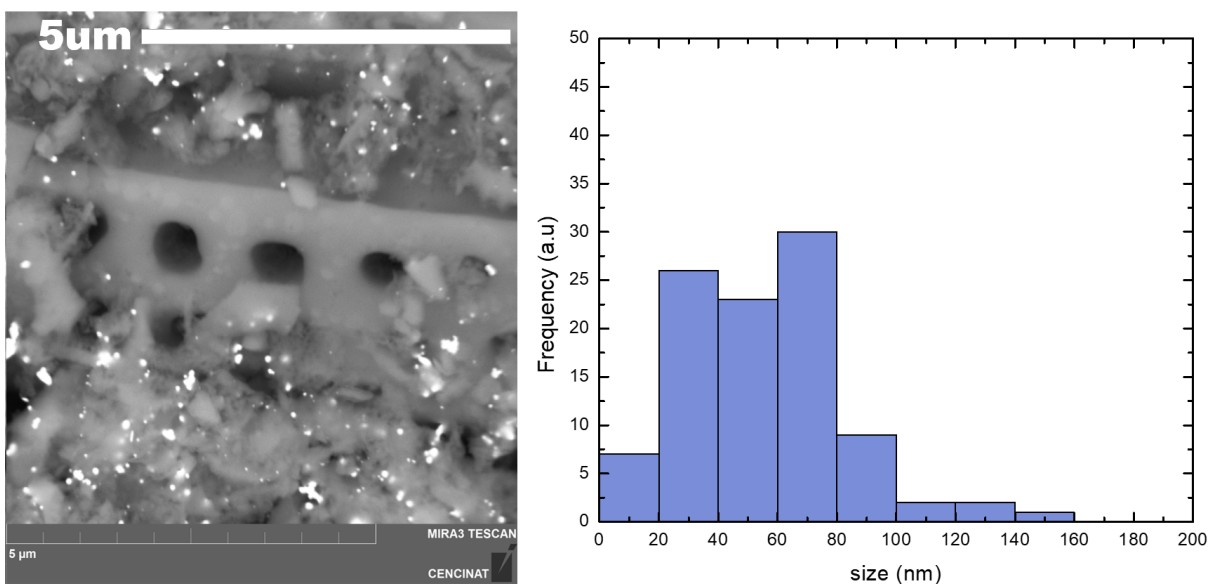
Figure 5.17: SEM micrographs of dealuminated diatom with broken structure doped with gold nanoparticles (DBG-*In-situ* protocol).

In figure 5.17 (left) can be observed the SEM micrograph of the sample DBG; it has a broken morphology due to the ground process and is doped with AuNPs with the *In-situ* protocol. To the right, a histogram of the nanoparticles showing a wide distribution (10-100)nm an average particle size of 60 nm. A total of 100 nanoparticles were measured.

Comparing figures 5.16 and 5.17, both have the same treatment for cleaning, and both of them were doped with gold nanoparticles, with the differences that figure 5.16 the nanoparticles were added following the *Ex situ* protocol. In figure 5.17, the nanoparticles were synthesized on the diatoms, following the *In-situ* method. In figure 5.16, the nanoparticles can be seen, in less amount than in figure 5.17, where it can be observed that there are a large amount of Au Nps on the diatom.
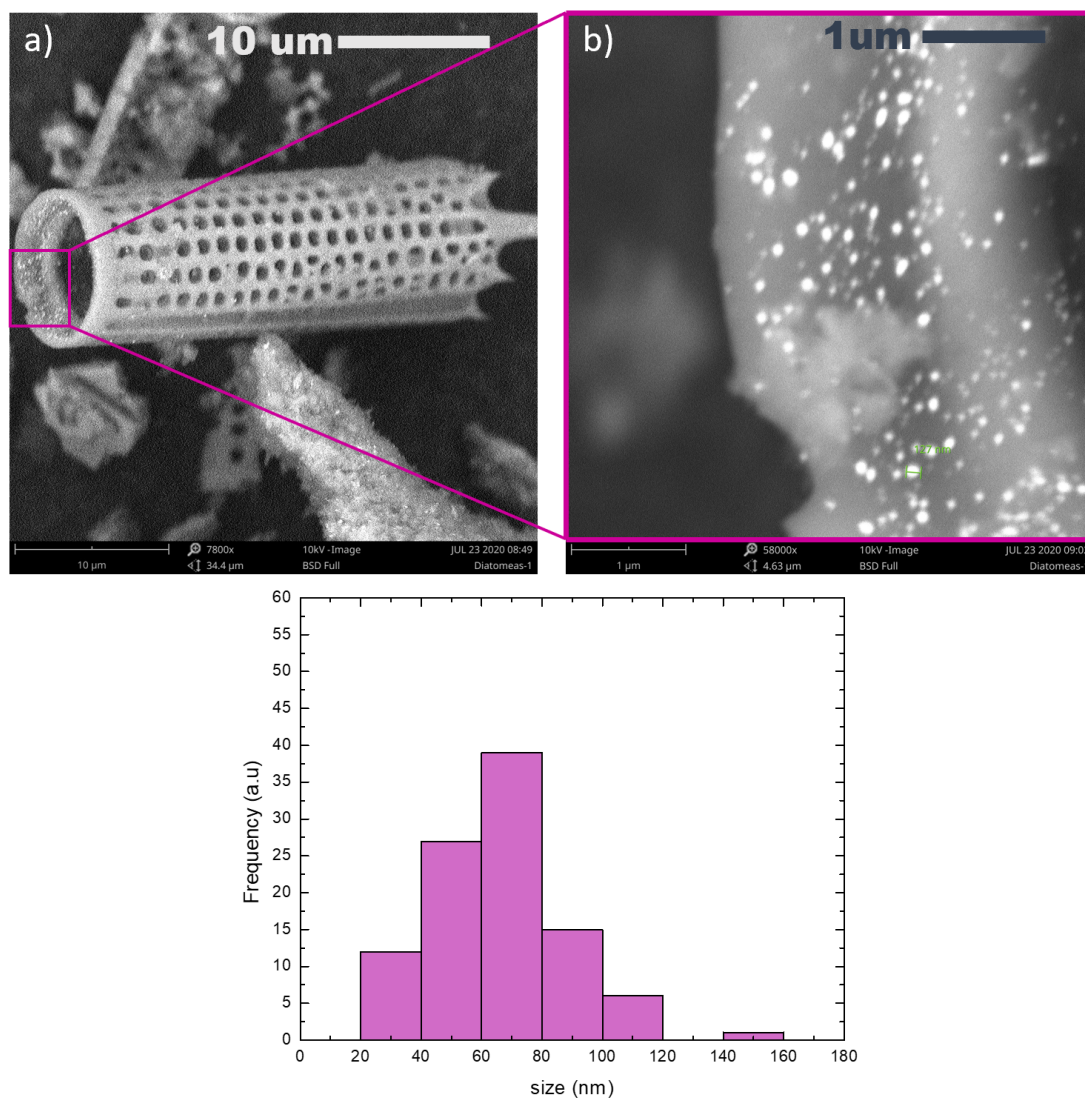
Figure 5.18: SEM micrographs of the diatom with complete structure doped with gold nanoparticles (DG); a) micrograph 10μm, b) magnified image of (a).

In figure 5.18 the sample (DG) of a diatom with its complete structure and doped with gold nanoparticles using the *In-situ* protocol; b) magnified image of (a), where the nanoparticles can be clearly observed. It can be observed that ther AuNps cover completely the diatom structure. In graph 5.18 c), a histogram of the sizes of the nanoparticles present in the diatom showing an average particle size of 60 nm, consistent

with the UV spectrum. A total of 100 nanoparticles were measured.

SEM micrographs showed the diatoms before nanoparticle decoration in full and broken morphology (without AuNps, Fig.5.14). In image 5.18, it can be seen the decoration of complete diatoms with AuNps prepared with the *In situ* treatment. In Fig. 5.16 it can be seen a lower AuNps doping in comparison with the latter mentioned image.

5.7   Energy Dispersive X-Ray Spectroscopy (EDX)

Energy Dispersive X-Ray Spectroscopy was used to determine the elements present in diatoms, specifically, a broken structure sample and a complete structure sample.
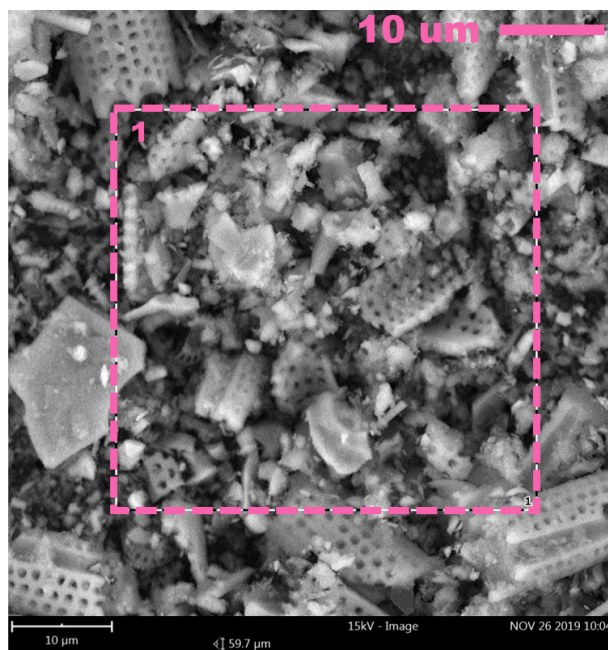
Figure 5.19: Area of the micrograph from were the EDX analysis was performed.

Area 1, Dealuminated diatom with broken structure				
Element number	Element symbol	Element name	Atomic concentration	Error
14	Si	Silicon	24.8	0.2
8	O	Oxygen	71.2	0.3
13	Al	Aluminum	3.5	0.2
20	Ca	Calcium	0.5	0.9

Table 5.6: EDX analysis, showing the elements present in the area selected in Fig.5.19

Figure 5.19 correspond to the micrograph of the diatom ground, in its center, the area marked by a pink square was analyzed by EDS, and the elements present in this area of the sample are specified in table 5.6. In the mentioned table, it can be appreciated what elements are present in the area, in what proportion. Also, there are stipulated an error that may be in the data quantification.

In the area analyzed were found silicon (24.8%), this is an expected element to be found because is the principal material of what a skeleton of a diatom is conformed[81]. The presence of Aluminium, Oxygen, and Calcium are in low quantities and this may be because of leftovers of the process of purification of the diatom frustrule. The cleaning process tries to eliminate all the impurities presents. This impurities may vary depending on their local environment, and this could include clay, terrigenous particles, volcanic glass, organic matter, with the composition of inorganic oxides such as Al_2O_3, Fe_2O_3, $CaCO_3$, MgO, CaO, P_2O_5, K_2O, and Na_2O[8,82].

The next sample to be discussed corresponds to the diatom with its structure complete doped with gold nanoparticles by the *In situ* method (figure 5.20). There are marked 5 sections in total, in those sections are where the EDX analysis was performed, 4 of them correspond to spots, and 1 to a general area.
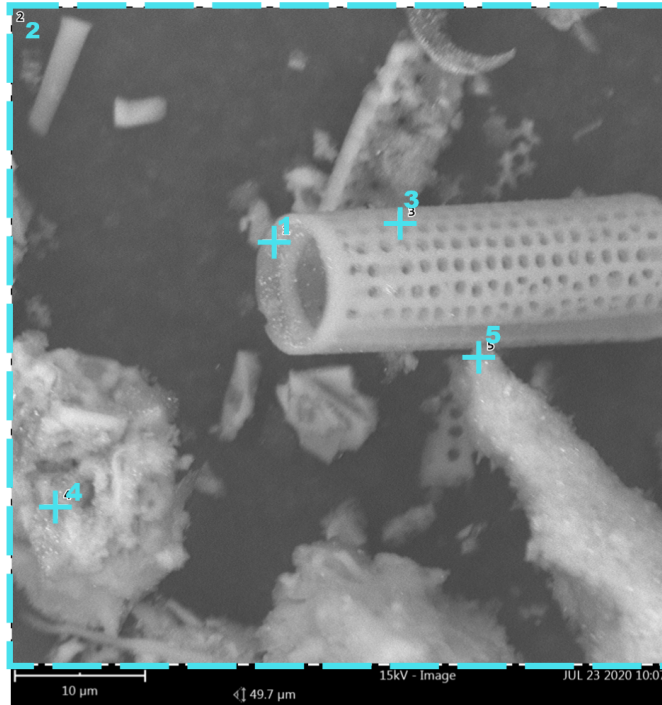
Figure 5.20: Area and spots of the micrograph where EDX analysis was carried out in the sample.

The first section to be analyzed is the one marked as "1" in the Fig. 5.20 with a cross mark color cyan, this corresponds to a spot. Is localized in the diatom in a zone what will be called the aperture. Subsequently, in table 5.7 can be found a summary of the elements found with the EDX of spot "1". In the mentioned table will be specified the chemical element, the atomic concentration, its weight, the oxide symbol and the stoichiometry concentration.

Spot: "1"				
Element symbol	Atomic conc.	Weight conc.	Oxide symbol	Stoich conc.
O	48.57	51.67		
C	44.62	35.63	C	86.76
Si	6.47	12.09	Si	12.59

Table 5.7: Content of EDX analysis, present elements in the spot "1", selected in Fig.5.20

In the spot analyzed, "1", were found silicon, this is expected element to be found, because is the

principal material of what a skeleton of a diatom is conformed is silica (SiO_2)[81]. There is presence of Oxygen as part of the silica structure and Carbon fromthe graphite sample holder.

The second section to be analyzed is the one marked as "2" in the Fig. 5.20 with a cross mark color cyan, this corresponds to the whole area in the image. It encompasses all the space that is inside the square in color cyan. In table 5.7 can be found a summary of the elements found with the EDX of the entire area "2".

Area: "2"				
Element symbol	Atomic conc.	Weight conc.	Oxide symbol	Stoich conc.
C	59.50	49.52	C	92.68
O	35.80	39.69		
Si	4.24	8.25	Si	6.61

Table 5.8: Content of EDX analysis, present elements in the area "2", selected in Fig.5.20

In the area analyzed, "2", were found the same elements as in spot "1", but in different concentration[81]. To emphasize, in Fig. 5.20 can be distinguished just one complete diatom.

The third section to be analyzed is the one marked as "3" in the Fig. 5.20 with a cross mark color cyan, this corresponds to a spot. This spot is localized in the skeleton of the diatom, where the pores are located. In table 5.9 can be found a summary of the elements found with the EDX of the analyzed spot "3".

Spot: "3"				
Element symbol	Atomic conc.	Weight conc.	Oxide symbol	Stoich conc.
C	50.85	39.83	C	81.85
O	37.88	39.52		
Si	11.28	20.65	Si	18.15

Table 5.9: Content of EDX analysis, present elements in the spot "3", selected in Fig.5.20

In the spot analyzed, "3", were found the same elements as spot "1", silicon, oxygen and carbon as before.

The fourth section to be analyzed is the one marked as "4" in the Fig. 5.20 with a cross mark in color cyan, this corresponds to a spot. This spot is localized in an amorphous surface what it looks like an impurity. In table 5.10 can be found a summary of the elements found with the EDX of the analyzed spot "4". In the mentioned table will be specified the chemical element, the atomic concentration, its weight,

the oxide symbol and the stoichiometry concentration. This new element present come from impurities leftovers of the process of purification of the diatom frustrule. The cleaning process tries to eliminate all the impurities present however some remain, like clay, terrigenous particles, etc[8,82].

Spot: "4"				
Element symbol	Atomic conc.	Weight conc.	Oxide symbol	Stoich conc.
O	42.53	41.05		
C	31.97	23.17	C	55.64
Si	12.78	21.64	Si	22.23
N	9.78	8.26	N	17.01
Al	2.32	3.78	Al	4.04
Fe	0.63	2.10	Fe	1.08

Table 5.10: Content of EDX analysis, present elements in the spot "4", selected in Fig.5.20

The fifth and last section to be analyzed is the one marked as "5" in the Fig. 5.20 with a cross mark in color cyan, this corresponds to a spot. This spot is localized in a surface not-well defined, it resemble to be a diatom but also to a impurity. In table 5.11 can be found a summary of the elements found.

Spot: "5"				
Element symbol	Atomic conc.	Weight conc.	Oxide symbol	Stoich conc.
C	44.41	35.98	C	69.52
O	36.11	38.97		
N	13.88	13.11	N	21.73
Si	5.21	9.88	Si	8.16

Table 5.11: Content of EDX analysis, present elements in the spot "5", selected in Fig.5.20

Worth to mention once again, that this impurities may be leftovers in the medium of the general sample during the process of purification of the big sample.

From these analyses it can be observed that gold could not be detected, this can be due to the small particle size and the small amount of gold on the diatoms, therefore not enough signal gets to the EDS detector.

5.8 Raman

By using Raman Spectroscopy in Fig.5.21 it is shown how fluorescence is visible in the range from 0-3000[cm^{-1}] of the light spectra. What this mean is that our object of study (Diatoms) possess intrinsic fluorescence characteristics.
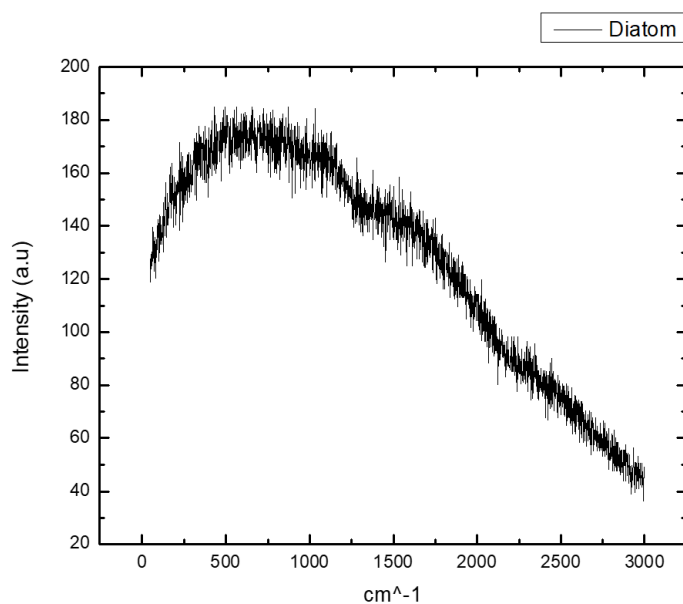
Figure 5.21: Raman shift of a natural diatom.

Raman shift of Diatoms doped with gold nanoparticles (AuNps) is shown below in Fig.5.22, in this kind of spectroscopy, AuNps are located between 450-500[cm^{-1}][83]. In Fig.5.22 (a) exhibits a whole spectra from 0-3000[cm^{-1}] in which AuNps peak is located nearly to 500[cm^{-1}] in x axis. A close up is made in Fig.5.22 (b) in order to observe the previously mentioned peak in even greater detail.
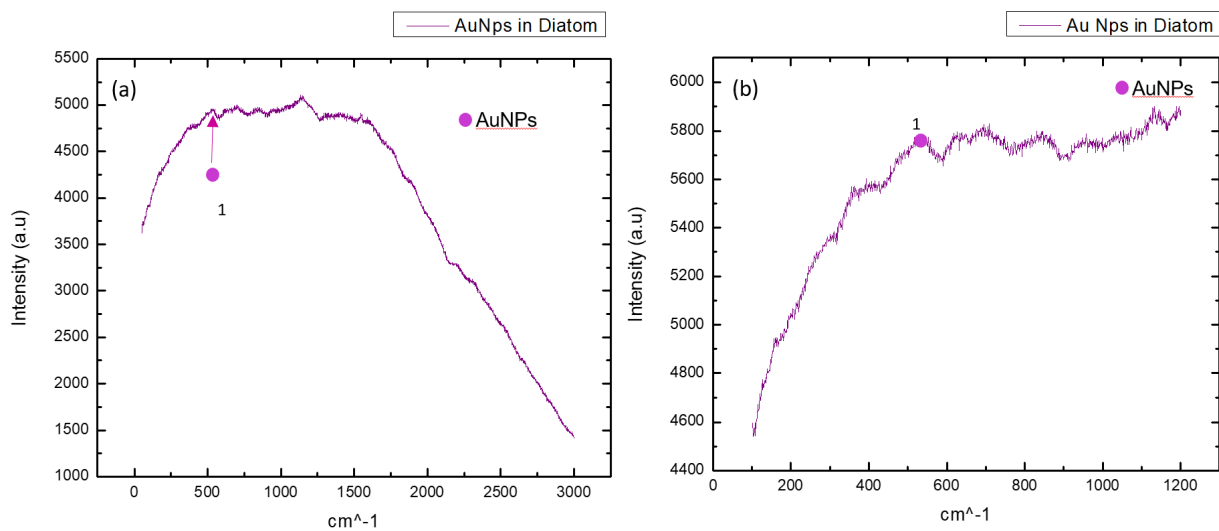
Figure 5.22: (a)Raman shift of a diatom doped with AuNPs in a general view, (b) close up from 200-1200[cm^{-1}]
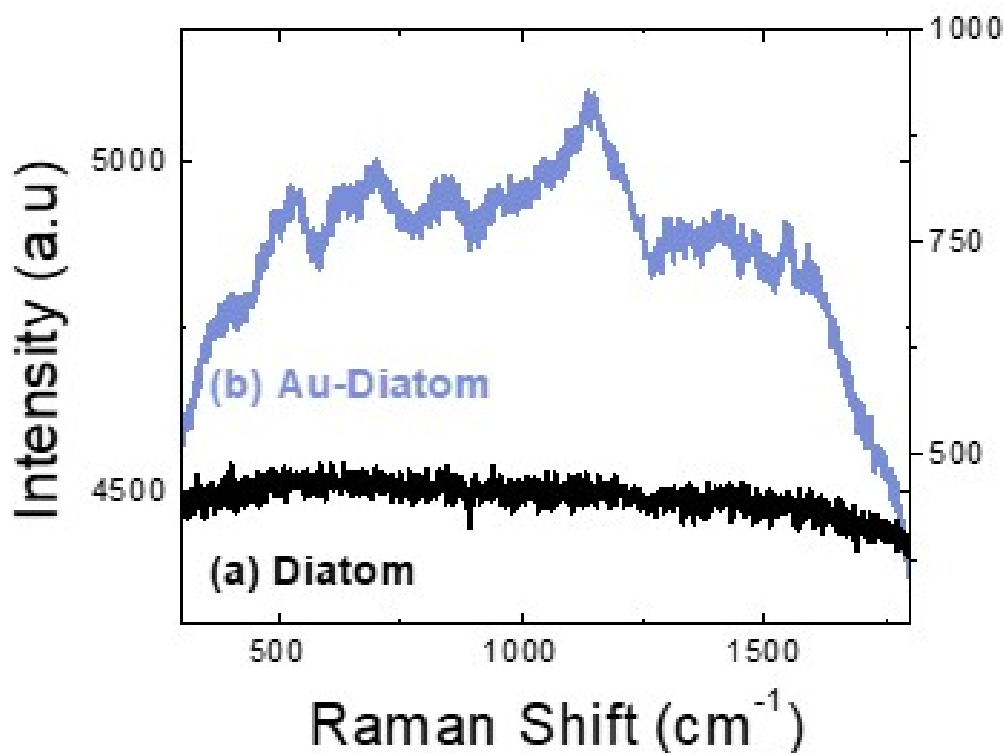
Figure 5.23: Raman of (a) Diatom and (b) Diatom doped with gold nanoparticles (Au-Diatom).

Figure 5.23 shows the Raman spectrum of the diatom (a) and the diatom doped with gold nanoparticles (b). Because of the fluorescence present from the diatom spectrum of 5.23 (a) it is very difficult to extract the structural information that Raman could give . However, despite all the noise present in the sample, it can be appreciated in the range of wavelength (500-1500) nm, the peaks belonging to gold nanoparticles, specially the characteristic peak around 1125 cm^{-1}; indicating the successful deposition of the AuNPs in the diatom surface[84].

5.9   Fluorescence microscopy

Fluorescence images of the diatoms doped with gold nanoparticles are shown in figure 5.24 and 5.25. Natural diatoms by themselves do not present any fluorescence, but as it could be confirmed with the

Raman shift in Fig. 5.23, the decoration with gold nanoparticles brings up the fluorescence output.
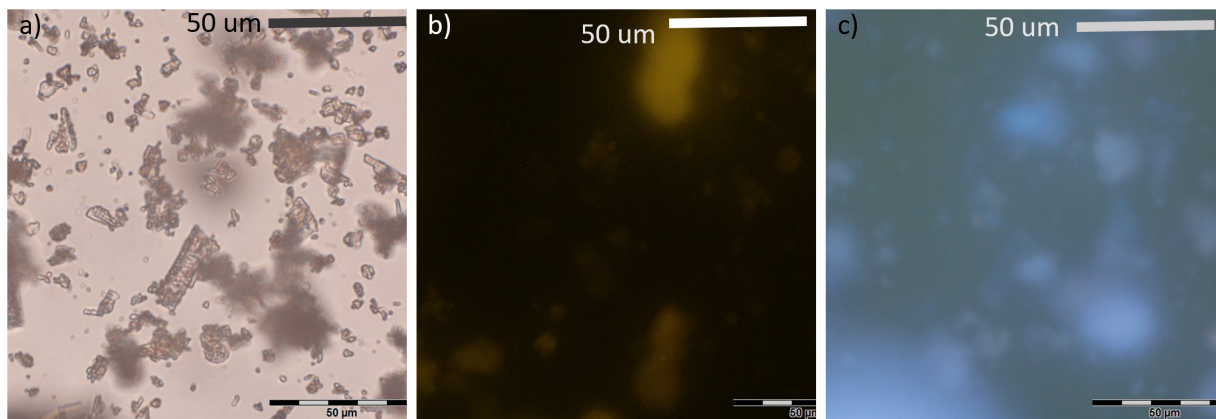
Figure 5.24: the decoration with gold nanoparticles brings up the fluorescence output. Image of fluorescence microscopy taken from a diatom sample doped with gold Nps (DG) loaded with Gentamicin a)optical microscopy image b) fluorescence image with green light of same diatoms samples, doped with gold Nps (DG) and loaded with Gentamicin and in c) fluorescence image of same sample taken with blue light.

Figure 5.24 is a fluorescence image of natural diatoms doped with gold nanoparticles (DG) and loaded with Gentamicin, (a) optical microscopy of natural the diatom decorated with gold nanoparticles (D), (b) the same image with the green incident light, and (c) the same sample with the blue incident radiation; indicating the fluorescence due to the presence of gold nanoparticles.

Figure 5.25 (b) shows the fluorescence image of diatoms sample doped with gold nanoparticles, without Gentamicin (a) optical microscopy, b) shows the fluorescence image of the sample with the green light applied, and c) shows the fluorescence image of the sample with the blue light applied confirming.
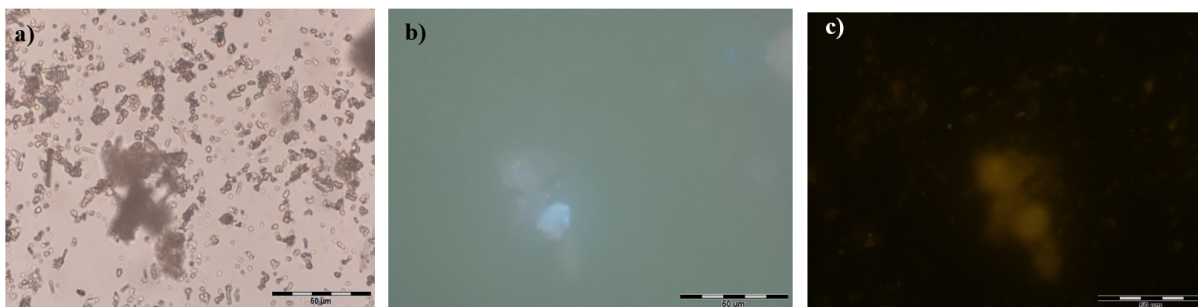
Figure 5.25: Image of the fluorescence microscope taken from a sample of diatoms doped with gold NPs(DG), without Gentamicin a) optical microscopy of diatoms with gold nanoparticles in b) fluorescence image with blue light c) fluorescence image with green light.

The fluorescence micrographs of the diatoms are displayed in figures 5.24 and 5.25. When we compare these figures, we notice that the fluorescence intensity increases with the loading of Gentamicin enhancing the fluorescence response. The incident light (green or blue) lead to excitation of the surface plasmon coherent electronic motion as well as the electrons. This behavior is consistent with the observed surface plasmon band in figure 5.11 corresponding to nanoparticles of 60 nm at (500-550) nm in the visible region, which may be attributed to the surface plasmon oscillation of free electrons[85], and is enhanced by the loading with Gentamicin. This is very useful in bioimaging to observed regions where the drug is delivered.

5.10   Drug Delivery

For the study of loading and release of Gentamicin in the diatom, the brand used was "Genbexil 160", belonging to the pharmaceutical *Life*. Its presentation is injectable solution in the concentration of 160 mg/mL, 2mL.

Figure 5.26: Genbexil 160 injectable solution.

5.10.1   Drug loading

UV-vis spectroscopy was used to study the drug loading and the drug release of Gentamicin in the different samples of diatoms, in figure 5.27 we can observe the calibration curve of Gentamicin. The importance of knowing how the calibration curve behaves lies in that in this way it is possible to obtain a broader vision about how much gentamicin has been released, and of course, how much has been loaded. Once the calibration curve is ready, it is easier to identify which of the samples have a better behavior.
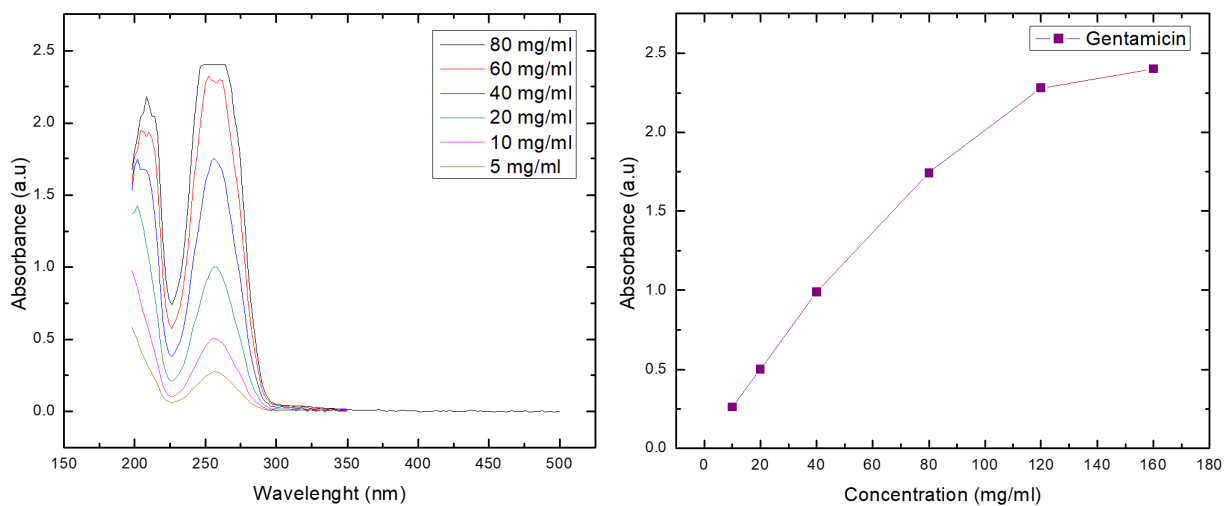
Figure 5.27: Calibration curve of Gentamicin. (a)spectra at different concentrations of gentamicin, (b) calibration curve made with spectra of (a), taken in wavelength 256 nm.

The UV-vis spectra measurement was divided into 2 stages. The first stage; The loading phase, this spectra was obtained after making a measure all day long for one day. The second stage; The release phase, the spectra of release was obtained after taking measurements for a period of nine days. Next The complete 9 samples above mentioned, will be detailed each one for separate.

The release stage will be detailed deeply in the following section in the so called Release of Gentamicin section at the end of the current chapter.

The gentamicin peak is located at 256[nm] in the UV spectrum[86], and this is why the wavelength was chosen as a reference for measuring the absorbance.

5.10.2   Sample dealuminized simple, complete structure, (D)

The first sample to be discussed will be dealuminized complete diatom, as mentioned in table 5.2, this sample will be referred as (D). This sample was treated with sulfuric acid and therefore functionalizing its structure with H groups.

Figure 5.28: UV-vis spectrum of sample "D", in (a) the spectrum of "absorbance vs wavelength", and in (b) the percentage of concentration vs the time.

In figure 5.28 (a) it can be observed the absorbance taken at different times in a period of 6 hours, a total of 15 spots were measured, in (b) the percentage of concentration of Gentamicin loaded is plotted, this adjustment was made with the calibration curve of "absorbance vs concentration of drug" in figure 5.27,

vs time. The wavelength chosen as the reference point to all the samples is 256 nm, because it showed the highest peak of Gentamicin and matched with the peaks in the literature for Gentamicin[86]. To measure the loading capability we took from the figure 5.28 (b) the maximum point that will be considered 0% of the drug loaded, and the minimum point, that in this case is located at the "time 120" is the maximum load of Gentamicin in the diatom, being this approximately 30% of the drug in solution. A subtraction of the minimum from the maximum will gave us the total drug loaded. In percentage, approximately a 70% was loaded, thanks to the calibration curve in figure 5.27, a simple procedure described in equation 5.1 tell that 10.4 mg/mL is the quantity loaded in the diatom "D".

$$concentration = \frac{72.22\% * 14.4 mg/mL}{100\%} = 10.4 mg/mL \tag{5.1}$$

Where 72.2% corresponds to the percentage loaded, 14.4 mg/mL corresponds to the maximum concentration loaded in the sample, and the 10.4 mg/mL corresponds to the concentration loaded. All the equivalence data can be observed in table 5.12.

Equivalence of percentage in concentration and absorbance of Gentamicin in sample "D"		
Absorbance	Percentage(%)	Concentration (mg/mL)
0.3611	100	14.444
0.2234	61.86652	8.936
0.1487	41.17973	5.948
0.139	38.49349	5.56
0.1205	33.37026	4.82
0.1133	31.37635	4.532
0.1145	31.70867	4.58
0.1117	30.93326	4.468
0.1084	30.01939	4.336
0.1035	28.66242	4.14
0.1027	28.44088	4.108
0.1081	29.93631	4.324
0.1104	30.57325	4.416
0.1157	31.9856	4.62
0.1205	33.37026	4.82

Table 5.12: Equivalence of percentage, absorbance and concentration of Gentamicin loaded in "D".

5.10.3 Sample dealuminized dopped with gold nanoparticles, complete structure, "DG"
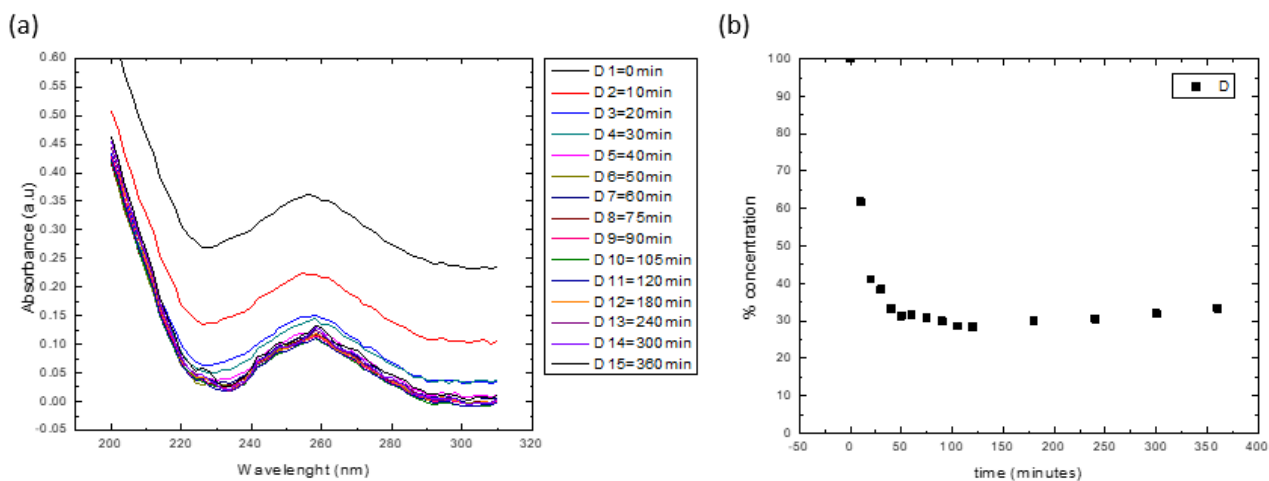

Figure 5.29: UV-vis spectrum of sample "DG",in (a) is found the spectra of "absorbance vs wavelength", and in (b) percentage of concentration vs the time.

The sample "DG" is dopped with gold nanoparticles, with the *In-situ* protocol.

To demonstrate the coating of the diatom with gold nanoparticles in figure 5.30 the change of color of the solution can be observed, where the diatoms are located. In the left one, the solution is right before adding the nanopartices, and in the image in the right, is after adding the nanoparticles, it can be seen a change of color, which that the nanoparticles are effectively there, this will later be confirmed with a measurement of UV-vis spectra of the solution.

In table 5.13 it can be appreciated the equivalence of values of the data DG. By observing in graph 5.29 (b), it can established that the maximun value, considered to be the 100% loaded in this sample, and based on the table 5.13, that the value in concentration is 10.816 mg/mL, and the minimum, following the same standards to obtain the maximun, will be 3.88 mg/mL, making a subtraction it will be obtained 6.936 mg/mL, this value equates to the 64.13%, and this value is the total loaded in the sample DG.

The reasons why this sample loaded less than the sample D may vary. On the other side it is a known fact that Gentamicin has a good linkage with AuNps[87].

Equivalence of percentage in concentration and absorbance of Gentamicin in sample "DG"		
Absorbance	Percentage(%)	Concentration (mg/mL)
0.2704	100	10.816
0.1463	54.10503	5.852
0.1241	45.89497	4.964
0.1127	41.67899	4.508
0.1102	40.75444	4.408
0.1164	43.04734	4.656
0.1092	40.38462	4.368
0.108	39.94083	4.32
0.1056	39.05325	4.224
0.0998	36.90828	3.992
0.097	35.87278	3.88
0.0994	36.76036	3.976
0.1035	38.27663	4.14
0.1302	48.15089	5.208
0.1061	39.23817	4.244

Table 5.13: Equivalence of percentage, absorbance and concentration of Gentamicin loaded in "DG".
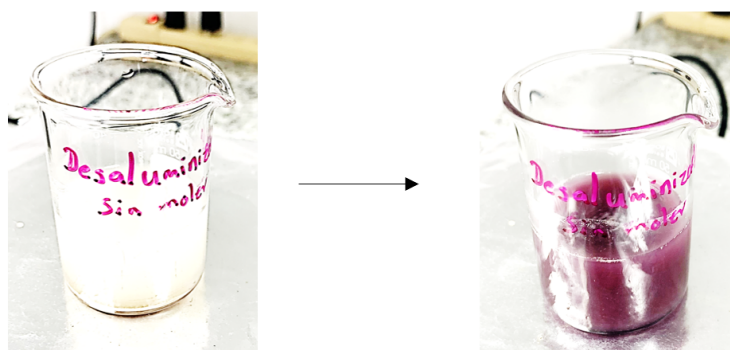
Figure 5.30: Process of dopping with gold nanoparticles of sample DG, it can be observed the change of color in the image in the right because of the presence of the nanoparticles.

5.10.4 Diatom dealuminized, broken structure "DB"

The sample "DB" has been treated equal as the sample "D", but with the difference that this one was ground, producing the breakage of its structure. In figure 5.31 (a) can be observed the absorbance taken at different times in a period of 6 hours, a total of 15 spots were measured, as it can be appreciated, the intensity in the absorbance axis is getting lower according time is passing, this can give us a clearly hint that the loading of the drug is happening. In (b) can be observed the percentage of concentration of Gentamicin loaded, referring as "100%" the maximum quantity registered loaded in the diatom DB. In table 5.14 there are the values of the graph in figure 5.31 (b), in its equivalences of the absorbance, percentage concentration and concentration.

In sample DB, the maximum loaded, in terms of concentration is 16.956 mg/mL, and the minimum is 4.108 mg/mL. Proceeding with a subtraction of this two values, we get 12.848 mg/mL as the total loaded drug in DB. Therefore, it can be expressed to as the 75.77% of drug was loaded into this diatom. The loaded of the drug on the diatom with the broken structure compared with the sample "D"could be related to an increase in the surface area of the sample leading to a higher capacity of absorption. Also to the easiness to cover the structure, because of the broken characteristics.
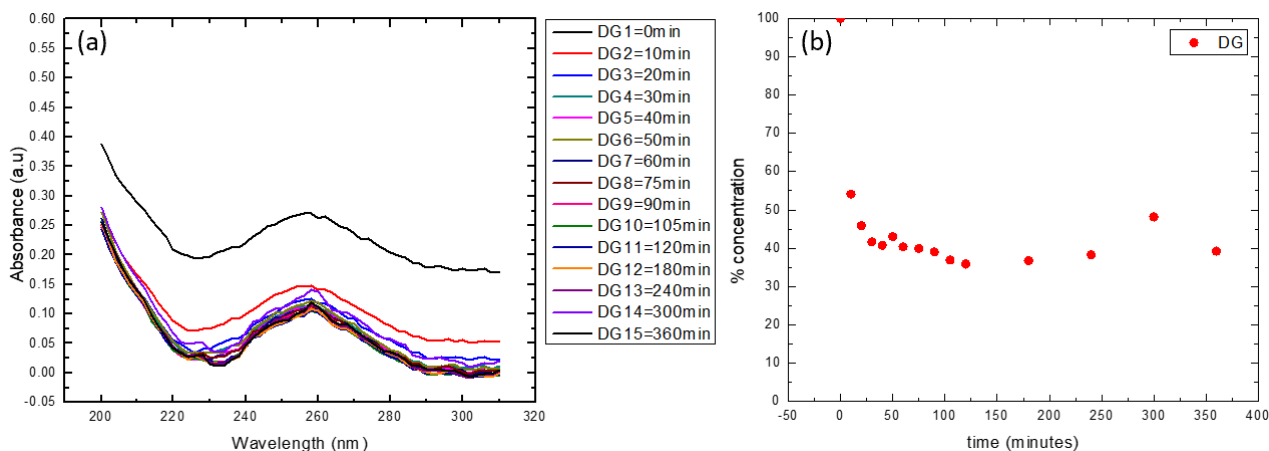

Figure 5.31: UV-vis spectrum of sample "DB",in (a) is found the spectrum of "absorbance vs wavelength", and in (b) percentage of concentration vs the time.

Equivalence of percentage in concentration and absorbance of Gentamicin in sample "DB"		
Absorbance	Percentage(%)	Concentration (mg/mL)
0.4239	100	16.956
0.1798	42.41566	7.192
0.1405	33.14461	5.62
0.0978	23.07148	3.912
0.1339	31.58764	5.356
0.1143	26.96391	4.572
0.1128	26.61005	4.512
0.1063	25.07667	4.252
0.1154	27.2234	4.616
0.1044	24.62845	4.176
0.1089	25.69002	4.356
0.1059	24.98231	4.236
0.1068	25.19462	4.272
0.1085	25.59566	4.34
0.1079	25.45412	4.316

Table 5.14: Equivalence of percentage, absorbance and concentration of Gentamicin loaded in "DB".

Sample dealuminized doped with gold nanoparticles, broken structure "DBG"

Figure 5.32: UV-vis spectrum of sample "DBG",in (a) is found the spectrum of "absorbance vs wavelength", and in (b) percentage of concentration vs the time.

The sample "DBG" has the exact same treatment as DG but with the difference that this sample was ground before being coated with the gold nanoparticles. figure 5.2 corresponds to the process of gold nanoparticles in this sample. In (a) can be observed the solution with the diatoms and in (b) when the gold nanoparticles have been synthesized and stabilized.

In graph 5.32 (a) are the spectra of UV-vis taking in a range of 6 hours, it can be seen that conforming the time is passing, the intensity in absorbance of Gentamicin is getting lower too, demonstrating that, eventually, the drug loading is happening, (b) shows the concentration of Gentamicin with respect of this sample, verifying what is seen in (a) conforming the time pass the curve is flattening.

In table 5.15 can be found the equivalence data belonging to the sample DBG in graph 5.32. The total loaded drug in this sample is 14.968 mg/mL. This was obtained by subtracting the maximum corresponding to the value 21.004 mg/mL and the minimum, corresponding to 6.036 mg/mL, this value is the equivalent to 71.26% of total drug loaded into the diatom. This behavior could be related to a higher surface area due to the broke structure and the functionalization with the gold nanoparticles leading a synergistic effect to a higher capacity of absorption of the gentamicin.

Equivalence of percentage in concentration and absorbance of Gentamicin in sample "DBG"		
Absorbance	Percentage(%)	Concentration (mg/mL)
0.5251	100	21.004
0.3176	60.48372	12.704
0.3189	60.73129	12.756
0.2749	52.35193	10.996
0.1848	35.1933	7.392
0.173	32.94611	6.92
0.183	34.8505	7.32
0.1801	34.29823	7.204
0.1509	28.73738	6.036
0.1552	29.55627	6.208
0.1566	29.82289	6.264
0.162	30.85127	6.48
0.164	31.23215	6.56
0.1659	31.59398	6.636
0.20.43	38.90687	8.172

Table 5.15: Equivalence of percentage, absorbance and concentration of Gentamicin loaded in "DBG".

Sample dealuminized doped with gold nanoparticles (Au/CTAB) (Ex-situ protocol), broken structure "DBE"
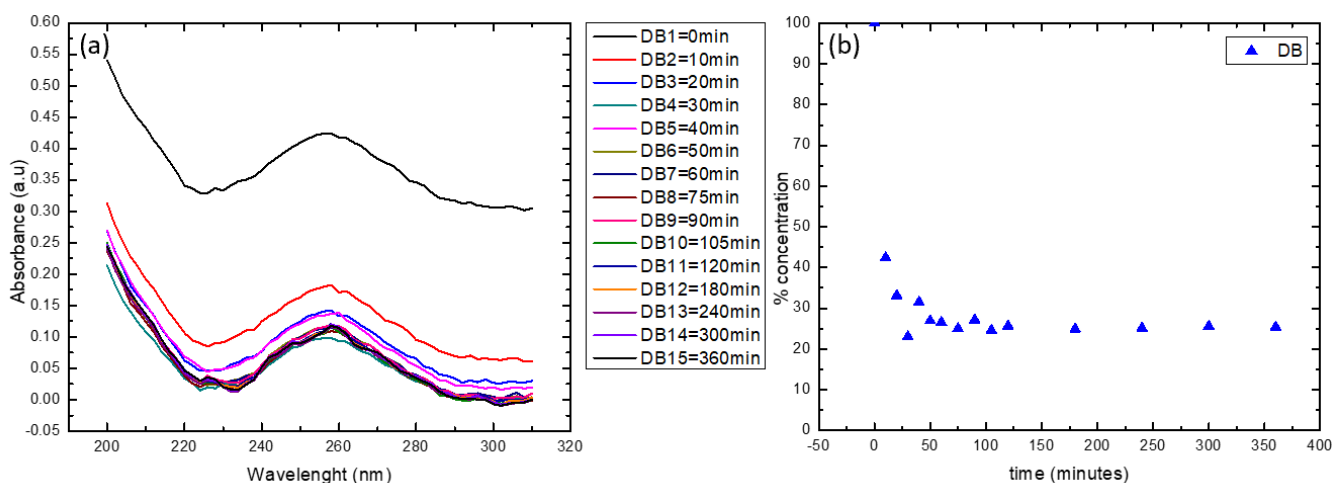

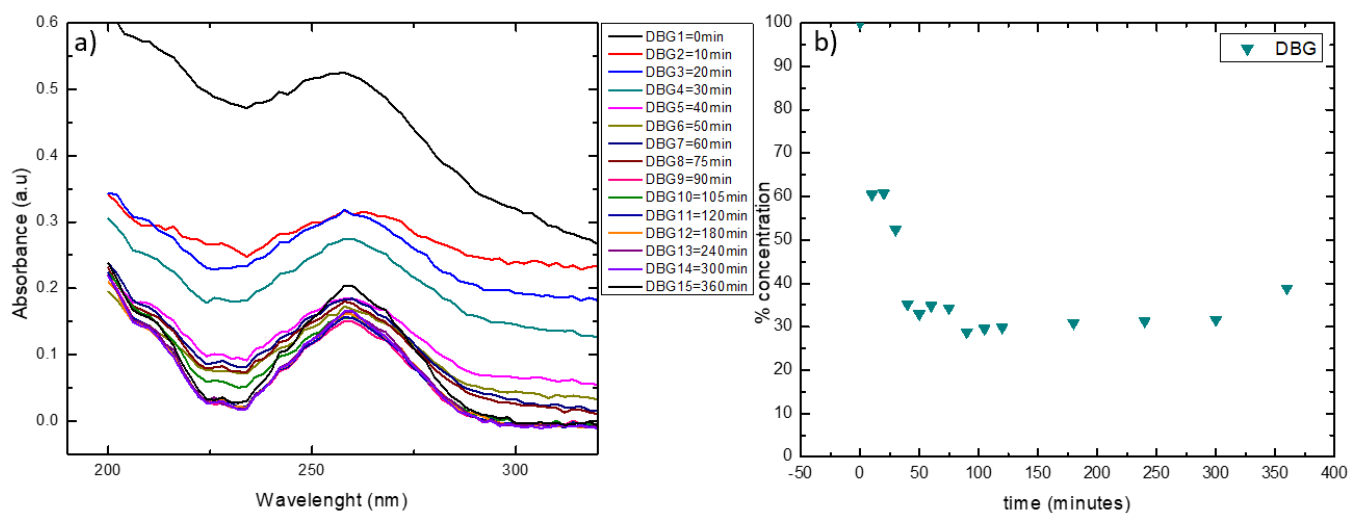Figure 5.33: UV-vis spectrum of sample "DBE",in (a) is found the spectrum of "absorbance vs wavelength", and in (b) percentage of concentration vs the time.

The sample "DBE", at first has the same treatment of cleaning as the sample DB. This sample is doped with gold nanoparticles as DBG, but, in this case, the nanoparticles were added to the diatom, following the "*Ex-situ* protocol", previously mentioned.

In figure 5.33 (a) the spectra of UV-vis took in a range of 6 hours, it can be seen that conforming the time is passing, the intensity in absorbance of Gentamicin is getting lower, (b) shows the concentration of Gentamicin with respect of this sample, verifying what is seen in (a) conforming the time pass the curve is trying to flattening and stabilizing.

In table 5.16 can be found the equivalence data belonging to the sample DBG in graph 5.33. The total loaded drug in this sample is 5.416 mg/mL. Corresponding to 43.56% of total drug loaded into the diatom. Between the sample of the same nature, that are DB, DBG and DBE, it can be observed that DBE is the sample that loaded less drug, referring about the percentage. This behavior could be related to the presence of the CTAB in the sample. CTAB confer cationic properties on AuNPs since it is a cationic surfactant and forms a bilayer that prevents the agglomeration of the nanoparticles due to electrostatic and steric interactions. On the other hand, Gentamicin is a positively charged molecule. One possible reason

is that the gentamicin molecule has a repulsive electrostatic effect on the Au-CTAB surfaces leading to reduce the absorption properties compared to the sample prepared using the In-situ method.

Equivalence of percentage in concentration and absorbance of Gentamicin in sample "DBE"		
Absorbance	Percentage(%)	Concentration (mg/mL)
0.3108	100	12.432
0.2186	70.33462	8.744
0.2520	81.37066	10.116
0.2116	68.08237	8.464
0.1913	61.55084	7.652
0.2201	70.81725	8.804
0.1755	56.46718	7.02
0.1926	61.96911	7.704
0.1882	60.55341	7.528
0.1754	56.43501	7.016
0.1773	57.04633	7.092
0.1848	59.45946	7.392
0.2065	66.44144	8.26
0.2378	76.51223	9.512
0.2111	67.92149	8.444

Table 5.16: Equivalence of percentage, absorbance and concentration of Gentamicin loaded in "DBE".
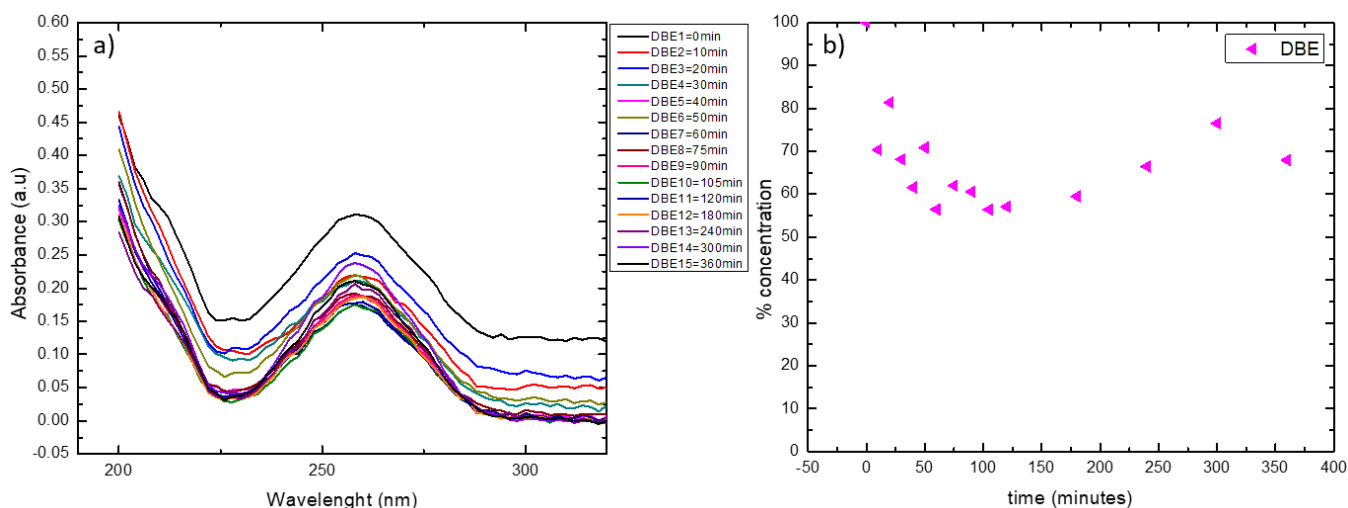
Sample ethanol-washed simple "E"

Figure 5.34: UV-vis spectrum of sample "E",in (a) is found the spectrum of "absorbance vs wavelength", and in (b) percentage of concentration vs the time.

The sample "E", according to previous sections, is diatom cleaned with ethanol 99% and sonication, letting taking out almost all the dirtiness and clay present in the sample. No other treatment like sulfuric acid or piranha was performed on it.

In figure 5.34 (a) the spectra of UV-vis took in a range of 6 hours, it can be seen that conforming the time is passing, the intensity in absorbance of Gentamicin is getting lower too, demonstrating that, eventually,the drug loading is happening, similar to the other samples with the sulfuric acid treatment, (b) shows the concentration of Gentamicin with respect of this sample,verifying what is seen in (a) conforming the time pass the curve is trying to flattening and stabilizing.

In table 5.17 can be found the equivalence data belonging to the sample E in graph 5.34. The total loaded drug in this sample is 7.036 mg/mL. This value is the equivalent to 64.13% of total drug loaded into the diatom. In this case, the loading of the drug is related to the functionalization of the sample with the OH groups from the ethanol treatment.

Equivalence of percentage in concentration and absorbance of Gentamicin in sample "E"		
Absorbance	Percentage(%)	Concentration (mg/mL)
0.2743	100	10.972
0.1868	68.10062	7.472
0.1441	52.53372	5.764
0.1114	40.61247	4.456
0.1186	43.23733	4.744
0.111	40.46664	4.44
0.1003	36.5658	4.012
0.1094	39.88334	4.376
0.1007	36.71163	4.028
0.101	36.821	4.04
0.1007	36.71163	4.028
0.0984	35.87313	3.936
0.1055	38.46154	4.22
0.1049	38.2428	4.196
0.1034	37.69595	4.136

Table 5.17: Equivalence of percentage, absorbance and concentration of Gentamicin loaded in "E".

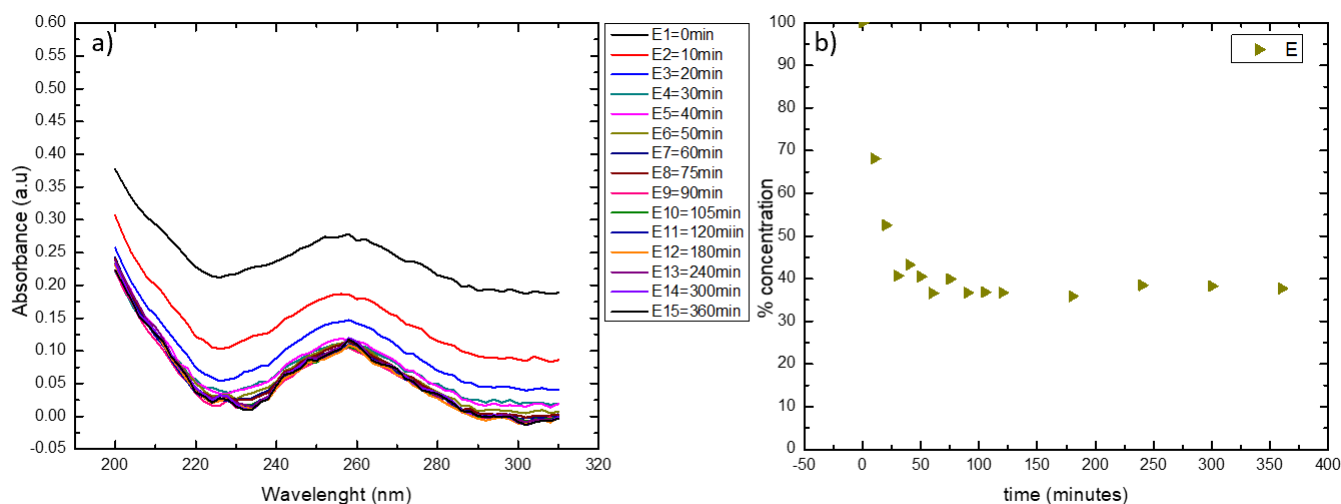**Sample ethanol-washed doped with gold nanoparticles, "EG"**

Figure 5.35: UV-vis spectrum of sample "EG",in (a) is found the spectrum of "absorbance vs wavelength", and in (b) percentage of concentration vs the time.

The sample "EG" corresponds to the same sample as "E", meaning that has the same cleaning strategy, ethanol 99%. The modification here is that it is doped with gold nanoparticles, by the "*In-situ* protocol".

In figure 5.35 are shown the graphs obtained in the measure of sample EG in the UV-vis spectrophotometer. In (a) the spectra of UV-vis taken in a range of 6 hours, it can be seen that the drug loading is taking place because, conforming the time pass, the intensity in absorbance of Gentamicin is getting lower, (b) shows the concentration of Gentamicin with respect of this sample,verifying what is seen in (a) conforming the time pass the curve is flattening and stabilizing. In table 5.18 can be found the equivalence data belonging to the sample EG in graph 5.35. The total loaded drug in this sample is 8.508 mg/mL. This value is equivalent to 66.99% of total drug loaded into the diatom. In the figure 5.36 it can be observed the process of AuNPs synthesis of the sample EG, a) is the step before adding gold, can be appreciate a yellowish solution because of the diatoms, b) a moment after adding gold and $NaBH_4$, the color turned into dark red, and c) after two days, the colloidal solution of this nanoparticles turn darker, into a blueish, with a tendency to black, attributed to agglomeration of the nanoparticles, as has been reported[79].

Equivalence of percentage in concentration and absorbance of Gentamicin in sample "EG"		
Absorbance	Percentage(%)	Concentration (mg/mL)
0.2743	100	12.7
0.1868	50.61417	6.428
0.1441	41.22835	5.236
0.1114	43.9685	5.584
0.1186	36.18898	4.596
0.111	38.17323	4.848
0.1003	37.66929	4.784
0.1094	34.20472	4.344
0.1007	33.92126	4.308
0.101	33.00787	4.192
0.1007	33.03937	4.196
0.0984	37.73228	4.792
0.1055	33.6063	4.268
0.1049	34.01575	4.32
0.1034	39.40157	5.004

Table 5.18: Equivalence of percentage, absorbance and concentration of Gentamicin loaded in "EG".

Figure 5.36: Process of doping diatoms washed with ethanol with gold nanoparticles.
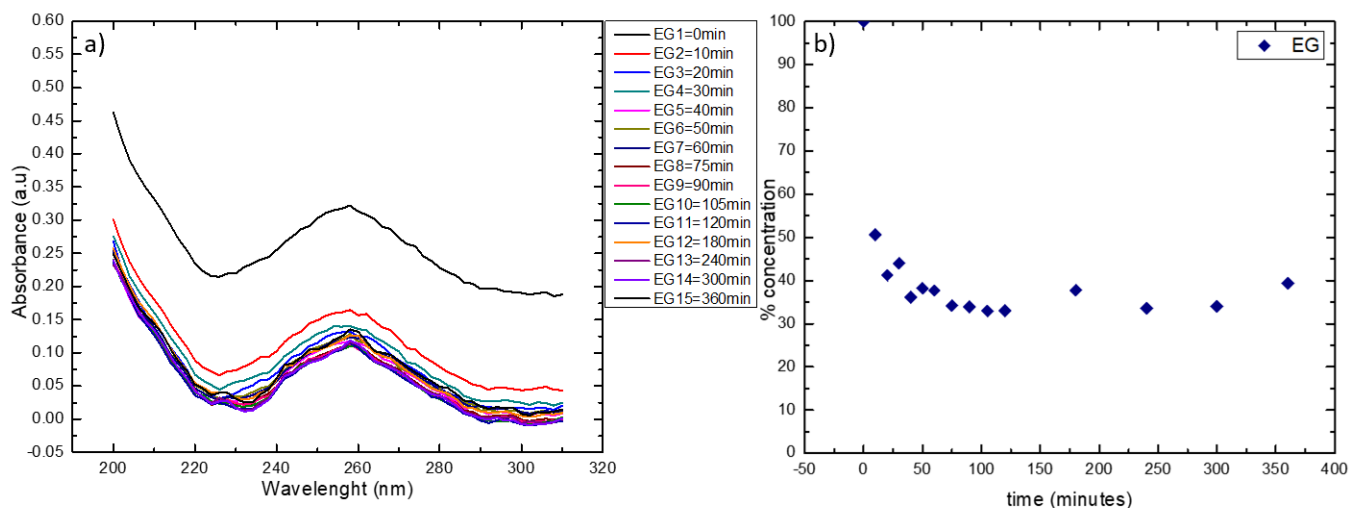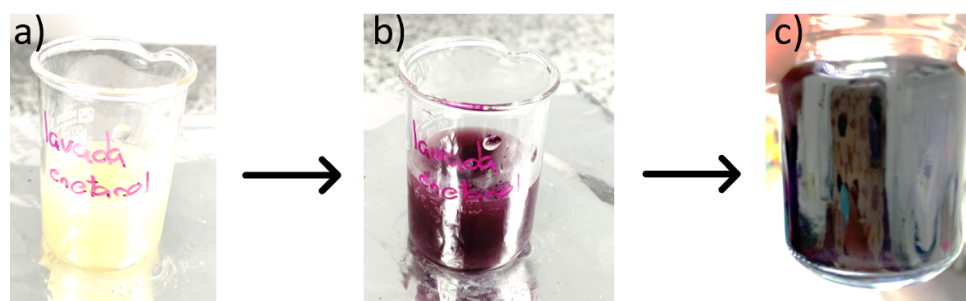
Sample diatom with piranha treatment, simple, "P"
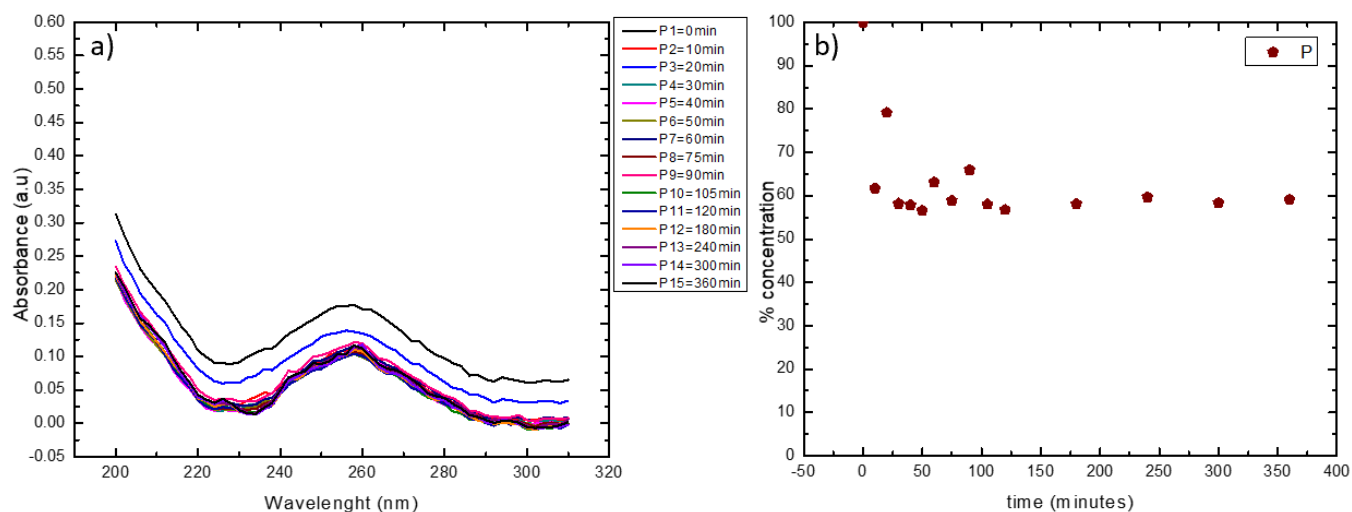
Figure 5.37: UV-vis spectrum of sample "P",in (a) is found the spectrum of "absorbance vs wavelength", and in (b) percentage of concentration vs the time.

The sample "P" corresponds to the sample of diatom that was treated with piranha solution, which is basically sulfuric acid and hydrogen peroxide concentrated.

In figure 5.37 are the graphs obtained in the measure of sample P in the UV-vis spectrophotometer. In (a) the spectra of UV-vis took in a range of 6 hours, with the help of the absorbance intensity, it can be shown that effectively the gentamicin is been loaded into the diatom, (b) shows the concentration of Gentamicin with respect of this sample,verifying what is seen in (a) the curve is flattening and stabilizing after some time.

In table 5.19 can be found the equivalence data belonging to the sample P in graph 5.37. The total loaded drug in this sample is 3.052 mg/mL. This value is equivalent to 43.43% of total drug loaded into the diatom. In this case, the loading of the drug is related to the functionalization of the sample with the H protons from the piranha treatment and a reduction of the pH of the media, leading a different mechanism of absorption in acidic conditions.

Equivalence of percentage in concentration and absorbance of Gentamicin in sample "P"		
Absorbance	Percentage(%)	Concentration (mg/mL)
0.1757	100	7.028
0.1084	61.69607	4.336
0.139	79.11212	5.56
0.1022	58.16733	4.088
0.1016	57.82584	4.064
0.0994	56.57371	3.976
0.1109	63.11895	4.436
0.1034	58.85031	4.136
0.1159	65.96471	4.636
0.1019	57.99659	4.076
0.0997	56.74445	3.988
0.1021	58.11042	4.084
0.1049	59.70404	4.196
0.1026	58.39499	4.104
0.1039	59.13489	4.156

Table 5.19: Equivalence of percentage, absorbance and concentration of Gentamicin loaded in "P".

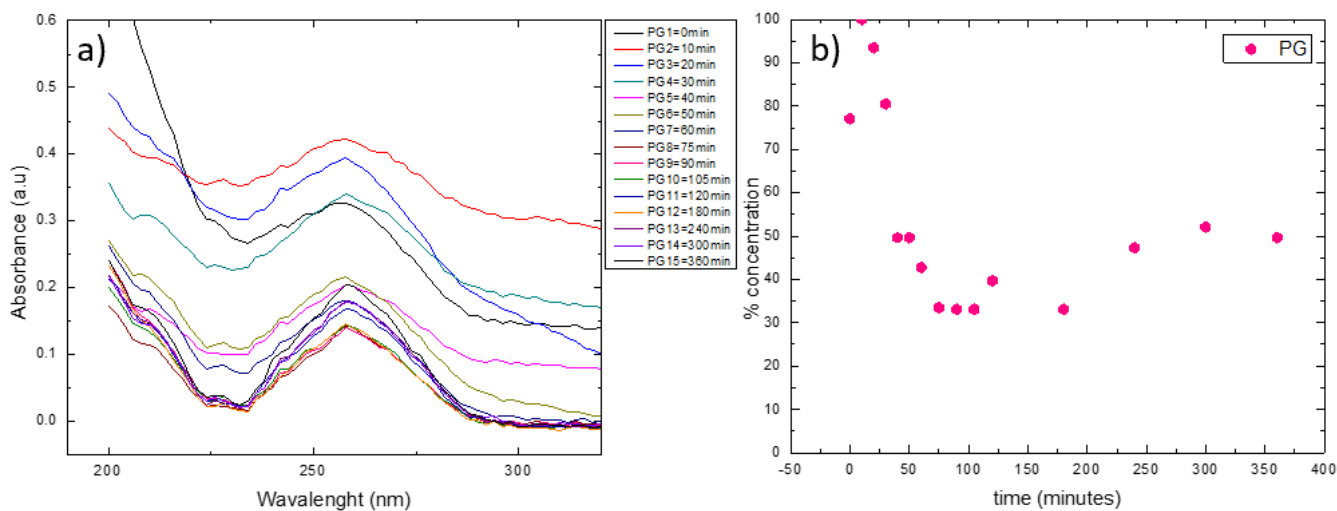**Sample diatom with piranha treatment doped with gold nanoparticles, "PG"**

Figure 5.38: UV-vis spectrum of sample "PG",in (a) is found the spectrum of "absorbance vs wavelength", and in (b) percentage of concentration vs the time.

The sample "PG" corresponds to the same sample as "P", meaning that has the same cleaning strategy, Piranha treatment. The modification here is that it is doped with gold nanoparticles, utilizing the "*In-situ* protocol".

In figure 5.38 are the graphs obtained in the measure of sample PG in the UV-vis spectrophotometer. In (a) the spectra of UV-vis took in a range of 6 hours, thanks to the constant measure of the intensity of the absorbance, it can be assure that the loading of the gentamicin is happening, (b) shows the concentration, in terms of percentage, of Gentamicin with respect of this sample,verifying what is seen in (a) the curve is flattening and stabilizing conforming the time passes.

In table 5.20 can be found the equivalence data belonging to the sample PG in graph 5.38. The total loaded drug in this sample is 11.312 mg/mL. This value is equivalent to 66.89% of total drug loaded in the solution with the diatoms. Compared to the sample of its same nature, piranha treatment, PG seems to catch a bit more in comparison with P but, sample P has the characteristic to be a little bit stabilized. This evidence the advantage of doping the diatom with the gold nanoparticles.

Equivalence of percentage in concentration and absorbance of Gentamicin in sample "PG"		
Absorbance	Percentage(%)	Concentration (mg/mL)
0.3258	77.05771	13.032
0.4228	100	16.912
0.3953	93.49574	15.812
0.3403	80.48723	13.612
0.21	49.66887	8.4
0.21	49.66887	8.4
0.1807	42.73888	7.228
0.1416	33.49101	5.664
0.14	33.11258	5.6
0.14	33.11258	5.6
0.1679	39.71145	6.716
0.14	33.11258	5.6
0.2	47.30369	8
0.22	52.03406	8.8
0.21	49.66887	8.4

Table 5.20: Equivalence of percentage, absorbance and concentration of Gentamicin loaded in "PG".

General results of loading of gentamicin		
Sample	Total loaded (%)	Total loaded (g/mL)
D	72.22	10.4
DG	64.14	6.94
DB	75.77	13.05
DBG	71.26	14.96
DBE	43.56	5.42
E	64.13	7.03
EG	66.99	8.51
P	43.43	3.05
PG	66.89	11.31

Table 5.21: Summary of loading results of the 9 analyzed samples.

5.10.5 Release of Gentamicin

The release of Gentamicin loaded in diatoms was measured in a total period of nine days. The first day, in the firsts hours, the spectra were taken in short range of time, to have a better value of the burst release[14]. Every 10 minutes the first hour, the next one every 15 minutes, every half hour the next hour, and the other 3 hours were measured every hour. The 9 samples analyzed had successfully loaded Gentamicin. In this section will be analyzed how much of the drug was released in the period of time that was measured. The wavelength selected as reference to measure the absorbance by Gentamicin is at 256 nm, same as the one for loading process.

Release sample D

Figure 5.39: UV-vis release spectrum of Gentamicin in sample D, (a) release in days, (b) release of first day.

5 mL of Simulated Body Fluid solution (pH 7.4) was added to a 0.1 g of drug-loaded diatom of the sample D. For the first hour, every ten minutes, 0.25 μl of aliquot was taken for UV-vis spectroscopic analysis at 256 nm. For the second hour, the same process was repeated, but this time every 15 minutes. The same process was followed for the third hour, just instead of every 15 minutes, it was passing half an hour, and for the next three hours, the analysis was made with an hour of difference. For the next days, the aliquot was taking once a day, at the same hour every day. For sample D, the graph of release is in Fig. 5.39, as it can be observed, a burst release occurs in the first day. This is in accordance with other authors that on the first day should be the highest release[14]. In (b) we can tell that the release on the first day, reaches almost 20% of what it was loaded. In the next days, the release seems to be more controlled, tending to be stable. On the eighth day, sample D reaches 27,3% of release, which is equivalent to a 3.94 mg/mL in concentration. This means that 73% of the drug is still retained in the sample and could be delivered with prolonged time.
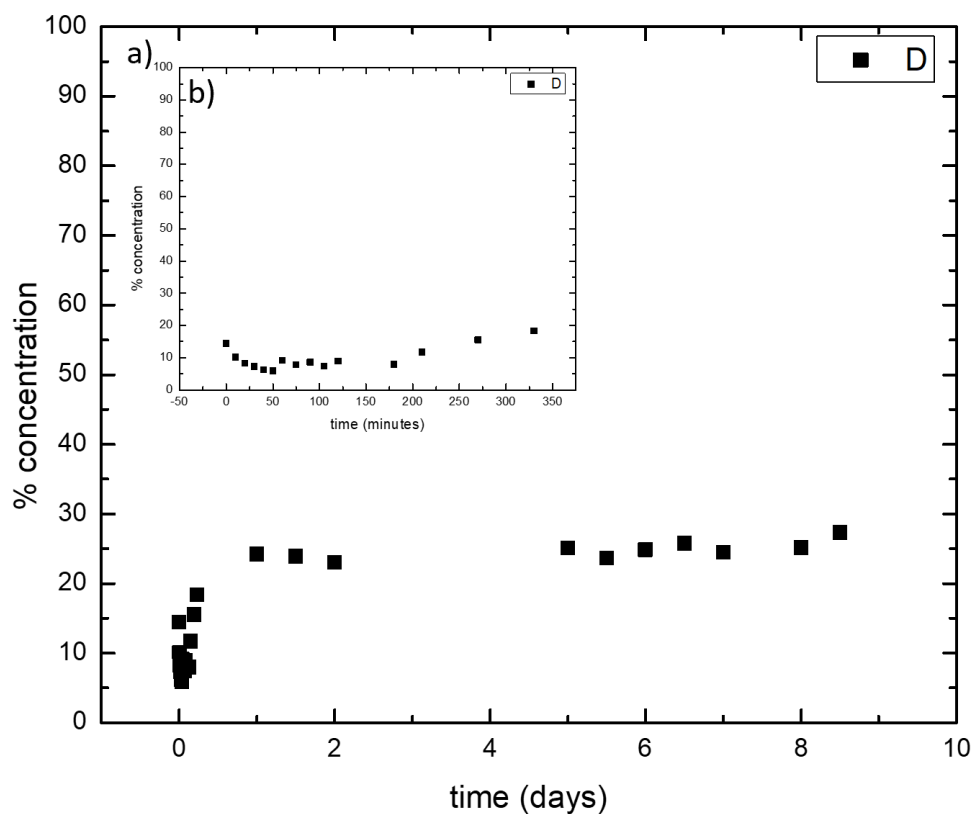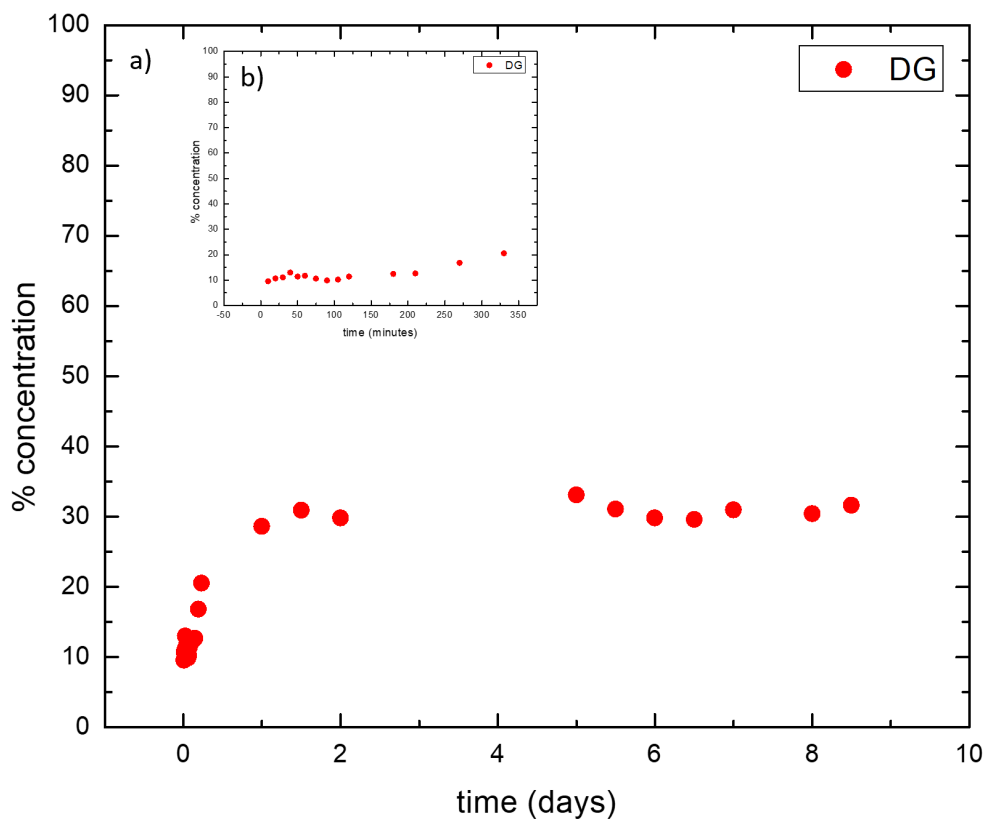
Release sample DG

Figure 5.40: UV-vis release spectrum of Gentamicin in sample DG, (a) release in days, (b) release of first day.

5 mL of Simulated Body Fluid solution (pH 7) was added to a 0.1 g of drug-loaded diatom of the sample DG. For sample DG, the graph of release is in Fig. 5.40, as it can be observed, a slower burst release than sample D, occurs in the first day, releasing approximately 25% of the loaded Gentamicin in the first day. This is in agreement with other authors that on the first day should be the biggest release[14]. In (b) we can tell that the release on the first 6 h, reaches almost 20.52% of what it was loaded. In the next days, the release seems to be more controlled, tending to be stable. On the eighth day, sample DG reaches 31.61% of release, which is equivalent to a 3.42 mg/mL. Although it releases a little less in concentration in comparison with sample D, in percentage, it releases a little faster.

Release sample DB

Figure 5.41: UV-vis release spectrum of Gentamicin in sample DB, (a) release in days, (b) release of first day.

For sample DB, the graph of release is in Fig. 5.41, as it can be observed, a burst release occurs in the first day. In (b) we can tell that the release on the first 6h, reaches 15.03% of what it was loaded. In the next days, the release seems to be more controlled, tending to be stable. On the eighth day, sample DB reaches 21.7% of release, which is equivalent to a 3.7 mg/mL in concentration. Therefore, 87.3% of the drug still remains in the diatome, and could be release with prolonged time.

Release sample DBG

Figure 5.42: UV-vis release spectrum of Gentamicin in sample DBG, (a) release in days, (b) release of first day.

5 mL of Simulated Body Fluid solution (pH 7) was added to a 0.1 g of drug-loaded diatom of the sample DBG. For sample DBG, the graph of release is in Fig. 5.42, as it can be observed, a burst release occurs on the first 6h. In (b) we can tell that the release on the first 6h, reaches 18.6% of what it was loaded. In the next days, the release seems to be more controlled, tending to be stable. On the eighth day, sample DBG reaches 23.95% of release, which is equivalent to a 5.03 mg/mL in concentration, retaining 76% of the drug.
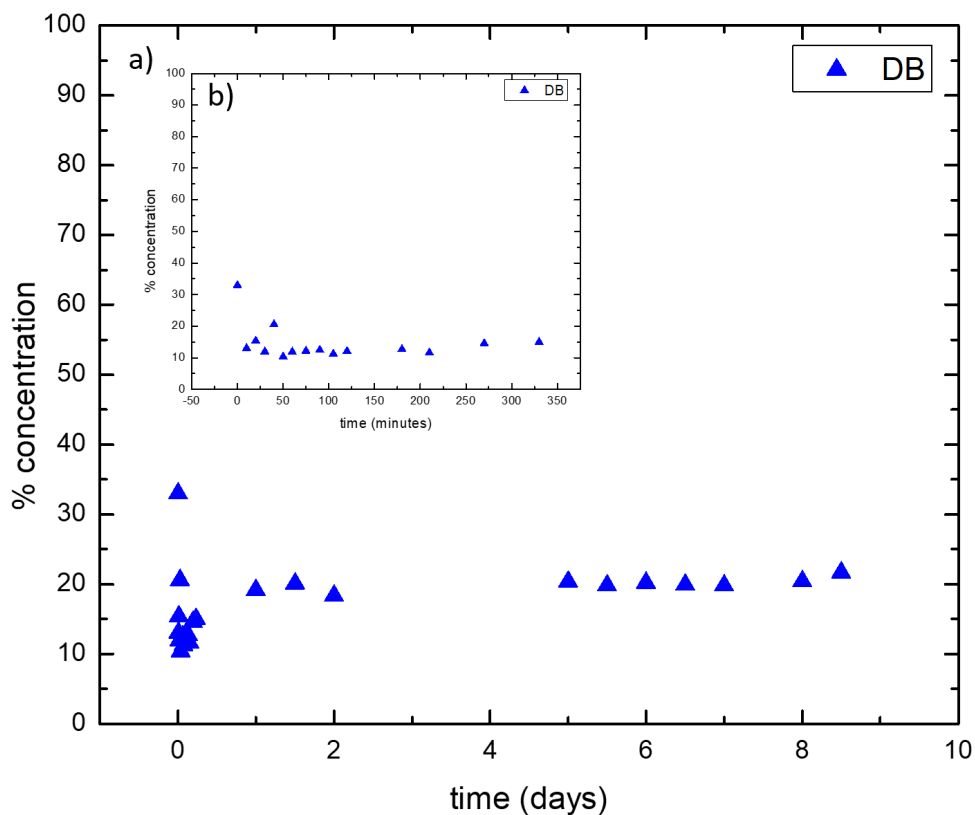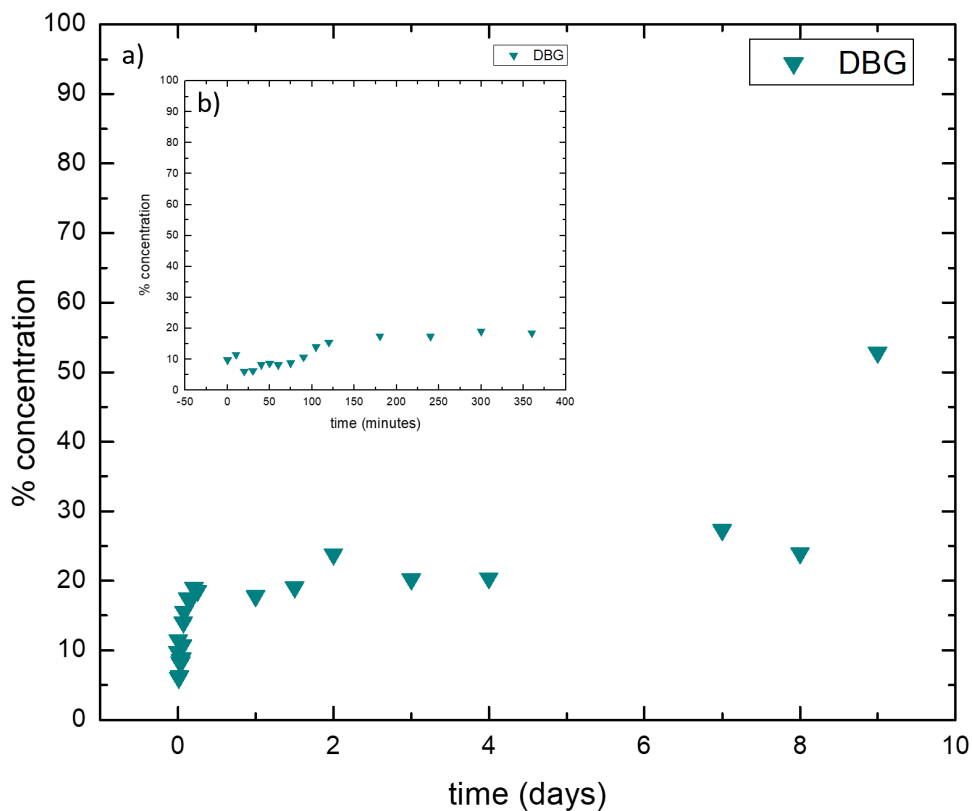
Release sample DBE

Figure 5.43: UV-vis release spectrum of Gentamicin in sample DBE, (a) release in days, (b) release of first day.

5 mL of Simulated Body Fluid solution (pH 7) was added to a 0.1 g of drug-loaded diatom of the sample DBE. For sample DBE, the graph of release is in Fig. 5.43, as it can be observed, a burst release occurs in the first 6h, reaching 34.10% of what it was loaded. In the next days, the release seems to be more controlled, tending to be stable. On the eighth day, sample DBE reaches 72.27% of release, which is equivalent to 8.98 mg/mL, retaining only 27.73% of the loaded drug. It can be seen that is a big difference in the percentage of drug release compared to DB and DBG with DBE. Therefore DBE figure 5.43, shows that there is a relative fast release, however depending on the treatment this is in general a good behavior for an antibiotic. Between DB and DBG there is almost no difference, except how they behave during the

first 6h . DBG has a controlled release of Gentamicin, while DB presents a more random behavior as seen in 5.43 (b), to later have a more stable behavior (a).
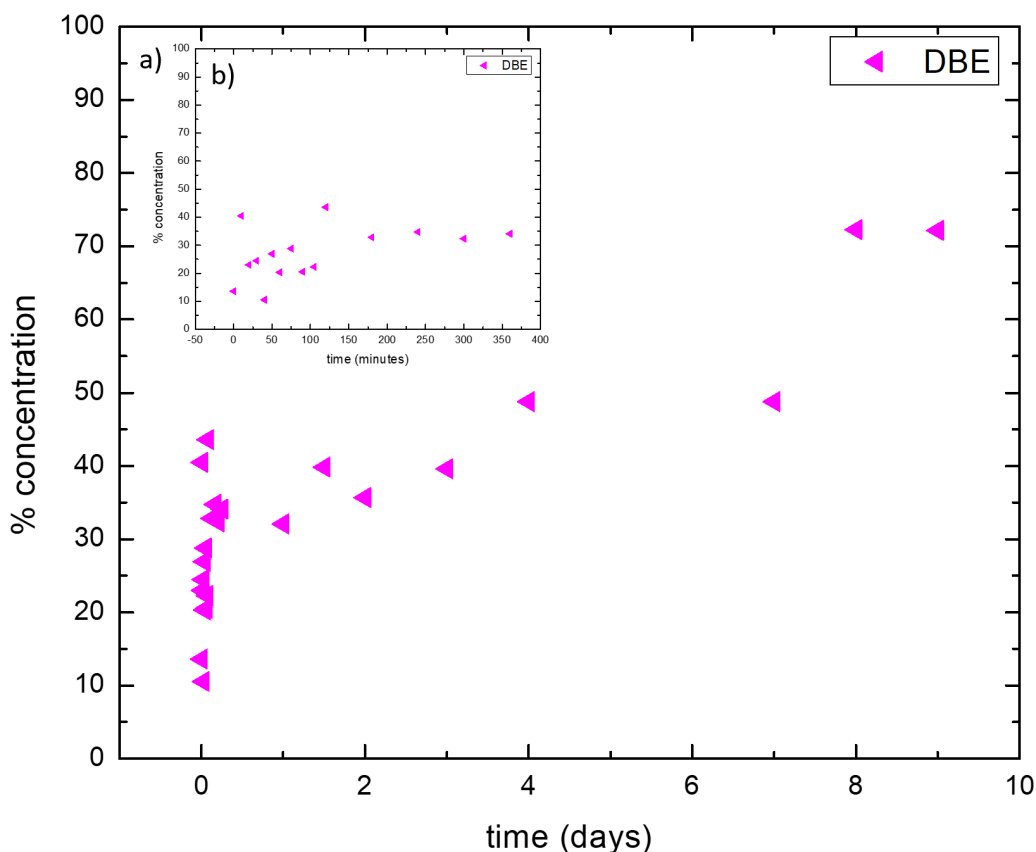
Release sample E

Figure 5.44: UV-vis release spectrum of Gentamicin in sample E, (a) release in days, (b) release of first day.

5 mL of Simulated Body Fluid solution (pH 7) was added to a 0.1 g of drug-loaded diatom of the sample E. For sample E, the graph of release is in Fig. 5.44, as it can be observed, a burst release occurs in the first 6h. In (b) we can tell that the release on the first 6h, reaches 20.01% of what it was loaded. In the next days, the release seems to be more stable. On the eighth day, sample E reaches 31.64% of release, which is equivalent to a 3.48 mg/mL in concentration, retaining 68.36% of the drug.
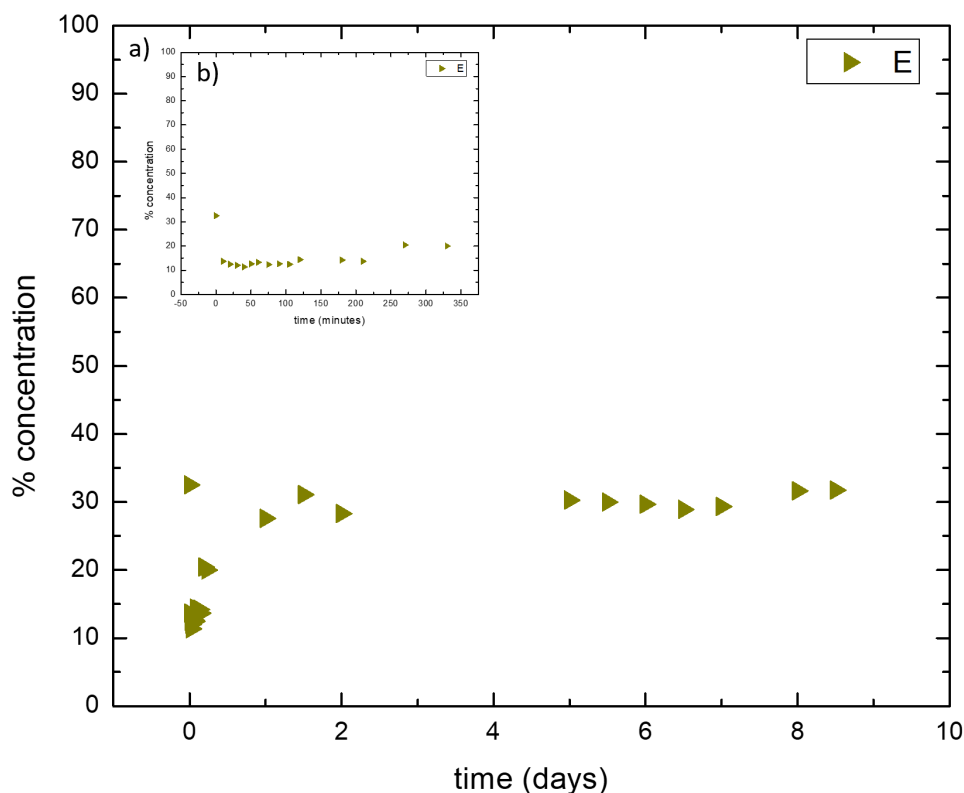
Release sample EG

Figure 5.45: UV-vis release spectrum of Gentamicin in sample EG, (a) release in days, (b) release of first day.

5 mL of Simulated Body Fluid solution (pH 7.4) was added to a 0.1 g of drug-loaded diatom of the sample EG. For sample EG, the graph of release is in Fig. 5.45, as it can be observed, a burst release occurs in the first day. In (b) we can tell that the release on the first 6h, reaches 18.43% of what it was loaded. In the next days, the release seems to be more stable. On the eighth day, sample EG reaches 26.14% of release, which is equivalent to a 3.32 mg/mL in concentration, retaining 68.36% of the drug.

Release sample P
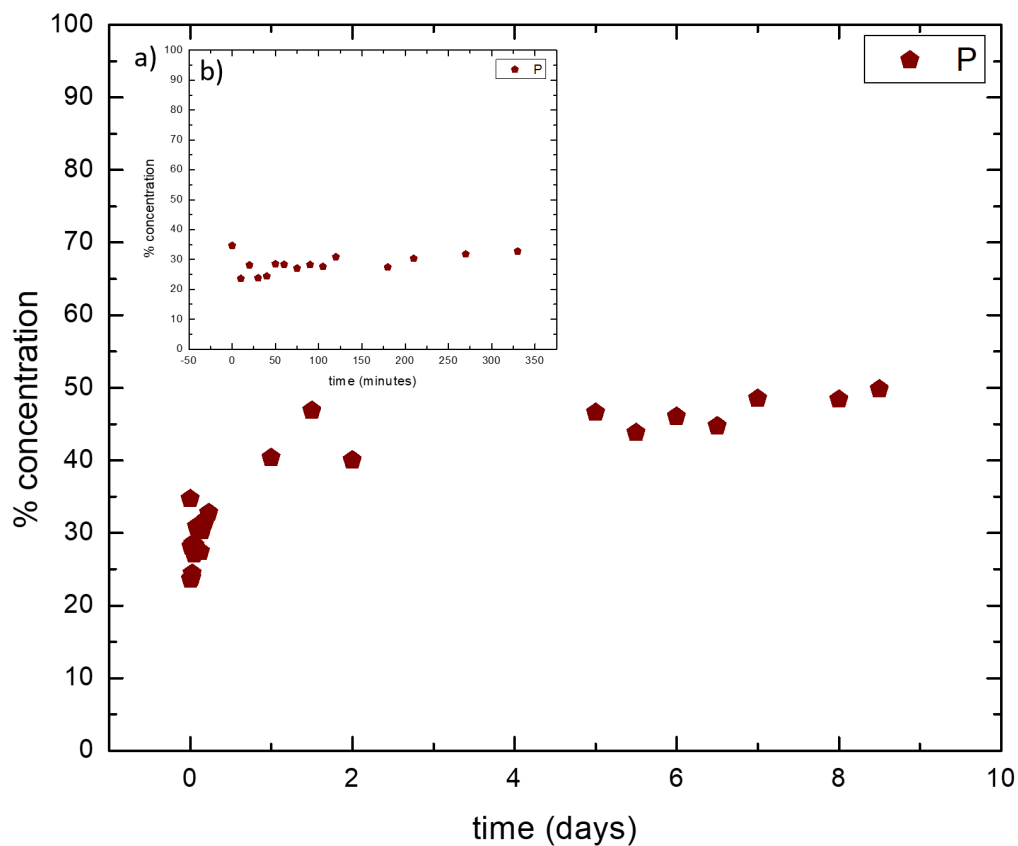
Figure 5.46: UV-vis release spectrum of Gentamicin in sample P, (a) release in days, (b) release of first day.

For sample P, the graph of release is in Fig. 5.46, as it can be observed, a burst release occurs in the first day. In (b) the release on the first 6h, reaches 32.78% of what it was loaded. In the next days, the release seems to be more stable. On the eighth day, sample P reaches 49.8% of release, which is equivalent to a 3.5 mg/mL in concentration, retaining 50.2% of the drug loaded.
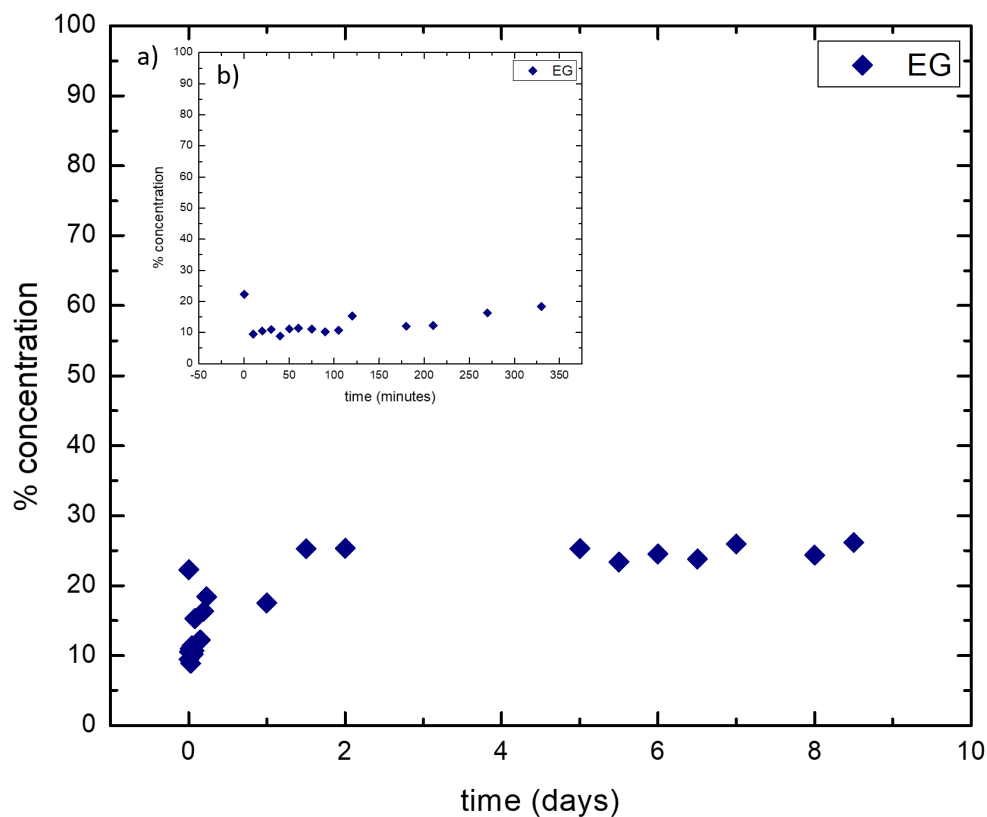
Release sample PG
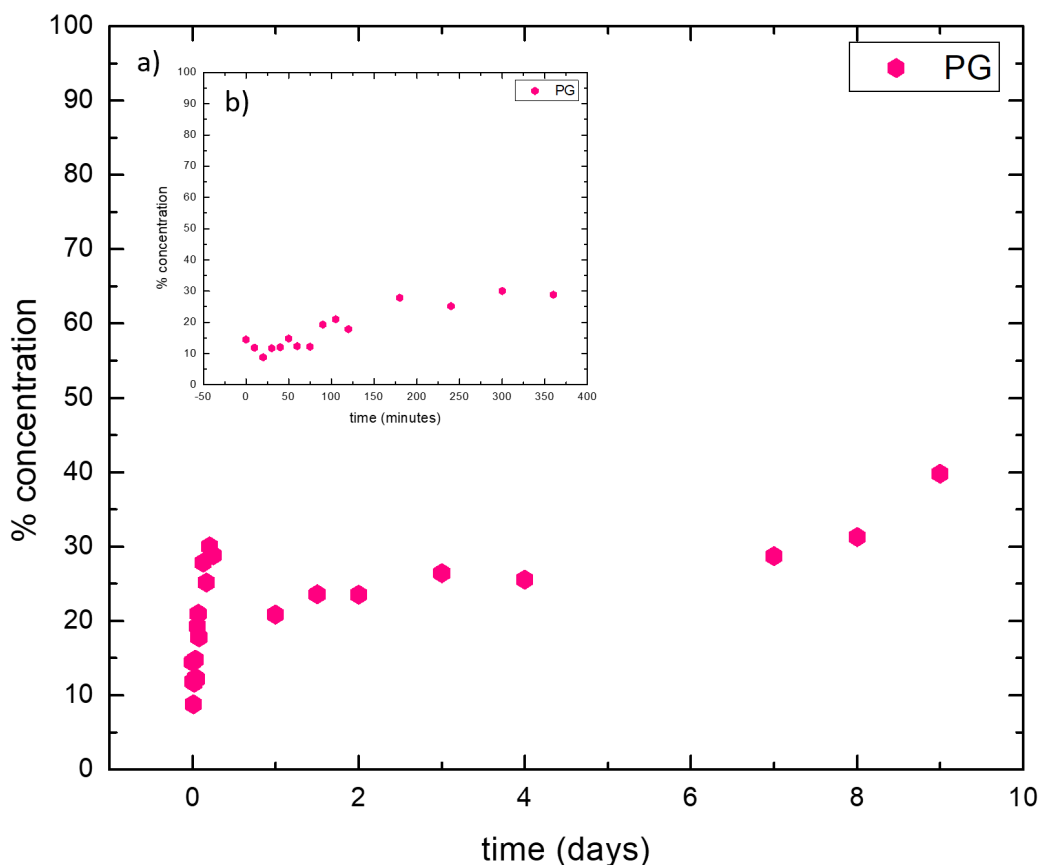
Figure 5.47: UV-vis release spectrum of Gentamicin in sample PG, (a) release in days, (b) release of first day.

For sample PG, the graph of release is in Fig. 5.47, as it can be observed, a burst release occurs in the first day. In (b) the release on the first 6h, reaches 28.85% of what was loaded. In the next days, the release seems to be more stable. On the eighth day, sample PG reaches 31.26% of release, which is equivalent to a 5.29 mg/mL in concentration. Between samples P and PG, P has a burst release less controlled, and in the rest of the days releases almost the half of all the loading. In the other hand, PG on the first day has a better control releasing, and on the other days behaves in a controlled and stable manner, with a slower release.

General results of loading and release of gentamicin		
Sample	Total loaded (%)	Total released at the 8th day (%)
D	72.22	27.31
DG	64.14	31.61
DB	75.77	21.7
DBG	71.26	23.95
DBE	43.56	72.27
E	64.13	31.64
EG	66.99	26.14
P	43.43	49.80
PG	66.89	31.26

Table 5.22: Summary of results of the 9 analyzed samples.

Figure 5.48: UV-vis release spectra of Gentamicin in all samples. D "Dealuminated", DG "Dealuminated-gold", DB "Dealuminated broken", DBG "Dealuminated broken-gold, DBE "Dealuminated broken-Au/CTAB", E "Ethanol", EG "Ethanol-gold", P "Piranha" and PG "Piranha-gold".
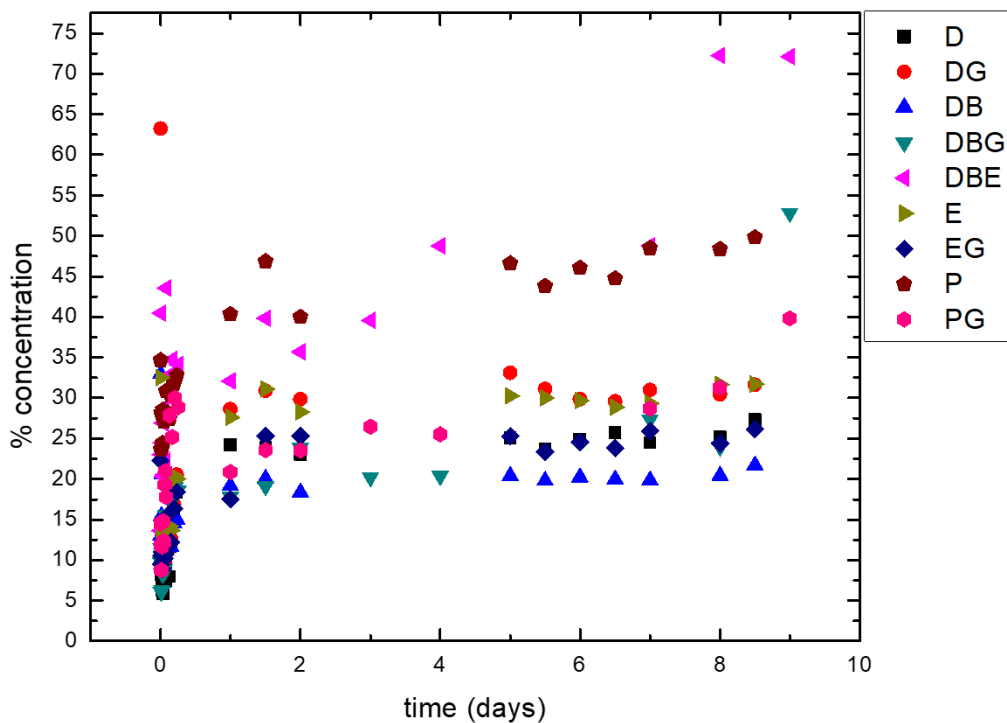
From Table 5.21 we can compare the different behavior of the diatoms with different treatments and doped with gold nanoparticles as follows: The DB sample is the one that shows the highest drug load and has a 30 percent release after 8 days. The DBE sample, despite showing a release with good behavior, has released almost all its content after 8 days, it is the one with the fastest released. In general, gold-doped samples are moderately loaded and demonstrate more controlled release than samples without AuNPs. The controlled released can be appreciated as they release in a stable and continuous manner, releasing less than the 50% in the first 8 days, the only exception of the samples is the DBE, as mentioned before, it released almost its complete content by the first 8 days. Sulfuric acid (dealuminated treatment) functionalized samples were 5, of which 3 have a broken structure and 2 have their structure complete. Of the different treatments made to diatoms, the ones that show the best performance are those functionalized (dealuminated treatment) with sulfuric acid, with the increase in surface area and the OH groups, giving

better engagement with the gold nanoparticles.

The P and PG samples are involved in the absorption-desorption into an acidic pH medium, allowing the functionalization with H^+, this process leads to another absorption mechanism (loading mechanism). Due to the amine groups content of Gentamicin, such groups will show a bigger affinity to OH groups because of its negativity. Thus, the final product after piranha treatment are the functionalization with OH groups over the diatom surface. In table 5.22 it can be appreciated how the P and PG samples show a good load and a moderated released in P sample, and on the other hand, in the PG sample the released shows to be in better control due to its gold doping in comparison with the same sample but in normal conditions.

Regarding to E and EG sample, after being washed with ethanol, Gentamicin is purely loaded over diatom, after this treatment, it does not show linkages with any different group that is not typical of the diatom itself. In table 5.22 it can be appreciated that E and EG samples show an acceptable load and a much lower release, considering the initial concentration loaded. In contrast with other samples, the released quantity is much more lower as it can be in table 5.17 and table 5.18.

Chapter 6

Conclusions & Outlook

In this work we studied the gentamicin drug delivery process, diatoms were previously treated using different methods. Then, diatoms were doped with gold nanoparticles using an *in-situ* reduction and an *ex-situ* protocol with CTAB. The presence of the gold nanoparticles on the diatoms was corroborated using surface area, SEM, XRD, and RAMAN techniques. We confirm the fluorescence properties of the samples using Raman and fluorescence microscopy, due to the interaction of the gold nanoparticles with the diatom surfaces. The loading and drug release of the gentamicin demonstrate that the functionalization and doping with gold nanoparticles modify the release behavior, reaching a maximum of 72% in eight days in the case of the sample coated with Au/CTAB nanoparticles. The DB sample is the one that shows the highest drug load and has a 30 percent release after 8 days. In general, gold-doped samples are moderately loaded and demonstrate more controlled release than samples without AuNPs, this samples showed the highest drug retention after 8 days which implies that with prolonged time they could further release the remaining drug. This work contributes to the use of green and sustainable biosilica natural materials in Ecuador and the understanding of the drug release of the gentamicin on diatoms using different treatments and decorating with gold nanoparticles that the specific site where the particles are delivering the drug can be followed by bioimaging procedures. For future work, a more detailed characterization of the samples must be done and further extended experiments of the drug release as a function of the time are needed.

Bibliography

[1] Chao, J. T.; Biggs, M. J.; Pandit, A. S. Diatoms: a biotemplating approach to fabricating drug delivery reservoirs. Expert Opinion on Drug Delivery **2014**, 11, 1687–1695.

[2] Davis, S. S. Drug delivery systems. Interdisciplinary Science Reviews **2000**, 25, 175–183.

[3] Venkatesan, J.; Lowe, B.; Kim, S.-k. Application of Diatom Biosilica in Drug Delivery. 2015, 245–254.

[4] Castro, D.; Chavez, E.; Cuasquer, J. Use of natural diatoms for drug delivery. Bionatura **2020**,

[5] Maher, S.; Kumeria, T.; Aw, M. S.; Losic, D. Diatom Silica for Biomedical Applications : Recent Progress and Advances. 2018, 1800552, 1–19.

[6] Aw, M. S.; Simovic, S.; Addai-Mensah, J.; Losic, D. Silica microcapsules from diatoms as new carrier for delivery of therapeutics. Nanomedicine **2011**, 6, 1159–1173.

[7] Zhang, H.; Shahbazi, M. A.; Mäkilä, E. M.; da Silva, T. H.; Reis, R. L.; Salonen, J. J.; Hirvonen, J. T.; Santos, H. A. Diatom silica microparticles for sustained release and permeation enhancement following oral delivery of prednisone and mesalamine. Biomaterials **2013**, 34, 9210–9219.

[8] Dolatabadi, J. E. N.; de la Guardia, M. Applications of diatoms and silica nanotechnology in biosensing, drug and gene delivery, and formation of complex metal nanostructures. Trends in Analytical Chemistry **2011**, 30, 1538–1548.

[9] Delasoie, J.; Zobi, F. Natural diatom biosilica as microshuttles in drug delivery systems. Pharmaceutics **2019**, 11, 1–21.

[10] Uthappa, U. T.; Sriram, G.; Brahmkhatri, V.; Kigga, M.; Jung, H. Y.; Altalhi, T.; Neelgund, G. M.; Kurkuri, M. D. Xerogel modified diatomaceous earth microparticles for controlled drug release studies. New Journal of Chemistry **2018**, 42, 11964–11971.

[11] Onesto, V.; Villani, M.; Coluccio, M. L.; Majewska, R.; Alabastri, A.; Battista, E.; Schirato, A.; Calestani, D.; Coppedé, N.; Cesarelli, M.; Amato, F.; Di Fabrizio, E.; Gentile, F. Silica diatom shells tailored with Au nanoparticles enable sensitive analysis of molecules for biological, safety and environment applications. Nanoscale Research Letters **2018**, 13.

[12] Terracciano, M.; Napolitano, M.; De Stefano, L.; De Luca, A. C.; Rea, I. Gold decorated porous biosilica nanodevices for advanced medicine. Nanotechnology **2018**,

[13] Vance, D.; Little, S. H.; De Souza, G. F.; Khatiwala, S.; Lohan, M. C.; Middag, R. Silicon and zinc biogeochemical cycles coupled through the Southern Ocean. Nature Geoscience **2017**, 10, 202–206.

[14] Bariana, M.; Aw, M. S.; Kurkuri, M.; Losic, D. Tuning drug loading and release properties of diatom silica microparticles by surface modifications. International Journal of Pharmaceutics **2013**, 443, 230–241.

[15] Brinkmann, N.; Friedl, T.; Mohr, K. Diatoms; 2009; pp 326–330.

[16] Tommasi, E. D.; Gielis, J.; Rogato, A. Marine Genomics Diatom Frustule Morphogenesis and Function : a Multidisciplinary Survey. 2020,

[17] Zamora, J. V. MICROFOSSILS BIOSTRATIGRAPHY AND PALEOENVIRONMENTAL RE-CONSTRUCTION OF THE LATE PLEISTOCENE LACUSTRINE SAN MIGUEL FORMATION, GUAYLLABAMBA BASIN, ECUADOR. 2020.

[18] Faraday, M. Experimetal realtions of gold (and other metals) to light. Philosophical Transactions **1857**, 145–181.

[19] Calipinar, H.; Ulas, D. Development of Nanotechnology in the World and Nanotechnology Standards in Turkey. Procedia Computer Science **2019**, 158, 1011–1018.

[20] Baker, J. R.; Ward, B. B.; Thomas, T. P. Nanotechnology in Clinical and Translational Research. **2004**, 123–135.

[21] Zia-ur Rehman, M.; Qayyum, M. F.; Akmal, F.; Maqsood, M. A.; Rizwan, M.; Waqar, M.; Azhar, M. Recent Progress of Nanotoxicology in Plants. Nanomaterials in Plants, Algae, and Microorganisms **2018**, 1, 143–174.

[22] Holkar, C. R.; Jain, S. S.; Jadhav, A. J.; Pinjari, D. V. SCALE-UP TECHNOLOGIES FOR FOR GREEN ENERGY :. Nanomaterials for Green Energy **2020**, 433–455.

[23] Yeh, Y. C.; Creran, B.; Rotello, V. M. Gold nanoparticles: Preparation, properties, and applications in bionanotechnology. Nanoscale **2012**, 4, 1871–1880.

[24] Küünal, S.; Rauwel, P.; Rauwel, E. Plant extract mediated synthesis of nanoparticles. Emerging Applications of Nanoparticles and Architecture Nanostructures **2018**,

[25] Turkevich, J.; Stevenson, P. C.; Hillier, J. A study of the nucleation and growth processes in the synthesis of colloidal gold. Discussions of the Faraday Society **1951**, 11, 55–75.

[26] Frens, G. Controlled Nucleation for the Regulation of the Particle Size in Monodisperse Gold Suspensions. Nat. Phys. Sci. **1973**, 241.

[27] Brust, M.; Walker, M.; Bethell, D.; Schiffrin, D. J.; Whyman, R. Synthesis of Thiol-derivatised Gold Nanoparticles in. **2000**, 801–802.

[28] Murphy, C. J.; Gole, A. M.; Stone, J. W.; Sisco, P. N.; Alkilany, A. M.; Goldsmith, E. C.; Baxter, S. C. Gold Nanoparticles in Biology: Beyond Toxicity to Cellular Imaging. Accounts of chemical research **2008**,

[29] Jain, P. K.; Eustis, S.; El-Sayed, M. A. Plasmon coupling in nanorod assemblies: Optical absorption, discrete dipole approximation simulation, and exciton-coupling model. Journal of Physical Chemistry B **2006**, 110, 18243–18253.

[30] Hans-Dieter Barke, S. Y., Al Hazari Redox Reactions. Misconceptions in chemistry **2009**, 207–234.

[31] Ojea-jime, I.; Campanera, J. M. Molecular Modeling of the Reduction Mechanism in the Citrate-Mediated Synthesis of Gold Nanoparticles. **2012**,

[32] Zhao, Drug Delivery Systems. 2015; `https://www.nibib.nih.gov/node/42846`.

[33] Pal, D.; Nayak, A. K. Alginates , Blends and Microspheres : Controlled. 2015, 89–98.

[34] Hasnain, M. S. Drug delivery: present, past, and future of medicine. Applications of Nanocomposite Materials in Drug Delivery **2018**, 255–282.

[35] Ranade, V.; Cannon, J. Drug Delivery Systems. **2011**,

[36] Bhowmik, D.; Gopinath, H.; Pragati Kumar,; Duraivel, S.; Sampath Kumar, K. Controlled Release Drug Delivery Systems. The pharma innovation **2012**,

[37] Thomas, L. Chemically Controlled Drug Delivery Systems. 2019; `https://www.news-medical.net/health/Chemically-Controlled-Drug-Delivery-Systems.aspx`.

[38] Higuchi, T. Mechanism of Sustained-Action Medication. Journal of Pharmaceirtical Science **1963**, 1145–1149.

[39] Kumar, V.; Kaur, G.; Pickrell, G. R. Biomedical, Therapeutic and Clinical Applications of Bioactive Glasses; Elsevier Ltd., 2019; pp 521–544.

[40] Davis, J. L. Equine Internal Medicine; 2018; Chapter 2, pp 79–137.

[41] Rochon, M.-E.; Moussa, A.; Autmizguine, J. Infectious Disease and Pharmacology; 2019; Chapter 13, pp 155–166.

[42] Wade, K. C.; Benjamin, D. Infectious Diseases of the Fetus and Newborn Infant, 7th ed.; 2011; Vol. 74; Chapter 37, pp 1160–1211.

[43] Alden, C. L.; Khan, K. Handbook of Toxicologic Pathology, vol 2, 2nd ed.; 2002; Chapter 33, pp 255–338.

[44] Ã, T. K.; Takadama, H. How useful is SBF in predicting in vivo bone bioactivity ? 2006, <u>27</u>, 2907–2915.

[45] Pentassuglia, S.; Agostino, V.; Tommasi, T. EAB-electroactive biofilm: A biotechnological resource. Encyclopedia of Interfacial Chemistry: Surface Science and Electrochemistry **2018**, 110–123.

[46] Wang, H.; Chu, P. K. Characterization of Biomaterials; Elsevier: Hong Kong, 2013; Chapter 4, pp 105–174.

[47] Hooijschuur, J. H. UV/Vis spectrometry basics. 2020; `www.chromedia.org/chromedia`.

[48] Worsfold, P. J.; Kingdom, U. Encyclopedia of Analytical Science, 3rd ed.; Elsevier, 2017; pp 1–5.

[49] Campbell, D.; Pethrick, R.; White, R. Polymer Characterization, 2nd ed.; 2018; p 481.

[50] Katoch, A.; Bhardwaj, R.; Goyal, N.; Gautam, S. Synthesis, structural and optical study of Ni-doped Metal-organic framework for adsorption based chemical sensor application. Vacuum **2018**, 158, 249–256.

[51] Sindhu, P. S. Fundamentals of Molecular Spectroscopy., 1st ed.; 2006; p 426.

[52] Omidi, M.; Fatehinya, A.; Farahani, M.; Akbari, Z.; Shahmoradi, S.; Yazdian, F.; Tahriri, M.; Moharamzadeh, K.; Tayebi, L.; Vashaee, D. Biomaterials for Oral and Dental Tissue Engineering; 2017; pp 97–115.

[53] Raval, N.; Maheshwari, R.; Kalyane, D.; Youngren-Ortiz, S. R.; Chougule, M. B.; Tekade, R. K. Basic Fundamentals of Drug Delivery; Elsevier, 2018; Chapter 10, pp 369–400.

[54] Hafner, B. Scanning Electron Microscopy Primer. 2007.

[55] Wang, G. C. Slag processing. The Utilization of Slag in Civil Infrastructure Construction **2016**, 87–113.

[56] Holbrook, R. D.; Galyean, A. A.; Gorham, J. M.; Herzing, A.; Pettibone, J. Frontiers of Nanoscience; Elsevier, 2015; Vol. 8; pp 47–87.

[57] Yesilkir-Baydar, S.; Oztel, O. N.; Cakir-Koc, R.; Candayan, A. Nanobiomaterials Science, Development and Evaluation; Elsevier, 2017; pp 211–232.

[58] Boyd, D.; Yao, Z. Application of modern transmission electron microscopy (TEM) techniques to the study of phase transformations in steels. 2012, 507–531.

[59] Hodoroaba, V. D. Characterization of Nanoparticles: Measurement Processes for Nanoparticles; Elsevier., 2019; Chapter 4.4, pp 397–417.

[60] Adya, A. K.; Canetta, E. Animal Biotechnology: Models in Discovery and Translation; Elsevier, 2013; Chapter 14, pp 247–263.

[61] Speight, J. G. Environmental Inorganic Chemistry for Engineers; Elsevier, 2017; Chapter 5, pp 231–282.

[62] Le Pevelen, NIR FT-Raman; Elsevier, 2017; pp 98–109.

[63] Eyring, M. B. Encyclopedia of Physical Science and Technology, 3rd ed.; Elsevier, 2003; pp 637–643.

[64] Kloprogge, J. T. Infrared and Raman Spectroscopies of Clay Minerals, 1st ed.; Elsevier., 2017; Vol. 8; Chapter 6, pp 150–199.

[65] Crammer, B.; Ikan, R. Organic Chemistry, Compound Detection. Encyclopedia of Physical Science and Technology 2003, 459–496.

[66] Parracino, M. A.; Martín, B.; Grazú, V. Photoactive Inorganic Nanoparticles: Surface Composition and Nanosystem Functionality; 2019; pp 211–257.

[67] Zhang, J. X.; Hoshino, K. Molecular Sensors and Nanodevices; 2019; pp 231–309.

[68] Atabaev, T. S.; Hong, N. H. Nano-sized Multifunctional Materials: Synthesis, Properties and Applications; Elsevier Inc., 2018; Chapter 4, pp 73–88.

[69] Steager, E. B.; Wong, D.; Sakar, M. S.; Kumar, V. Microbiorobotics: Biologically Inspired Microscale Robotic Systems, 2nd ed.; Elsevier, 2017; Chapter 9, pp 163–195.

[70] Belyansky, M. Handbook of Thin Film Deposition, 4th ed.; Elsevier, 2018; Chapter 8, pp 231–268.

[71] Kohli, R.; Mittal, K. Developments in Surface Contamination and Cleaning; Elsevier, 2019; Vol. 12; Chapter 3, pp 23–105.

[72] Tamiri, T.; Zitrin, S. Encyclopedia of Forensic Sciences, 2nd ed.; Elsevier, 2013; pp 64–84.

[73] Patel, J. P.; Parsania, P. H. Biodegradable and Biocompatible Polymer Composites: Processing, Properties and Applications; Elsevier, 2017; Chapter 3, pp 55–79.

[74] Nasrollahzadeh, M.; Atarod, M.; Sajjadi, M.; Sajadi, S. M.; Issaabadi, Z. Interface Science and Technology; 2019; Vol. 28; pp 199–322.

[75] Schneider, D. Particle world. 2019, 20–23.

[76] McLaughlin, R. B. In An Introduction to the Microscopical Study of Diatoms; Delly, J. G., Gill, S., Eds.; 2012.

[77] Edlund, M. B.; Stoermer, E. F.; Taylor, C. M. Aulacoseira skvortzowii sp. nov. (Bacillariophyta), a poorly known diatom from Lake Baikal, Russia. Journal of Phycology 1996, 32, 165–175.

[78] Ruggiero, I.; Terracciano, M.; Martucci, N. M.; De Stefano, L.; Migliaccio, N.; Tatè, R.; Rendina, I.; Arcari, P.; Lamberti, A.; Rea, I. Diatomite silica nanoparticles for drug delivery. Nanoscale Research Letters **2014**, 9, 1–7.

[79] Rodríguez-Fernández, J.; Pérez-Juste, J.; Mulvaney, P.; Liz-Marzán, L. M. Spatially-directed oxidation of gold nanoparticles by Au(III)-CTAB complexes. Journal of Physical Chemistry B **2005**, 109, 14257–14261.

[80] Dalagan, J.; Enriquez, E. Interaction of Diatom Silica with Graphene. Philippine Science Letters **2013**, 6, 119–127.

[81] Gnanamoorthy, P.; Anandhan, S.; Prabu, V. A. Natural nanoporous silica frustules from marine diatom as a biocarrier for drug delivery. Journal of Porous Materials **2014**, 21, 789–796.

[82] Aw, M. S.; Simovic, S.; Yu, Y.; Addai-Mensah, J.; Losic, D. Porous silica microshells from diatoms as biocarrier for drug delivery applications. Powder Technology **2012**, 223, 52–58.

[83] Govindaraju, S.; Ramasamy, M.; Baskaran, R.; Ahn, S. J.; Yun, K. Ultraviolet light and laser irradiation enhances the antibacterial activity of glucosamine-functionalized gold nanoparticles. International Journal of Nanomedicine **2015**, 10, 67–78.

[84] Tian, F.; Bonnier, F.; Casey, A.; Shanahan, A. E.; Byrne, H. J. Surface enhanced Raman scattering with gold nanoparticles: Effect of particle shape. Analytical Methods **2014**, 6, 9116–9123.

[85] Abdelhalim, M. A. K.; Mady, M. M.; Ghannam, M. M. Physical properties of different gold nanoparticles: Ultraviolet-visible and fluorescence measurements. Journal of Nanomedicine and Nanotechnology **2012**, 3, 1–5.

[86] Ikram, F.; Qayoom, A.; Shah, M. R. Synthesis of epicatechin coated silver nanoparticles for selective recognition of gentamicin. Sensors and Actuators, B: Chemical **2018**, 257, 897–905.

[87] Salouti, M.; Heidari, Z.; Ahangari, A.; Zare, S. Enhanced delivery of gentamicin to infection foci due to Staphylococcus aureus using gold nanorods. Drug Delivery **2016**, 23, 49–54.